THE UNIVERSITY OF MICHIGAN

INDUSTRY PROGRAM OF THE COLLEGE OF ENGINEERING

HEAT TRANSFER FROM ACOUSTICALLY RESONATING GAS FLAMES IN A CYLINDRICAL BURNER

William N. Zartman

A dissertation submitted in partial fulfillment
of the requirements for the degree of
Doctor of Philosophy in The
University of Michigan
1960

July, 1960

IP-445

Doctoral Committee:

Professor Stuart W. Churchill, Chairman
Professor John A. Clark
Associate Professor Don E. Rogers
Professor Lawrence H. Van Vlack
Professor Edwin H. Young

ACKNOWLEDGEMENTS

I wish to express my appreciation to:

The doctoral committee for their advice and assistance during this investigation.

Dr. S. W. Churchill, the chairman of the doctoral committee, for his interest, suggestions, and encouragement.

The Department of Chemical and Metallurgical Engineering and Esso Research and Engineering Company for their financial support of this research.

Dow Chemical Company for providing a fellowship.

The Industry Program of the College of Engineering for its help in reproduction of this report.

TABLE OF CONTENTS

TABLE OF CONTENTS (CONT'D)

TABLE OF CONTENTS (CONT'D)

LIST OF FIGURES

LIST OF FIGURES (CONT'D)

LIST OF FIGURES (CONT'D)

LIST OF FIGURES (CONT'D)

NOMENCLATURE

a	speed of sound, ft/sec
A	area, ft^2; A_s for inside surface area; A_T for total area
C	a constant
C_p	specific heat at constant pressure, Btu/lb°F; C_{ps} for heat capacity of species S; $\overline{C}_p$ for mean heat capacity of a mixture
D	diameter, ft.
E	combustion efficiency, i.e., the fraction of available heat released by chemical reaction
E_F, E_L	intensity of emmission of radiant energy at the wave lengths of the sodium D-lines and in the direction of sight, (energy)/(area)(time); E_F for the flame; E_L for the lamp
f	sonic frequency, cps; or friction factor
F_D	drag of flameholder and tube walls, lb force per lb mass
g_c	conversion factor, ft(lb mass)/ft(lb force) sec^2
G	mass velocity, lbs/$hrft^2$
h	local coefficient for convective heat transfer, Btu/$hrft^2$°F; h_x for a position x along the tube; h_∞ is the predicted coefficient for fully developed turbulent flow; h' for the coefficient without combustion
J_m	cylindrical Bessel function
k	thermal conductivity of fluid, Btu/$hrft^2$°F per ft; k_s for evaluation at the surface temperature
L	length, feet; commonly the distance from flameholder; L_b for the burning length, exclusive of any spray quench; L_e for acoustically resonating length, feet
m	a wave number for transverse modes of oscillation
M	molecular weight, lb mole; $\overline{M}$ for the mean value of a mixture
n, n_x	wave numbers; n for radial modes of oscillation; n_x for longitudinal modes of oscillation

NOMENCLATURE (CONT'D)

Nu	Nusselt number, hD/k; Nu_s for evaluation at the surface temperature
P	absolute pressure, psia; or the root-mean-square pressure amplitude of a sonic oscillation; P_o for the sound pressure amplitude at 130 db, 0.0092 psi
Pr	Prandtl number, $C_p\mu/k$; Pr_s for evaluation at the surface temperature
q	rate of heat transfer per unit area, Btu/hrft^2; q_R for the radiant heat flux
Q	rate of heat transfer, Btu/hr; Q_i for the integration of the profile of local fluxes; Q_w for the heat absorbed by the tube's cooling water; Q_t for the total heat loss from the flame per unit mass of fluid, Btu/hrlb
$Q_r(T_o)$	heat released due to chemical reaction at reference temperature T_o, Btu/lb
$Q_R(T_o)$	heat released by complete combustion at reference temperature T_o, Btu/lb
r	radius, inches; r_i and r_j for the radii of thermocouple tips, i and j; r_s for the inside tube radius
R	inside radius of tube, feet
Re	Reynolds number, DG/μ; Re_s for evaluation at the surface temperature
t	time, hour
T	temperature, °F or °R; T_{SLR} for the temperature measured by the SLR method; T_b for the bulk mean fluid temperature; T_s for the surface temperature
u	fluid velocity, ft/sec; or coordinate in complex mapping problem
v	coordinate in complex mapping problem
V	volumetric rate of flow, ft^3/hr
W	mass rate of flow, lb/hr

x	distance along tube, feet; or coordinate in complex mapping problem
y	mol fraction; or coordinate in complex mapping problem
z	plane in complex mapping problem

Greek Symbols

α_F	absorptivity of flame
α_{mn}	values that satisfy a condition in the solution of the wave equation
ϵ	emissivity; ϵ_g for the flame; ϵ_s for the tube surface
μ	viscosity of fluid, lb/hrft
π	3.1416
ρ	density, lb mass/ft^3
θ	angular coordinate, radians
ϕ	actual fuel-to-air ratio in inlet mixture divided by the stoichiometric fuel-to-air ratio

Subscripts

av	average
D	drag due to flameholder and tube walls
f.h.	flameholder
g	gas
i	inlet conditions
o	outside or outer surface
r	partial derivative with respect to r

s	surface
w	water
1,2	any two positions, usually 1 for upstream of flameholder and 2 for conditions near the exit

Abbreviations

cps	cycles per second
db	decibels
div	divergence or dot product
f.h.,fh	flameholder
gpm	gallons per minute
grad	$i \frac{\partial}{\partial x} + j \frac{\partial}{\partial y} + k \frac{\partial}{\partial z}$
level	distance from exhaust end of tube, excluding spray quench
ℓn	natural logarithm
mil	0.001 inch
SCFM	standard cubic feet per minute (at 60°F and 1 atm)
SLR	sodium line reversal
SPL	sound pressure level

ABSTRACT

Heat transfer from premixed propane-air flames to the cooled walls of a five-inch diameter, ramjet-type burner was studied with and without flame-generated, acoustically resonating oscillations. The oscillations generated were transverse oscillations, i.e., screeching combustion, of approximately 4000 cps and longitudinal oscillations, i.e., organ pipe, of approximately 350 cps. Bluff-body flameholders with greater than 90 per cent blockage of the free-stream area were used to stabilize the flame from 8 to 18-1/2 inches from the end of the tube. The inlet flow velocity upstream of the flameholder varied from 13 to 18 feet per second.

Local heat-flux densities and local inside wall temperatures were measured with and without combustion at five stations downstream from the flameholder. Flame temperatures were measured by a sodium-line-reversal technique at two of these stations. Flame temperatures were also determined from pressure-drop measurements and a thermocouple traverse of the flame in a lean propane-air mixture. Flame temperatures varied from 1600°F to 2800°F as the propane-to-air ratio was varied in the range of combustible lean mixtures. Local coefficients for convective heat transfer were evaluated using the measured values of heat flux, wall temperature, and flame temperature. The coefficients for heat transfer from the flame could be evaluated only at two stations. However, coefficients for heat transfer without combustion were evaluated at all five stations. In order to calculate flame temperatures at points other than where the flame temperatures were measured, coefficients for heat transfer from the flame were assumed to be proportional to the coefficients measured without combustion.

The sound level and frequency of the oscillations were measured and recorded with a high intensity microphone in the combustion tube upstream of the flameholder. Control of the oscillations were obtained by the use of various flameholders, and by a spray-quench muzzle on the end of the burner. Flameholders that stabilized the flame close to the tube wall were prone to screech. The spray-quench muzzle damped out the longitudinal oscillation.

Profiles of the local heat-flux density and of the flame temperature along the combustion tube are presented. The heat flux density was increased significantly by the oscillations; however, the temperature profiles were not changed significantly. The sonic oscillations had a greater effect on the heat transfer phenomena than on the combustion efficiency. The local coefficients for heat transfer 13-1/2 inches downstream of the flameholder can be represented by the expression

$$\frac{h}{h^*} = 0.044 \frac{P}{P_o} + 1.08$$

The quantity h is the measured, local coefficient for convective heat transfer from the flame at the sound pressure amplitude, P; h^* is the coefficient determined from cold flow measurements and corrected for the change in physical properties due to the combustion; and P_o is the sound pressure amplitude of the stable burner. The sound level ranged from 130 db to 160 db, which corresponds to a range in pressure amplitude, P, from 0.0092 to 0.29 psi. The effect of frequency or mode of oscillation on the heat transfer was insignificant.

INTRODUCTION

The fields of heat transfer from vibrating fluids and from flames have recently received increased attention. The recent emphasis on more powerful jet engines has lead to problems of flame-generated oscillations and the prediction of heat transfer rates. The field of combustion is a very complex one, and a fundamental understanding of the many variables and phenomena involved is lacking. Some of the variables in ramjet-type combustion studies include: fuel, oxidant, flow rates, mixture ratios, geometry of flameholder, combustion chamber design, inlet temperature, inlet turbulence, and pressure level.

Combustion instabilities are a whole field of investigation in themselves. The causes, mechanisms, and nature of flame-generated oscillations have been investigated. For ramjet-type burners properly designed to isolate the fuel and oxidant supplies from any instabilities in the combustion chamber, the flame-generated oscillations, including those associated with screeching combustion, have been shown to be acoustically resonating waves with the mechanism of generation connected to periodic formation of vortices at the flameholder. The effect of oscillations on phenomena such as the recombination of dissociated combustion species and the gas-side boundary layer, which can be influential in determining heat transfer rates, is unknown.

Work on heat transfer from flame-generated oscillations is sparse and incomplete. In an early study by Berman and Cheney[7], only overall rates of heat transfer from a small rocket chamber were measured with shock-type and sinusoidal combustion instabilities. In a more recent investigation by Sundstrom[78], local heat fluxes along the burner

were measured with longitudinal oscillations, but heat transfer coefficients were not evaluated. In a work related to this field, Tailby[80] studied the effect on heat transfer rates of sonic vibrations imposed on a diffusion flame. The majority of work on the effect of vibrations on heat transfer has been done for natural convective heat transfer. Recently Harrje[22] and Jackson, Harrison, and Boteler[28] studied heat transfer from pipe flow with sonic vibrations applied.

Since no heat transfer studies have been conducted on screeching combustion and since the fields of heat transfer from vibrating fluids and heat transfer from high temperature flames are in the frontier stage of investigation, it is felt that a heat transfer study of screeching combustion can make a contribution to all three of these subjects. Screeching combustion is particularly interesting because of reports that burner walls have rapidly eroded when an unexpected screeching or transverse oscillation was generated. The objectives of the present study are

(1) to design a burner in which an intense transverse oscillation as well as a longitudinal oscillation can not only be generated but also damped;

(2) to make quantitative measurements of heat transfer rates at several points along the combustion chamber;

(3) to measure flame temperatures at one or two points along the chamber and hence to evaluate local heat transfer coefficients.

Preliminary studies in two uninstrumented burners were necessary before a burner to accomplish the first objective could be designed.

In the present investigation of propane-air flames, the measurements include flame temperatures, pressure drops, local heat fluxes at five locations, and the sound pressure level and sound frequency. Various flameholders and sound attenuators are used to control the oscillations, both longitudinal and transverse waves being studied. Experimental data are presented for local rates of heat transfer downstream from the flameholder and for local heat transfer coefficients.

LITERATURE SURVEY

The work in the fields of combustion instability, heat transfer from chemically reacting systems, and heat transfer from vibrating fluids has on the whole been done in the last decade and at an increasing rate. Heat transfer data for individual ramjets, special burners, and for nozzles is fairly abundant; however, basic studies on heat transfer from flames are limited. The work on the effect of vibrations on heat transfer has dealt mainly with natural convection and with specialized cases. Only recently has any basic study dealt with forced convection. Some exploratory investigations have been made on the interactions of vibrations and combustion, and some rather definitive studies have been made on flame-generated oscillations, but very little work has been done on the subject of heat transfer from vibrating flames.

The literature on all combinations of the three subjects, heat transfer, sonic oscillations, and combustion, is reviewed. The order of presentation follows the general arrangement of heat transfer combined with the other two, then vibrations and combustion, and finally a short treatment of one problem in the field of combustion -- turbulent flame speeds and stabilization. This latter treatment gives a good indication of the state of knowledge in the whole field of combustion. The problems connected with combustion processes are complex and as yet largely unresolved.

Heat Transfer from Flames

A review of the literature dealing with the problem of heat transfer from chemically reacting systems is presented first. The

possible mechanisms of heat transfer include forced and natural convection, conduction, radiation, catalytic surface reactions, transference of excess energy by collision of high energy gas molecules with the solid wall, and exothermic displacement of chemical equilibria. In the case of flame temperatures below 3000°F, Mach numbers significantly below one, and cold burner walls, the only important mechanisms are convection and radiation.

Radiation from Flames

The radiant contribution for non-luminous flames can be estimated by the methods presented by Hottel in McAdams[48], if the flame temperature and composition are known. Prediction of the radiation involves prediction of the flame temperature and composition. Only the heterogeneous molecules make a significant contribution to the radiation from non-luminous flames. Luminous flames, which are characterized by their yellow color and are commonly associated with the diffusion flame, have a greater emmissivity than the non-luminous ones, mainly because of the presence of carbon particles. Here the accurate prediction of the radiation is more difficult because of the added problem of estimating the size and concentration of the carbon particles.

Convective Heat Transfer

The convective contribution to the heat transfer can be affected significantly by a number of variables. Under some conditions, the coefficient for convective heat transfer from the flame to the wall may be estimated from one of the common correlations developed for fluids flowing in a pipe. Summerfield[77] reviews a number of theories of convective

heat transfer in turbulent flow with regard to high temperature combustion chambers.

Zellnik[91] studied the problem of high temperature difference between a hot gas and cold wall. He discovered that the well-known Dittus-Boelter relation

$$Nu = 0.023Re^{.8}Pr^{1/3} \tag{1}$$

correlated the data well if the fluid properties were evaluated at the bulk temperature. A factor $(T_b/T_s)^{.33}$ must be applied to the right side of the equation when the fluid properties are evaluated at the surface temperature.

For gas film convective heat transfer coefficients in rocket motor combustion chambers and nozzles, Greenfield[18] recommends the expression

$$h_g = (0.029\ G^{0.8}\ C_p\mu^{0.2})/D^{0.2} \tag{2}$$

Bartz[4] presents an equation for rapid estimation of rocket nozzle convective heat transfer coefficients. He points out that variations in velocity and temperature boundary layer thickness are secondary while mass flow rate per unit area is the dominant factor in determining heat transfer rates in the nozzle.

Heat Transfer from Chemically Reacting Systems

Hirschfelder[25] has analyzed heat transfer from chemically reacting gases. He presents an equation for calculating the thermal conductivity based on the classical treatment of Eucken for gaseous mixtures; however, local chemical equilibrium must exist.

Kilham[35] studied heat transfer from carbon monoxide-air and hydrogen-air flames to a rotating refractory tube. He assumed that at equilibrium the rate of heat transfer from flame gases to the tube by forced convection and radiation was equal to the heat loss by radiation to the surroundings. Experimental heat transfer coefficients for the carbon monoxide-air flame agreed closely with values predicted from McAdams' correlation[48] for pure convection. The lack of agreement with the hydrogen-air flame was attributed to recombination of radicals at the surface of the tube.

Schotte[70] shows analytically and experimentally that heat transfer coefficients for flow with gas-phase, instantaneous chemical reactions can be predicted by using calculated effective thermal conductivities and effective specific heats in conventional heat transfer correlations. Methods are described for obtaining these effective physical properties.

Studying heat transfer in a tube for the dissociating system $N_2O_4 = 2NO_2$, Brokaw[9] found the experimental data in accord with the usual Nusselt-Prandtl-Reynolds number correlation for this type of convective heat transfer. The thermal conductivities and kinematic viscosities were computed using rigorous expressions from the kinetic theory of gases. The thermal conductivity includes a large contribution arising from the diffusional transport of chemical enthalpy.

Heat Transfer from Particular Burners

Ziebland[92] performed heat transfer experiments in small rocket-type combustion chambers and found the experimental heat transfer coefficients exceeded the computed values by two-fold. He attributed the

difference between experimental and computed values mainly to the unestablished flow pattern near the inlet of the combustor. He also noted that the calculated emissivities may have been low due to the extrapolation of low pressure emissivity data to high pressure.

Shorin and Pravoverov[74] in measuring local heat transfer rates from laminar diffusion flames found that radiant heat transfer predominated. In a 6-inch diameter gas turbine combustion chamber, Winter[89] estimated that 50 to 80 per cent of the heat transfer was by radiation.

Hammaker and Hampel[20] studied heat transfer from a diffusion flame burning inside small diameter tubes. The fuel was injected through a jet at the entrance to the tube with air being sucked in from the surroundings. The heat transfer rates were fairly constant from a point six inches from the inlet to over forty inches. Neither inside flame temperatures nor internal heat transfer coefficients were estimated.

In equipment similar in design to that of Hammaker and Hampel, Tailby and Ashton[79] studied heat transfer from a diffusion flame, varying the fuel-to-air ratio, gas burner characteristics, excess air entrained into the system, and horizontal tube length. Both convective and total radiant heat transfer were measured. Radiation was the dominant of the two in the heat transfer from the lower portion of the tube, while convection dominated in the upper sections. Luminous radiation from the flame constituted the major portion of the total radiation. The results were not compared with any of the usual empirical heat transfer expressions. Earlier Tailby and Saleh[81] did a similar study in a vertical diffusion burner.

In their heat transfer study of hot combusted gases flowing through a water-cooled tube, Timofeev and Uspenskii[82] measured gas temperatures, radiant heat transfer, and local total heat transfer at several positions along the length of the tube. The radiant contribution agreed with an analytical prediction. The coefficients for convective heat transfer were scattered about an empirical curve from the literature. The total heat transfer coefficient correlated well with the Reynolds number, indicating the dominance of convection over other effects.

Effect of Oscillations on Heat Transfer Rates

Several contributions have been made on the effect of vibrations, sonic or mechanical, on heat transfer rates. A few of the more noteworthy investigations in the areas of natural convection as well as forced convection are discussed below.

Holman and Mott-Smith[26] give experimental evidence that the heat transfer coefficient for free convective heat transfer from a horizontal cylinder may be increased by more than 100 per cent in the presence of strong constant pressure sound fields. No appreciable effect occurred until the sound pressure level exceeded about 134 db. The heat transfer coefficient is independent of frequency except near this critical sound level where the frequency effect was slight. In a qualitative analysis, the authors attempted to explain the test results as an effect of the interaction of the phenomenon of acoustical streaming with the free convection boundary layers.

In an experimental study similar to that of Holman and Mott-Smith, Fand and Kaye[16] found that a critical sound pressure level

exists between 136 and 140 db, depending on the frequency, above which the heat transfer increases rapidly with increasing intensity.

Kubanski[39] studied the influence of standing sound waves on heat transfer by natural convection from a heated horizontal tube. The natural convective heat transfer coefficients were increased by two-fold or more as a result of the vibrations. An optical study of the flow field revealed the presence of acoustical streaming.

Jackson and others[28] imposed sound waves on air flowing through a horizontal tube and studied the effect upon natural and forced convective heat transfer. At a sound pressure level above 118 db, the free convective forces influenced the heat transfer coefficient only slightly. Above 118 db free convection was apparently negligible and the effect of sound appeared to be an increase of 30 to 40 per cent in the heat transfer coefficient at 140 db.

In a discussion of Jackson's paper, Kreith[38] points out that in this case the wave motion may be a resonance phenomenon controlled primarily by the over-all geometry of the system and may therefore affect the mechanics of the boundary-layer waves only indirectly by virtue of its effect on the flow far away from the boundary. One would, therefore, look for an explanation rather in terms of macroscopic flow phenomena, whereas in some other cases the vibration may affect the microscopic motion of the boundary layer directly. It was also pointed out that the 118 db figure is probably only a relative value.

Harrje[22] imposed axial-type sinusoidal pressure and velocity fluctuations on a steady flow of hot gas under conditions of fully established turbulent pipe flow. The fluctuations produced a maximum increase

in the steady-state heat flux of less than 10 per cent. However, the heat-flux increase was found to be almost linearly dependent on the amplitude of the unsteady component of velocity.

Havemann[23] studied heat transfer from rapidly compressed and oscillating gases in a cylinder. He found that the increase in heat transfer over a gas at rest was dependent on the amplitude of the pressure fluctuations and, to a lesser extent, on the frequency of oscillation. Vibrating wires of differing diameters were studied by Lemlich[43] for the effect on natural convection rates. The heat transfer coefficient was increased by four-fold for low temperature differences. West and Taylor[86] improved heat transfer 70 per cent in a double pipe heat exchanger by applying 100 pulses per minute to the water. Martinelli and Boelter[51] increased coefficients for heat transfer five-fold by vibrating a cylinder in natural convection under water. On the basis of acoustic streaming, i.e., flow created by the acoustic disturbance, Kubanski[40] explains the increased heat transfer in these experiments by Martinelli and Boelter and Lemlich.

Havemann and Rao[24] found that if the frequency is low enough the effect of pulsations becomes negligible as might be expected. This minimum frequency appears to be about 20 to 30 cps for fluids that are not highly viscous.

Morrell[55] proposed a method for calculating heat transfer rates in resonating gaseous pipe flow. His method treats the oscillations as shock waves and uses the relations that apply to shock waves in deriving his correlation, which therefore has limited applicability.

Heat Transfer from Oscillating Flames

Berman and Cheney[7] conducted a study of combustion instability in a three-inch rocket chamber. They observed no abnormal heat transfer rates from flame-generated sinusoidal-type oscillations with amplitudes up to 100 psi peak to peak. However, shock-type instability, with amplitudes up to 500 psi, was accompanied by heat transfer rates up to 2.5 times the normal values. Tischler and Male[83] state that the combustion-driven oscillation known as screeching can cause abnormally high heat transfer rates. They mention an air-cooled engine which had as much as 1/4 inch of solid stainless steel eroded from the chamber in runs of a second duration.

Tailby and Berkovitch[80] applied sonic vibrations to the gas stream of a diffusion flame burning at the inlet of a water-cooled tube and measured the total heat transfer as well as the radiation to the tube. The main effects of the sound were to increase the heat transfer by factors of 2 to 3 in the lower parts of the tube and to shift the position of maximum heat transfer upstream. Also the vibrations in general reduced flame temperature, shortened the flame, and reduced its luminosity at high sound levels.

In a water-cooled, 1-inch diameter tube, Sundstrom[78] measured local heat transfer rates from propane-air flames with and without self-sustaining longitudinal oscillations. He concluded that flame-generated longitudinal oscillations flattened the peak in the heat transfer curve for damped combustion, and shifted the peak of the damped curve toward the flameholder.

Combustion Instabilities

A combustion instability is any repetitive perturbation around steady conditions of the flow pattern, flame temperatures, and/or flame speed. A combustion instability is often revealed by sonic measurements because the instability is usually a cyclic or periodic variation, having a frequency within the spectrum of sound. Except for instabilities associated with rough burning of a rich fuel mixture or with uneven fuel injection, combustion instability has been found to be an acoustically resonant phenomenon.

Acoustically Resonant Frequencies

The resonant frequencies of the various possible modes of oscillation within a combustion chamber may usually be predicted through the standard wave equation.[54] This classical wave equation is strictly valid only for small perturbations of the fluid; however, numerous investigators[8,21,33,62,83] have found that the classical equation predicts the frequencies well, considering that within a combustion chamber there are large temperature and velocity fluctuations across the radius and length and with time. Maslen and Moore[54], after analyzing flame-generated transverse waves in a combustion chamber, concluded that such waves have frequencies independent of amplitude and do not steepen with time, i.e., do not form detonation waves.

The standard wave equation was solved originally by Rayleigh.[66] Morse[56] presents the solution for a cylinder with both ends closed. The slight modification to arrive at the solution for a cylinder with one end open and one closed is readily made. The frequencies of the

various acoustical modes for this cylinder are then given by the expression

$$f_{m,n,n_x} = \frac{a}{2}\sqrt{\left(\frac{n_x + 1/2}{L_e}\right)^2 + \left(\frac{\alpha_{mn}}{R}\right)^2} \qquad (3)$$

Any choice of the wave numbers, m,n,n_x, as positive integers or zero corresponds to a possible natural mode of acoustical oscillation within the cylinder. The three wave numbers can be viewed as representing three sets of waves. When $n = m = 0$, the longitudinal waves or organ pipe solutions are given by the wave equation. Here the motion is parallel to the axis of the cylinder. The waves, for which motion is entirely radial and for which $n_x = m = 0$, are those which focus the sound along the cylinder axis and are called radial waves. The transverse waves for which $n_x = n = 0$ are those which travel close to the curved walls of the tube and have little motion near the cylindrical axis. Of course any combination of these three pure waves is a possible mode of acoustic, resonant oscillation within the cylinder also.

The primary longitudinal or organ-pipe oscillation is of a lower frequency than the fundamental transverse or radial oscillation in the normal burner, the length of which is greater than its diameter. The primary longitudinal mode has a pressure antinode and velocity node at the closed end and a pressure node and a velocity antinode at the open end of the cylinder.

Conditions for Flame-Generated Oscillations

An intermittent source of energy is required to drive the oscillation and overcome the ever-present damping forces in the system. In the

case of a self-sustaining flame-driven oscillation, Rayleigh's hypothesis[66] states that an oscillating component of the rate of heat release must be in phase with the oscillating component of the pressure. This hypothesis has been justified analytically using thermodynamic principles by Putnam.[62] By employing one additional assumption, Putnam is able to explain the amplification in his burner of certain natural frequencies. This assumption dictates that the point of heat release must be near the point of maximum pressure amplitude in the combustion tube.

Flame-Generated Longitudinal Oscillations

Putnam[65] has written a comprehensive review of organ-pipe oscillations in combustion systems. He groups the burners in which oscillations occur into diffusion burners, flash tubes, gauze-tone burners, rocket-shaped burners, burners utilizing secondary air, and ramjet-type burners. The acoustical behavior of each system is described and possible driving mechanisms for producing the observed oscillations are indicated. In one study[64] a bank of hypodermic tubes was employed to lead the gases from the mixing chamber to the combustion chamber. The combustion chamber was considered a driver which forced slugs of gas in the hypodermic needle ports to oscillate. Burning of the incremental pulses of combustible mixture periodically issuing from the ports furnished energy to drive the oscillation when the pulses burned in phase with the oscillating component of the pressure in the chamber. Putnam and Dennis[62] found that longitudinal oscillations are most likely to occur when the flameholder is near a pressure antinode.

Bailey[2] studied some organ-pipe oscillations in a tube with a gauze-type flameholder. He proposed a driving mechanism depending on a flame speed which is a function of position as well as mixture strength. The resultant instability is found to be in accordance with Rayleigh's criterion.

Dunlap[15] studied resonance of a propane-air flame in a 1 x 1 x 12-inch combustion chamber, acoustically open at both ends. Agreement was obtained between experimentally observed frequencies and those predicted by assuming a longitudinal resonance of hot and cold gases. The flame was not prone to resonate at extremely rich or lean mixtures. Dunlap noted, as Putnam later verified, that the oscillation of any particular mode occurred when the flameholder was in the region of a pressure antinode for the mode. He postulated the following driving mechanism, which satisfies Rayleigh's hypothesis. Standing sound waves in the combustion chamber produce a variation in pressure and temperature at the flame front with time. The dependence of flame speed on temperature and pressure results in a cyclic variation of burning rate.

Sensitive Time Lag Criterion

Crocco, Grey, and Harrje[13] have postulated a theory based on a sensitive time lag for ignition of a gobule of unburned gas to explain flame-generated oscillations. They have observed that there is an upper limit to the chamber length above which a mode of longitudinal pressure oscillation cannot occur in a combustion chamber. They state that this upper chamber limit cannot be explained by any other mechanism advanced to date (December, 1958).

Working with a plungerjet rocket engine, Shieber[73] discovered this upper chamber limit and found stable operation above that length. The most noteworthy thing in Shieber's work, however, is the fact that the onset of instability was sooner and the amplitude greater when the larger of two replaceable exhaust nozzles was installed in the engine. In fact, he states that the smaller of the two throats practically inhibits pressure oscillations.

Generation of Transverse Oscillations

The question of which mode of resonant oscillation to expect in a given burner does not have as yet an explicit answer. The propensity of a burner to amplify transverse waves appears to be strengthened by several factors. A bluff-body-type flameholder of high blockage, a short combustion chamber of reasonable diameter, high wall temperatures, high inlet temperature of fuel, Mach number close to but below one, and fuel-to-air ratio near stiochiometric are all believed to make a burner more prone to screech.[3,45,67,85]

The tendencies of fourteen different fuels and three fuel blends to produce high frequency oscillatory combustion were measured by Tischler and Pass[58] in a 200-pound thrust, water-cooled, liquid-oxygen-fuel rocket engine. In this apparatus, the fuels in order of increasing screeching tendency were 1) hydrazine (it did not screech at all), 2) branched-chain paraffins, aromatics, and amines, 3) straight-chain paraffins. This trend of screeching tendency correlated with increasing fuel evaporation rate. An explanation was given by a combustion model that indicated combustion, for which flame propagation through a gaseous

mixture is rate controlling,is more sensitive to pressure changes than is combustion,for which fuel-droplet burning is rate controlling.

The bulk of the experimental evidence points to the fact that the acoustical modes of first order are the preferred modes of oscillation in rocket engines.(83) Maslen and Moore(54) point out on the basis of viscous energy dissipation in the boundary layer that the low-order modes are, indeed, more easily driven than the higher-order modes. Also they found that for large length-to-diameter ratios longitudinal waves are most likely to occur. They determined analytically and experimentally that while strong longitudinal waves in the chamber will inevitably develop shock fronts, the strong, transverse-wave pressure distribution is symmetrical.

Screeching Combustion

Blackshear, Rayle, and Tower(8), and Harp, Velie, and Bryant(21) developed a microphone probe to investigate the phenomena of screech and to ascertain if it was truly a transverse or radial solution to the wave equation. With the probe microphones, the frequency, the relative amplitude, and relative phasing of the oscillations were measured at various positions within a screeching combustor. Through this detailed probing they verified that the phenomenon of screech is truly an acoustically resonating oscillation and was the first transverse mode in their 6-inch diameter afterburner.

Tischler and Male(83) present some enlightening photographs of transverse waves in cylindrical combustion chambers. A streak photograph reveals a continuous trace of helical form for the transverse wave as

it travels along the axis of the burner. This helical form indicates that the transverse wave is rotating or spinning, i.e., the pressure head travels around the periphery of the chamber. The transverse wave can evidently be either in the standing (or sloshing) form or in the spinning form. The wave equation does not answer this question and the theoretical frequencies for either form are identical.

Mechanisms to Explain Screeching Combustion

Kaskan and Noreen[33] investigated transverse oscillations in a two-dimensional burner by searching for periodic flame-area variation during oscillation. Their screech limits for propane-air prescribed that a minimum inlet velocity of 35 feet per second was necessary to induce screeching combustion. Changing screens upstream from the flameholder and thus changing the inlet turbulence level had no effect on the screech limits.

High speed motion pictures revealed that the transverse oscillation was accompanied by the periodic formation of vortices, which distorted the flame front. The frequency with which these vortices were formed was equal to the frequency of oscillation, which was about 4000 cps. The vortices were also shown to have a definite phase relationship with the oscillatory parameters such as velocity and pressure. The vortices appeared to form as a result of the oscillatory part of the velocity, thus possibly providing the feedback between gas oscillation and driving force, which appears necessary in self-maintaining vibrations. Furthermore, Kaskan and Noreen mentioned as a driving mechanism the periodic variation in flame area caused by the periodic vortex formations at the

flameholder lip. The authors' pictures of the flame with a longitudinal oscillation also revealed the formation of vortices with the periodicity of the oscillation. Here the vortices also distort the flame, but in a more longitudinal fashion. Kaskan and Noreen's pictures show that both oscillations can also exist at the same time independently of one another.

Kaskan and Noreen's theory that variations in flame area drive the transverse mode is open to debate. Smith and Springer[75] argue that the pressure and temperature rise accompanying the acoustic wave increases the reaction rate in phase, or nearly so, with the pressure, and the necessary temperature rise is more conceivable than an equivalent increase of flame area.

Rogers and Marble[67] made a study similar to that of Kaskan and Noreen in a two-dimensional, rectangular burner, using air and vaporized gasoline. Their high speed motion pictures also showed that the high frequency oscillation is accompanied by vortices shed periodically from the flameholder lip with the same frequency as the oscillations. However, they have postulated a different driving mechanism for these oscillations, which they have stated very concisely.

> A mode of transverse oscillation is excited as the result of periodic transport of combustible material associated with the vortices into the hot wake of the flameholder. The vortices, in turn, are generated at the flameholder lips by the fluctuating transverse velocity. When the ignition time delay lies in the proper range, the phase relationship between oscillations in transverse velocity and combustion intensity is such that the oscillation is amplified.[67]

Recently Barker[3] in similar equipment verified this mechanism of screech generation.

The analysis of heat-driven oscillations by Merk[52] is not too applicable because it is for a special burner with long multiple ports which introduce the gas to the combustion chamber and serve as stabilizers. He analyzes the fluctuating heat transfer from these long metal burner ports.

Methods for Damping Oscillations

Putnam and Dennis[63] studied the suppression of flame-driven, organ-pipe oscillations with acoustical dampers. The effectiveness of the quarter-wave tube was found to be critically dependent on length, but relatively insensitive to location as long as the tube is placed in the region of the pressure antinode. It did not have to be placed near the particular antinode where energy was fed into the oscillation. Other means of suppression included holes drilled in the side of the tube and placed within 10 per cent of a wave length from a pressure antinode. Helmholtz resonators were also effective. Some of their work dealt with reflectors near the exit of the combustion tube.

The most successful damping of screeching combustion was obtained with a perforated liner inside the combustion chamber.[8,21,37] This was the only method found in the NACA studies that completely eliminated screech under all operating conditions.

Effects of Oscillations on Combustion

Some of the effects of transverse and longitudinal oscillations on the combustion phenomenon are available in the literature. The changes

brought about by a transverse or longitudinal oscillation are given mostly in a qualitative manner, however. Screeching combustion results in increased flame propagation, increased mixing, increased combustion efficiency, and higher operating temperature of combustor parts and shell.[8,33,54,84]

Another study by NACA, this one by Mickelsen[53], analyzes the effect transverse waves have on fuel-oxidant mixing in a cylindrical burner. In the burner that he has analyzed, the fuel is injected into the oxidant stream at a short distance upstream from the flameholder.

Several investigations have been made by applying a sound field to the flame. Tailby's work was mentioned earlier under heat transfer studies since he also measured heat transfer from his flames.

In Kippenham's experiment[36], high frequencies, 26 kc to 58 kc, were imposed on the combustion zone of pre-mixed propane-air flames and were found to have little effect on the normal flame velocity. The combustion zone configuration, however, was changed. The usual cone for laminar flames became a flattened bowl shape and for turbulent flames became a suspended violently agitated zone. Both possessed remarkable stability. The negative effect on flame velocity would seem to confirm Markstein's[50] opinion that the oscillation phenomena which occur in tubes should be ascribed primarily to variations of flame surface area rather than of burning velocity.

Loshaek, Fein, and Olsen[47] applied a sound wave with a frequency of 12,700 cps to a laminar propane-air flame. The sound altered the flashback limit so that the flame became more stable and altered the

blowoff limit so that the flame became less stable. The burning velocity and flow velocity profiles were unchanged.

In Hahnemann's experiment[19], intense sound vibrations of 5000 cps were imposed upon a stationary propane-air flame issuing from a nozzle. In addition to a slight increase of the flame velocity, a fundamental change both in the shape of the burning zone and in the flow pattern could be observed. This was explained as a transition at the nozzle from jet flow to potential flow.

Havemann[23] studied the effect of oscillations on flames burning inside tubes. He found that the apparent flame velocity increased with amplitude and frequency of oscillation. Schmidt, Steinicke, and Neubert[69] also noted an increase of flame velocity with amplitude for a combustion wave propagating in a tube.

Theories of Flame Stabilization

Theories or experiments attempting to explain the stabilization of a flame on a bluff body, the turbulent flame speeds, or the propagation of flames are plentiful, but their conclusions or explanations are varied and conflicting. It is worthwhile reviewing some of this literature to understand the current state of knowledge in the field of combustion.

Longwell's[46] view is that stabilization occurs in a zone with a high mixing intensity and approximately homogeneous composition. The stability range depends on the residence time in that zone. Under certain conditions combustion appears to proceed homogeneously as a second-order chemical reaction. This hypothesis of Longwell serves to explain

many gross features associated with flame stabilization behind bluff objects in high velocity air streams.

Wright and Becker[90] studied the ignition of combustible material by means of two streams flowing parallel to each other. They found that a propagating flame is established only when the residence time of combustible material in the mixing zone is long enough to lead to ignition of a mass adequate to serve as a secondary ignition source. This result was applied to the explanation of bluff-body flame stabilization and blowoff.

The existing theories of flame stabilization seem to differ only in their degree of simplification of one of the two fundamental aspects, i.e., the chemical kinetic viewpoint or the fluid mechanical one (including heat transfer). The theories are based explicitly either upon energy balance (Williams, Hottel, and Scurlock[88] and Khitrin and Goldenberg[34]) or on mass balance (Longwell, Frost, and Weiss[46]) or on mass balance (Longwell, Frost, and Weiss[46]) or on purely kinetic considerations (Zukoski and Marble[93]).

Cheng and Kovitz[11], however, tackle the problem without an initial assumption of the preponderance of chemical kinetics or fluid mechanics. Their work begins with Adamson's work[49] and the extension of his work by the authors in the Sixth Symposium.[10] Another recent contribution was made by Karlovitz[31] when he presented a theory which permits the direct calculation of the combustion wave area from the turbulent parameter and the laminar burning velocity.

The work on flame stabilization by Zukoski and Marble[93] makes an interesting point. The authors state that the most important

consideration is the time spent by the fresh gas in the shear layer rather than the residence time in the wake.

Turbulent Flame Speeds

Many variables interact complexly in flame spreading and no accurate, simple description seems likely. Neither the concept of a wrinkled laminar flame nor of an extended reaction zone, nor of homogeneous combustion fits the data generally; although any one concept may be acceptable over a restricted range. Petrein and Longwell[60] point out that burning is probably discontinuous in micro-time, making inapplicable theories assuming continuous burning.

Several theoretical works have suggested that the speed of combustion is influenced not only by the turbulence of the upstream flow, but also by the turbulence which occurs during combustion. These theories are those of Landau[42], Markstein[50], Scurlock[71], and Karlovitz.[32] Prudnikov[61] measured turbulence in flames by an optical diffusion method and found the turbulence to be increased by combustion. He also states that Westenberg[87], who came to the opposite conclusion, took measurements at a distance where turbulent intensity practically equals tube turbulence.

Friedman[17] feels that for low levels of turbulence the wrinkled flame model, first proposed by Damkohler[14], is valid and for very high intensities of turbulence the distributed reaction zone model is more appropriate. Through the effect of turbulence on radiation intensity, John and Summerfield[29] concluded that turbulent mixing breaks up what would be a continuous laminar flame sheet and that this break-up modifies chemical reaction and transport processes in the flame zone.

Shetinkov[72] used the model of micro-volume burning to calculate the turbulent flame velocity. In this model, which is contrasted with the surface mechanism model, the turbulent stream is regarded as consisting of individual turbulent moles or gobules which constantly appear and disappear.

APPARATUS

The attainment of accurate and meaningful heat transfer measurements is the primary objective of this design of a burner in which screeching combustion could be generated. A vertical, cylindrical design was chosen because the symmetry of a cylinder's walls is important to enable measurements at one point on the wall to yield representative heat transfer rates for that level. Also a vertical cylinder eliminates any density effects other than those along the tube axis.

One important property of the combustion chamber that could not be foretold from the literature is its propensity to screech with a propane-air flame. It was known that the burner diameter could be made too small to permit screeching combustion; however, since the air and fuel supply rates were limited, an upper limit was placed on the diameter. Therefore, preliminary experiments were conducted in two uninstrumented burners, one a four-inch pipe, and the other a five-inch pipe, both water cooled. Since higher screech intensities by 10 db were obtained in the 5-inch pipe, this size was picked for the investigation.

General Features of Complete System

A schematic diagram of the equipment is presented in Figure 1. The four streams, air, propane, cooling water for the combustion chamber, and cooling water for the flameholder, are shown entering the vertical assembly of mixing and combustion chambers. The details of each stream and each piece of equipment are given later.

Three pictures of the equipment are presented in Figures 2, 3 and 4. An overall view is presented in Figure 2. In back of and above

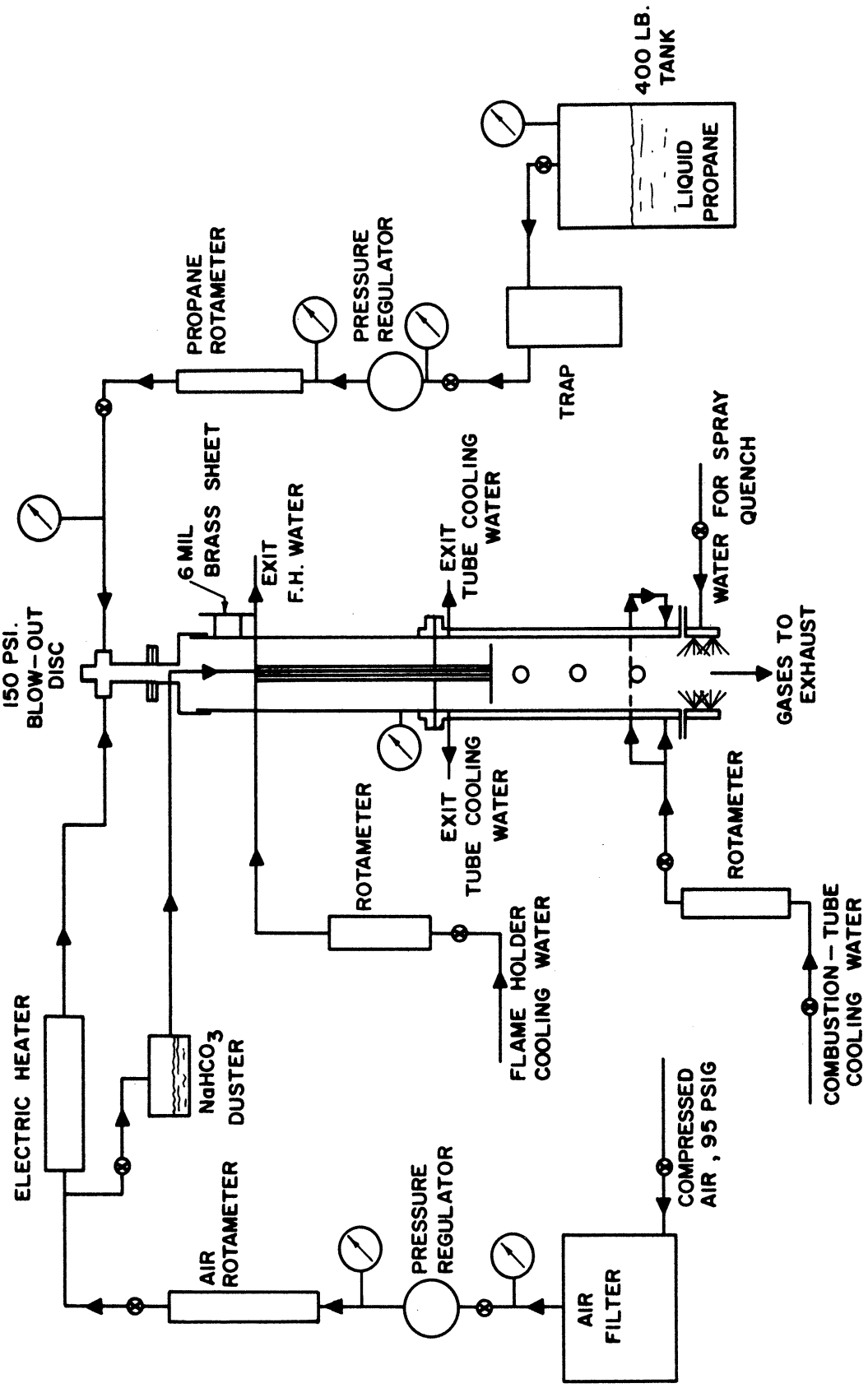

Figure 1. Schematic Flow Diagram of the Apparatus.

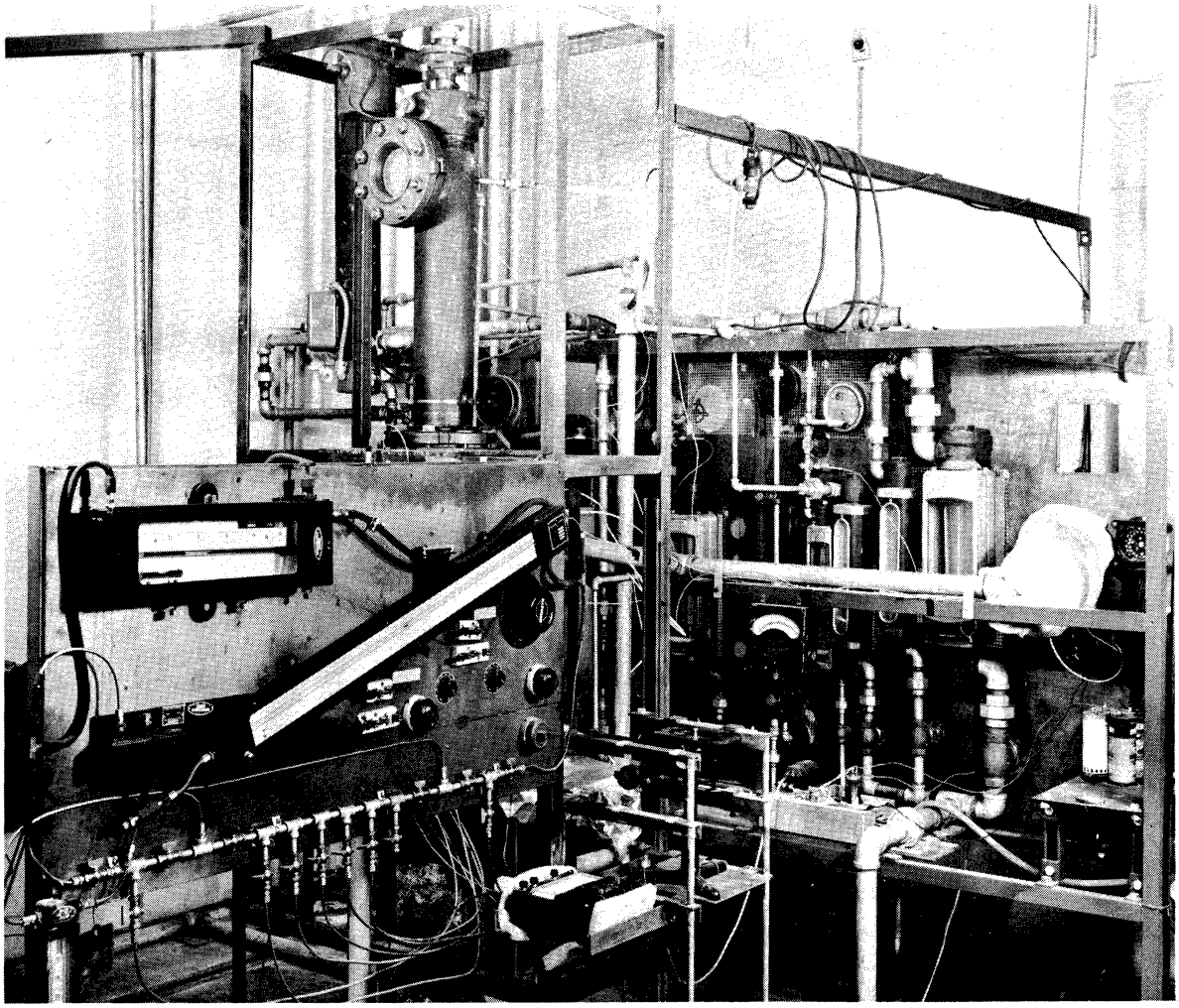

Figure 2. Photograph Showing the Manometer Panel on the Left, the Metering Panel on the Right, and the Vertical Mixing and Combustion Chambers in the Center, partially hidden.

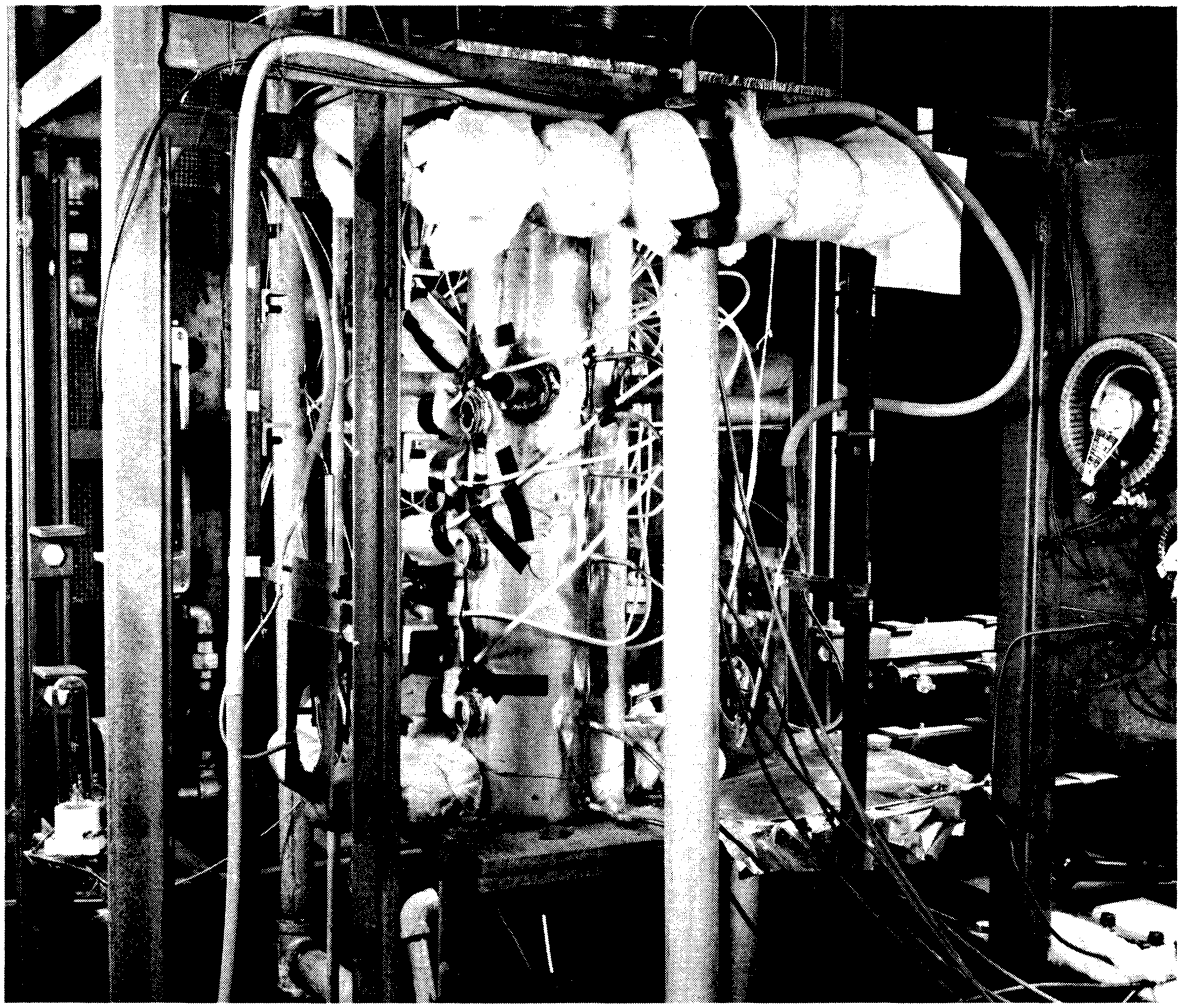

Figure 3. Photograph of the Combustion Chamber.

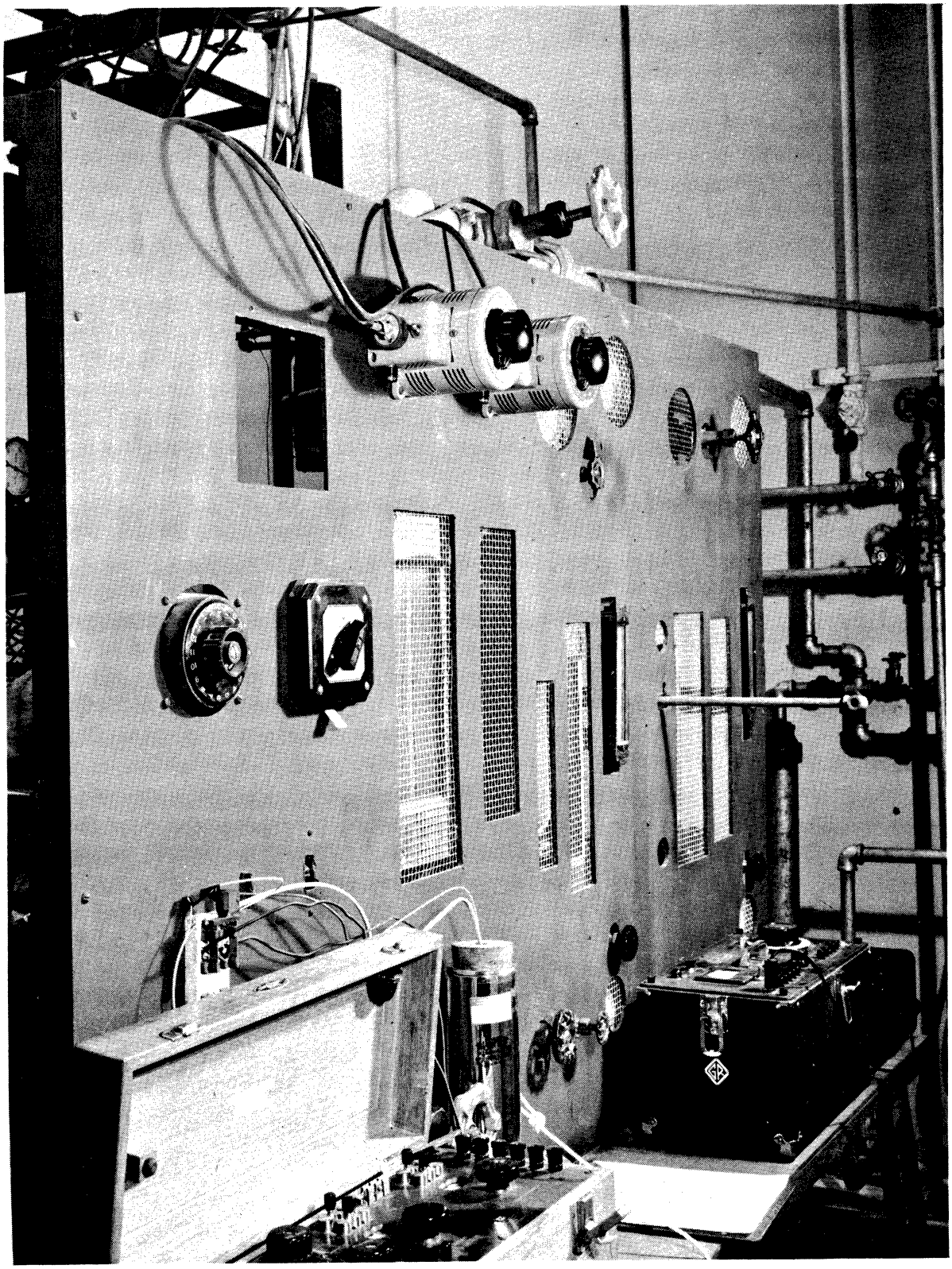

Figure 4. Photograph of the Metering Panel.

the manometer panel, the vertical mixing chamber is visible. The combustion chamber is hidden from view. In Figure 3, a view taken from in back of the manometer panel, the combustion chamber is shown with the pressure taps and one row of ports of windows visible. The last picture, Figure 4, shows the front of the metering panel.

General Features of Combustion Chamber

The instrumented chamber is constructed from a six-inch tube of hot rolled, low alloy stainless steel with a nominally 1/2 inch thick wall. The alloy is Croloy, which is a 9 per cent chromium, 1 per cent molybdenum steel. Its complete composition and a plot of its thermal conductivity versus temperature are given in Appendix D.

The inside surface of the tube was given a very smooth and even finish by a honing operation and the outside was cleaned up on a lathe. The final dimensions are an inside diameter of 4.920 ± 0.003 inches, an outside diameter of 5.937 ± 0.005 inches, and a length of 27 inches.

The local rates of heat transfer are measured at five thermally isolated stations, where the temperature gradients through the wall are measured by three thermocouples. These thermocouple sections are located at five positions along one side of the tube, at distances of 4, 10, 13, 15 and 17 inches from the exhaust end of the tube. Pairs of ports, 5/8 inch in diameter, are at three of these levels, the 4, 10, and 15-inch levels. Pressure taps are located at the 2-inch level and 25-inch level as well as at the 4, 10, 13, and 15-inch levels. The microphone mount is at the 22-inch level. The term level is being used to indicate the height or distance above the bottom or exhaust end of the burner. The

gas flows down and out the bottom of the tube. A schematic diagram of the mixing and combustion chambers is given in Figure 5.

Some miscellaneous items built into the chamber are a spark plug mount at the 2-inch level and four, 1/2-inch holes at the 16-inch level. Plugs, which completely fill the holes and make a smooth inside surface, were in these holes throughout all the recorded runs. Their purpose is to make it possible to place quarter-wave tubes at this position or some other acoustical dampers there.

Embedded Thermocouples for Heat Transfer Measurement

The thermocouple sections are one-inch square units that are thermally insulated from the rest of the tube and contain three thermocouples at three depths in the tube wall. Four slots, 30 mils wide, were milled deeply into the tube wall to form the four sides for each thermocouple section. These slots, which literally box off a one-inch square, reach within 20 mils of the inside surface. They are filled with strips of mica bonded with silicon resin. The tube was baked at 400°F for one hour to cure the resin. A diagram of a thermocouple section is shown in Figure 6.

The thermocouple assemblies are contained in holes, 42 mils in diameter, drilled from three edges of the boxed section to three different depths within the tube wall. The bottom of each hole is in the center of the square area, and thus the bottoms of all three holes are on the same radial line extending from the center of the tube.

The thermocouple assemblies were prepared from specially insulated and shielded thermocouple wire. This special wire consisted of

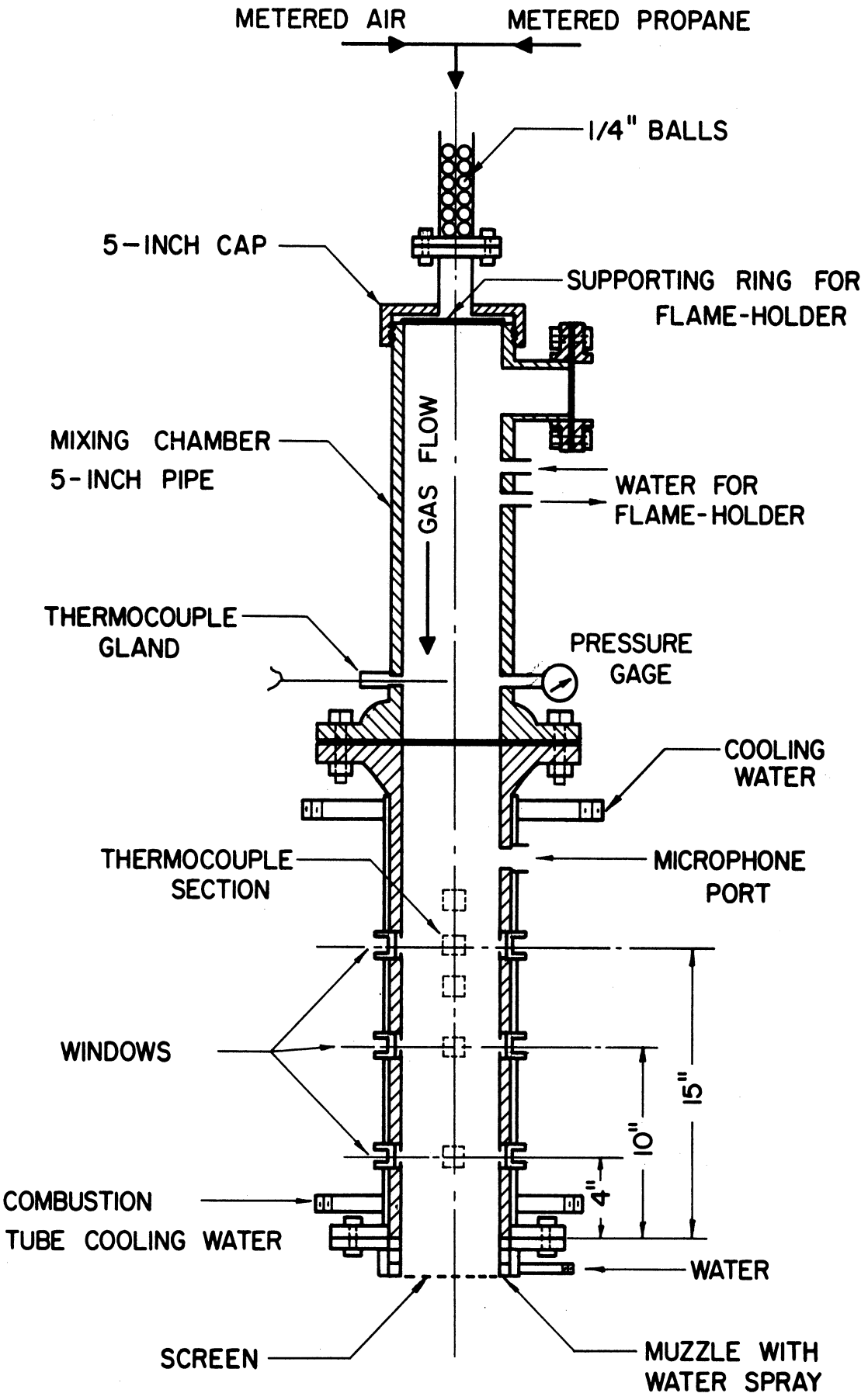

Figure 5. Detail of Combustion Chamber.

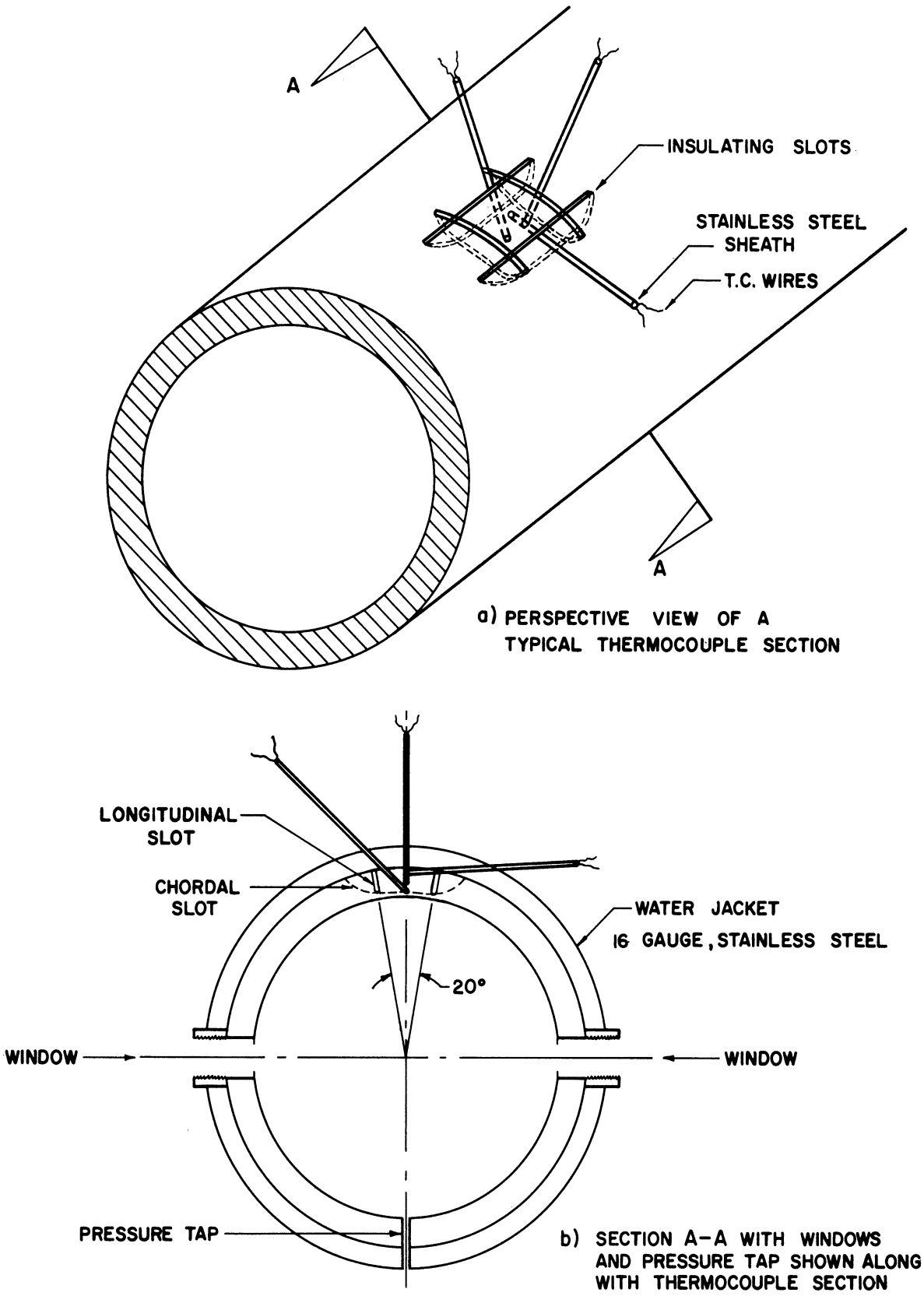

Figure 6. Detail of Thermocouple Section.

36-gauge chromel-alumel thermocouple wires packed with magnesium oxide within a stainless steel sheath, the outside diameter of which is 40 mils. Thermocouples were formed from this special thermocouple wire by cutting it into 6-inch lengths and carefully removing the sheath for a short distance at each end to expose the 36-gauge wires. A twisted tip was carefully silver-soldered and cut off cleanly just in front of the sheath's end. The thermocouple tip was held firmly by the packing and could not move from side to side. The tips were examined under a microscope and were rejected if they were more than 10 to 15 mils long. The thermocouple assemblies were then placed in each hole with the tips soldered to the bottom with a small chip of silver solder. The sheaths were soldered to the tube at the top of each hole so that the assembly was held firmly in place.

X-Rays to Locate Thermocouples Precisely

Since the angle and depth of each thermocouple hole was checked after drilling, the location of each thermocouple tip was known fairly accurately, probably to $\pm$ 10 mils. However, two uncertainties existed. The drill may have wandered, leaving the holes not perfectly straight. Also the thermocouple tip might not be soldered to the very bottom of the hole. Therefore, at the close of all the experiments, these two questions were checked by cutting out the thermocouple sections and taking x-ray pictures of them. The metal on the side, free of a thermocouple, was removed so that only a 1/32 inch of metal separated the plane of the thermocouple tips from the x-ray paper. The x-rays reveal that the holes are perfectly straight and that in every case the tip is at the very

bottom of each hole. The thermocouple locations were also measured from the x-ray negatives and are now known to the nearest 1/64 inch or $\pm$ 0.007 inches.

The bottom-most thermocouple is, on the average, 19 mils from the inside surface, the middle one is 210 mils above the first, and the top thermocouple is 219 mils above the second, or 60 mils from the outside surface.

Windows and Pressure Taps

Two ports, 5/8 inch in diameter, are located diametrically opposite each other at each of the three levels, 4, 10, 15 inch. The windows, which sealed each port in conjunction with a teflon gasket, are 1/8-inch thick vycor discs, 1 inch in diameter. They were originally designed to sit almost flush with the inside surface of the burner; however, difficulty was encountered in keeping the windows perfectly free and clean of the sodium bicarbonate dust. This problem was solved when the gasket assembly was modified to hold the windows about 3/4 inch from the inside chamber wall.

The pressure taps are 1/16-inch holes placed at six positions, 2, 4, 10, 13, 15, and 25-inch levels, along the remaining free quarter of the burner, i.e., directly opposite the thermocouple sections. The inside edge of each hole is rounded off smoothly. The pressure taps are connected with 3/16-inch copper tubing through a manifold of valves to either of three manometers for a wide range of measurements.

All three manometers are made by Meriam. The smallest is an inclined draft gauge indicating 0-0.5 inches of water, the intermediate

one is an inclined well-type manometer, indicating 0-10 inches of water, and the largest is a vertical U-tube manometer, indicating as much as 30 inches of water, differential pressure.

Flameholders

The flameholders employed in this study are all of the bluff-body type and are water cooled by means of a 3/16-inch copper tube coiled into three or four loops and silver soldered to the backside of the flameholder. The flameholder is a flat metal disc held firmly and precisely in the center of the stream by a 5/8-inch steel tube soldered to the center of the upstream side of the flameholder. This tube contains the leads to the copper-cooling coil and passes through two centering plates or spokes. One centering support is located between the flanges that join the combustion tube with the mixing chamber, i.e., at the 27-inch level. The other, a three-pronged centering wheel, is about 18 inches higher and fits snugly in the mixing chamber walls.

Several flameholders were used in the course of the experiment, but they all have a high blockage, being 90 per cent or more of the tube cross-section. Except for some slight differences in diameter within each group, the flameholders may be categorized in three groups according to variations of the basic geometry. These groups are 1) the plain 1/8-inch thick disc type, 2) the type with a 10-mesh screen placed in the annulus between the edge of the metal disc of the flameholder and the tube wall, and 3) the type with an effectively much thicker disc. The latter type includes one flameholder, the S-2, which was made thicker than the others by soldering a 1-1/4 inch wide ring of 1/16-inch thick

copper sheet to the back of the flameholder. The diameter of the copper ring is within 1/32 inch of the diameter of the flameholder disc. The 10-mesh screen used for the annulus of the flameholder has 0.047-inch-diameter, stainless steel wire. The flameholders are tabulated in Appendix A.

Sodium Injection Through Flameholder

In conjunction with the sodium-line-reversal system of measuring the flame temperature, a sodium salt is injected into the flame. The sodium salt, sodium bicarbonate powder, is introduced into the flame through a small hole in the center of the face of the flameholder. A small fraction of the air stream is used to entrain some of the sodium bicarbonate powder as this air blows across a vessel of the power. The air with entrained sodium bicarbonate travels down a 1/8-inch copper tube that is contained within the 5/8-inch supporting and centering tube, and enters the burner through a 1/32-inch diameter hole in the center of the flameholder. The rate of sodium salt injection is easily controlled by a valve in the small 1/4-inch air line through the duster.

Cooling Water and Spray Quench

The water jacket, surrounding the whole 27-inch length of the combustion chamber, was formed with a 16-gauge sheet of stainless steel. Two one-inch pipes diametrically opposed lead the water into the 1/4-inch annulus formed by the water jacket and provide more even cooling than one inlet pipe would. The vertical arrangement of the chamber has also provided a more even cooling by the water, since there is no tendency

for gas present in the water to accumulate anywhere and since the effect of density changes occurring in the water are symmetrical about the tube axis.

The spray quench, that could be placed over the exhaust end of the burner, is more correctly called a muzzle than a nozzle since its diameter is essentially the same as that of the main tube. This muzzle consists of an extra-heavy 5-inch pipe, 2-3/4 inches long, which has two circular rows of twelve 1/8-inch holes through its wall which allow the water from its own water jacket to quench the flame. A 10-mesh stainless steel screen of 0.047 diameter wire may also be placed in the muzzle below the water jets. A flange welded to the end of the burner serves to join the muzzle to the burner.

Mixing Chamber

The mixing chamber, which is also 27 inches long, was constructed from extra-heavy 5-inch pipe that was honed on the inside to give an even and smooth surface of 4.860 inches in diameter. A bourdon pressure gauge, 0-30 psi, and an iron-constantan, 24-gauge, thermocouple are located 4 inches above the flange-junction of the mixing and combustion chambers. A 4-inch diameter blowout or safety disc is located 21 inches above the flange junction. This blowout disc is a sheet of 0.006-inch brass shim stock, held between two 4-inch flanges. Its purpose is to relieve the pressure caused by a flashback; however, a better pressure release is provided by the failure of the 18-gauge copper wire that supported the flameholder and its centering rod.

The propane and air streams converge at a 1-inch cross and flow through a 6-inch length of 1-1/2 inch pipe packed with 1/4-inch ceramic balls. To the upper fitting of the cross is attached a 150 psi safety disc. A short length of connecting assembly, consisting of a 5-inch cap and a 1-1/2 inch flange, brings the gases into the top of the mixing chamber. The flow is broken up further by the steel piece, resting on the top of the 5-inch pipe of the mixing chamber, that supports the flameholder and the sonic piston. The 5-inch cap is fitted with four 1-inch couplings, so that the quarter-wave tubes can be attached here.

Sonic Orifice

Provision for three possible locations of a sonic plate or orifice has been made in order to isolate the air and propane streams from the oscillations generated in the burner. One location is the 1-1/2 inch flange just above the mixing chamber; another is between the 5-inch flange, connecting the combustion and mixing chambers; and the third sonic plate, being in the form of a piston, may be placed anywhere in the mixing chamber or in the combustion chamber above the flameholder.

The sonic plates have an even distribution of 70 to 75 , 1/16-inch diameter holes through which the flow of gas is maintained at sonic velocity. The 1/8-inch plate used between the 5-inch flanges has 75 of these holes besides the 5/8-inch center hole for the flameholder supporting rod. The sonic piston has 70 of these holes, is 1/2-inch thick, is supported by three 3/8-inch rods, and is sealed with the chamber walls by means of an O-ring.

Sodium - Line - Reversal System

The sodium - line - reversal system, denoted hereafter as SLR, which is employed to measure flame temperatures, involves a tungsten ribbon lamp, whose brightness temperature is calibrated as a function of electrical direct current, two lenses of equal size and focal length, a high quality spectrometer, a controlled and steady source of d.c. current, and a high quality d.c. ammeter. A schematic diagram of the SLR system is given in Figure 7.

The lamp is a 6 volt, 18 amp., tungsten-ribbon lamp, type T10, made by General Electric. The lenses have a 4-5/8 focal length, a 3-inch diameter, and are coated. The spectrometer is the Bausch and Lomb wave-length, laboratory spectrometer. The ammeter is a GE DP-11 with a dual range of 0-10 and 0-20 amp. The ammeter was purchased new for this project and had an accuracy of 1/2 of one per cent of full scale.

The brightness temperature of the lamp was calibrated by General Electric's Nela Park division with a vycor disc between the lamp and their pyrometer at five temperatures from 1500°F to 3500°F with respect to direct current. The accuracy of calibration is claimed to be $\pm$ 8°K and any aging of the lamp is claimed to be less than 1 per cent through the first forty hours of burning at full-rated current. The lamp used in the experiment is estimated to have been burned a total of about thirty hours at 70 per cent of rated current.

The mounting of the lamp, lenses, and spectroscope was done very carefully to achieve perfect alignment and focusing. The focal length of the lenses was checked before mounting and found to be 4-5/8 $\pm$ 1/64 inches. The lenses are mounted by means of lens holders and

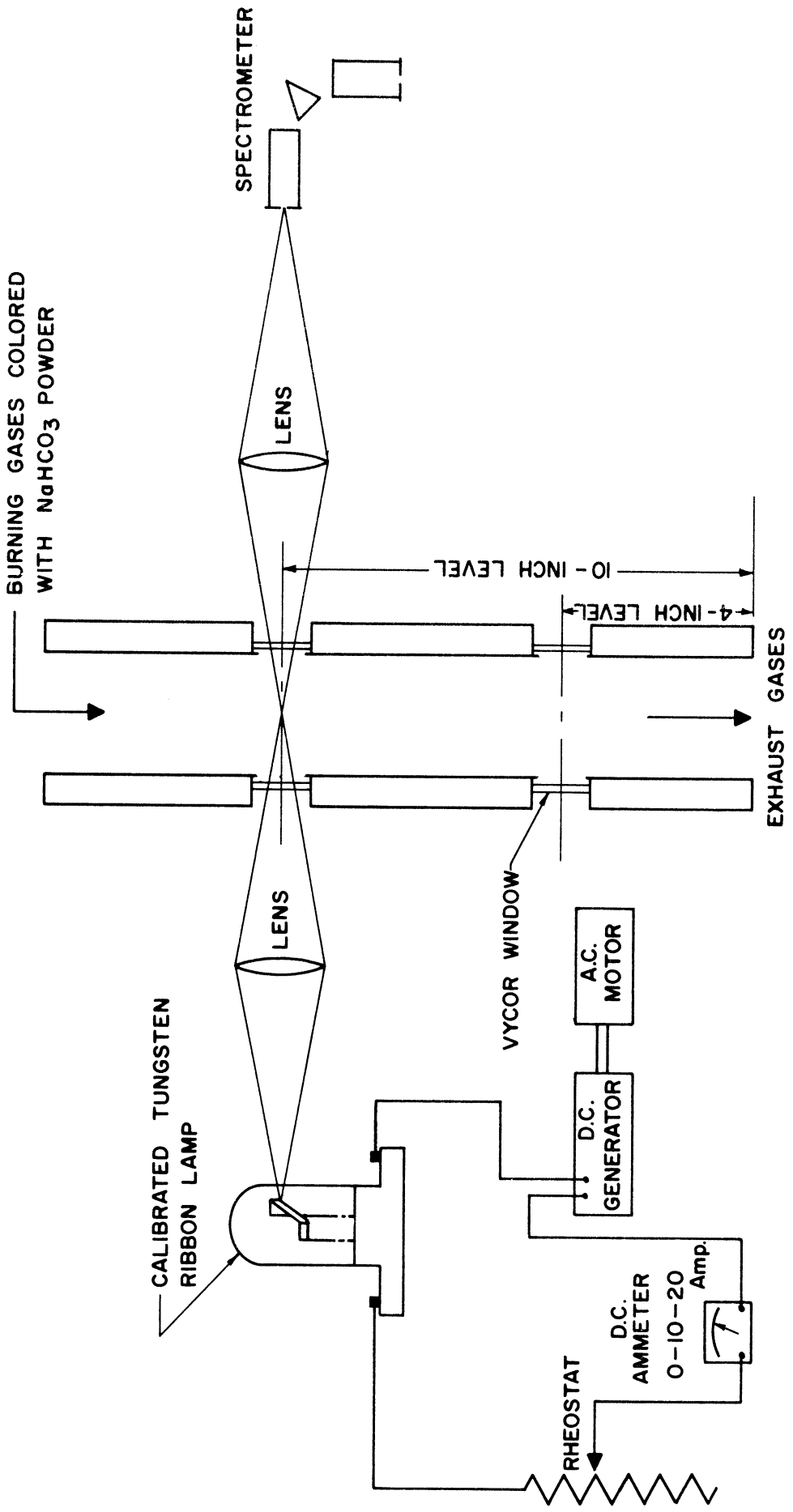

Figure 7. Schematic Diagram of Sodium - Line - Reversal System.

precisely placed slots on the basic framework surrounding the burner. The distance between lenses is 18-1/2 ± 1/32 inches, with the burner in the middle. The lamp and spectroscope are mounted so that the filament and spectroscopic slit are each 9-1/2 ± 1/32 inches from their respective lens.

Since measurements are to be taken at the 10-inch level as well as the 4-inch one, the four items in the optical line are mounted by means of tongues and slots at each level, so that they can be quickly lifted from one level to the other and slipped into position. In the case of the lens mounts, it was found prudent to attach leveling bulbs on the lens holders, so that it can be noted at a glance whether or not the lens holder has been completely and snugly slipped into its slot.

A direct current supply system was assembled that can be controlled to within 0.05 amp. from 6 amp. to 16 amp. and which gives a steady current. A 12-volt Autolite d.c. generator is driven at about 2100 r.p.m. by a 1/2 hp. electric motor. Two, 1-ohm 100-watt, and one 1-ohm 500-watt rheostats plus a 2-ohm 100-watt resistor are employed to control the current. An optical pyrometer by Leeds and Northrup of the disappearing filament type is an important part of the SLR equipment, serving to test the light scatter from the lens and window.

Extension Leads and Miscellaneous Thermocouples

The thermocouple assemblies embedded in the tube are connected by 16-gauge twisted thermocouple extension wire of chromel and alumel. Before the extension wires were silver soldered to the delicate 36-gauge wires, the weight of the extension leads was supported by means of tape.

The junctions are covered with Duco cement for support and thermal insulation as well as with fiberglass. The extension wires lead to a 24-couple switch box. A Leeds and Northrup portable, precision potentiometer, model #8662, is used to measure the e.m.f. between an ice bath and any of the thermocouples embedded in the tube or in the various streams. The potentiometer's standard cell was checked at the beginning and end of the experiments with a standard cell that had recently been calibrated by the National Bureau of Standards. No change was found in the potential of this project's standard cell. The potentiometer rests on two inches of foam rubber to insulate it from mechanical vibrations within the room and building.

All the iron-constantan thermocouples were checked in boiling water while the thermocouples embedded in the tube were checked at two temperatures. The burner was filled with fiberglass to prevent any heat transfer through the tube walls, so that all three thermocouples in each section would read the same. With cooling water circulating at a high rate, there was little temperature rise from inlet to outlet, about 0.1°F, and this was corrected by a linear interpolation. Thus readings were made at cooling water temperature, about 52°F, and at room temperature, about 75°F. Two of the embedded thermocouples were in error, but the remaining 13 all read the same. Of these two, one failed to function later in the project and the other never read correctly. One is in the 10-inch level section and the other in the 17-inch level.

Temperatures of all the various liquid and gas streams are measured with iron-constantan, 24-gauge thermocouples. Specifically,

they are located in the inlet and outlet water streams of the water jacket, the inlet and outlet streams to the flameholder's cooling coil, and in the propane and air stream just downstream from each rotameter. In the water streams the thermocouples are placed in wells, protruding at least three inches into the stream. Oil is placed in the well with the thermocouple. The well in the exit water jacket stream has six brass 14-mesh screens soldered along its length, and it protrudes seven inches into the stream. The pipes between the jacket and the thermocouple wells are insulated with fiberglass. The thermocouples in the gas streams are bare and are sealed with Conax thermocouple glands at their entrance into a stream.

Measurement of Sound in Chamber

The rigid, high intensity Massa microphone, model 141-B, which is located flush with the inside chamber wall at the 22-inch level is a crystal type microphone, completely enclosed in a stainless steel cover with a metallic diaphragm. It is suitable for use with the General Radio sound level meter, Type 1551-A, extending the range of the meter to 190 db. The General Radio sound analyzer, Type 760-B, is employed to measure the frequencies of an oscillation and to give the relative amplitude of different notes, if more than one is present. An Ampex 601 tape recorder was used to record the sound for a few conditions.

The microphone, sound level meter, and Ampex 601 tape recorder have flat frequency responses from 25 cps to (at least) 10,000 cps $\pm$ 2db. The range of the sound analyzer is 25 cps to 7500 cps $\pm$ 2 db, with a frequency accuracy of 1-1/2 per cent and a band width of 2 per cent.

Propane System

The propane was purchased from a commercial distributor and was analyzed twice on the mass spectrometer during this project and at least once on a previous project. The combined analyses indicate a composition of 98 per cent propane and 2 per cent propylene with a maximum variation of 1 per cent. The propane is stored outdoors in a four hundred pound tank, which is equipped with three 0.750 kw. immersion heaters, each with a 100 square inch area. These heaters provide the heat of vaporization when gaseous propane is withdrawn and are regulated with individual 110 volt variacs. A flash vessel approximately 9 inches in diameter and 15 inches tall is located in the propane line between the tank and metering panel to prevent any liquid propane from being entrained in the line from the storage tank.

A Moore nullmatic pressure regulator, model 42H, 0-100 psi, is upstream from the rotameter in the 1/4-inch pipe line to keep the propane at a constant pressure for accurate and steady metering. The rotameter which was calibrated by Fischer and Porter, the manufacturers, has a capacity of 10.6 SCFM of propane metered at 70°F and 50 psia.

Air Supply and Test Cell

The air is supplied by a 40 hp. compressor at 95 psig at a maximum rate of about 130 SCFM. The compressed air goes through a bed, approximately a 15-inch cubical, which is filled mostly with glass wool plus some 1/4-inch ceramic balls. This bed removes the oil drops entrained in the air from the compressor. The piping for the air line is 1-inch pipe. The air pressure is regulated upstream from the air rotameter by another Moore

nullmatic pressure regulator, type 42H, 0-100 psi. The air rotameter, which was calibrated by the manufacturers, Fischer and Porter, has a capacity of 152 SCFM of air metered at 50 psia and 70°F. A 1.5 kw electric heater is located in the air line downstream of the rotameter.

The apparatus section would not be complete without mentioning the cell or room in which the project was carried out. The room is an engine test cell in the University's Automotive Laboratory and is equipped with a high-capacity vacuum exhaust and ventilating system. Also the one-foot, poured concrete walls and double, explosion-proof doors enabled this extremely noisy project to be carried out with a minimum of disturbance to the others in the building.

EXPERIMENTAL THEORY AND ACCURACY

Several theories are involved in converting the measured data into meaningful and useful quantities. The thermocouple readings must be converted into heat transfer rates; the pressure drop measurements must be converted into combustion efficiencies; the SLR (sodium-line-reversal) measurements must be converted to average gas temperatures; and the mode of oscillation must be interpreted from the frequency measurements. The special theories or equations needed to process the data are presented in this section and the accuracies of the measurements are discussed. Derivations are presented in Appendix C, if they are special and not readily accessible in the literature.

Evaluation and Accuracy of Local Heat Fluxes

The appropriate heat transfer equation is readily deduced from the general equation for conduction through an isotropic solid,

$$\rho\, C_p \frac{\partial T}{\partial t} = \text{div}(k \text{ grad } T) \qquad (4)$$

In the case of the isolated thermocouple sections, several terms are zero, thus

$$\frac{\partial T}{\partial t} = \frac{\partial T}{\partial \theta} = \frac{\partial T}{\partial x} = 0 \qquad (5)$$

These simplifications are valid, because the data are taken under steady-state conditions, and because the insulated longitudinal and chordal slots prevent the flow of heat in those directions. The thermal conductivity of the tube may be assumed to have a constant, average value. This assumption is validated by Churchill[12] for a similar case but where the thermal

conductivity of the test object is even more dependent on temperature than is Croloy. He showed that the heat transfer rate calculated with the assumption of a constant average thermal conductivity differed negligibly from the result obtained by a more involved and rigorous procedure.

Therefore, the radial flux at the inside surface of the tube is given by

$$Q/A_s = \frac{k_{av}}{r_s} \frac{T_i - T_j}{\ell n\, r_j/r_i} \tag{6}$$

where $i \neq j$. In three of the five thermocouple sections, three temperatures are measured, giving two independent temperature gradients, and thus a check is made.

An overall check of the heat transferred through the tube walls is made, using the heat absorbed by the cooling water from the tube to check the integration of the locally measured heat transfer rates.

$$Q = W\, C_{p_w}\, \Delta T_w = \int_0^{A_T} (Q/A_s)\, dA_s \tag{7}$$

where ΔT_w is the net increase in water temperature due to heat transfer through the internal wall alone.

The presence of the thermocouples distorts the heat flux through the cylinder wall. By a conformal mapping technique an estimation of the error introduced is made, assuming the extreme case that the thermocouple holes are perfect insulators and that they lie perpendicular to the temperature gradients, i.e., parallel to the tube wall. This analysis, which is presented in Appendix C, indicates a maximum error of 3 per cent due to the distortion of the heat flux by the thermocouples.

The other simplified case to analyze is that of the thermocouple holes being vertical to the tube wall but still perfect insulators. Beck and Hurwicz[6] have analyzed this case and present their results in dimensionless distances and heat fluxes, so that the error is easily evaluated and is 4 per cent. The actual error in the heat flux caused by the presence of the thermocouples is thus no greater than 4 per cent.

The only remaining sources of error in the heat transfer measurements are the uncertainty of 7 mils in thermocouple location and an uncertainty of 3 microvolts in the e.m.f. measurement. The location uncertainty represents a possible error of 2.8 per cent, and the e.m.f. inaccuracy represents an error of 1/3°F in the temperature gradient or less than a 1/2 per cent error for heat fluxes over 10,000 Btu/hr.ft.

Accuracy of SLR Method

The principle of the sodium-line-reversal, SLR, method of flame temperature measurement is based on Kirchhoff's radiation law. At the matching condition, the following relation is fulfilled.

$$E_L = E_F + (1 - \alpha_F) E_L \qquad (8)$$

A detailed explanation of the SLR method is given by Reference (41).

The specifications of all the items in the SLR system are given in the Apparatus Section, and the calibration curve for the lamp is placed in Appendix D. The calibration of the lamp's brightness temperature versus its current is claimed to be accurate to $\pm$ 15°F by General Electric. The ammeter, having an accuracy of 1/2 of 1 per cent of full scale, is the source of a possible 5°F error in the range of use in this study.

Light scattering or absorption by the lens or window between the flame and spectroscope is of no consequence because the intensity of the lamp and flame would be reduced equally and the comparison is not altered. Since the lamp's calibration included the effect of the lamp-side window, the only uncertainty is the effect of the lamp-side lens. This error was evaluated with an optical pyrometer of the disappearing filament type and was found to cause a lowering of the apparent lamp temperature of no more than 20°F.

Any error due to inexact focusing of the lamp and the flame images on the spectrometer slit is held to a minimum. After the lamp, lenses, and spectrometer were mounted at the proper distances $\pm$ 1/32 inch, a check was made of the filament's image at the spectrometer slit and found to be in focus and exactly the same size as the filament.

The accuracy of the SLR measurement is reduced by one peculiarity of a flame, particularly in a large combustion chamber. Although all of the burner conditions were steady, including heat transfer rates, sound level, flow rates, and wall temperatures, there was a constant flickering of the flame temperature about a constant average value. However, an increase in lamp temperature of 30°F to 50°F would always produce steady dark D-lines, and a similar decrease in lamp temperature would always produce steady light D-lines. A safe estimate of this source of error is $\pm$ 50°F. The intense flame-generated oscillations did not cause any visible flickering of the D-lines, because their effects were averaged out in a shorter time than is visually perceptible.

Another possible source of error arises from the presence of radial temperature gradients in the flame. The radiation from the hot

central core of burned gases will be dominant in determining the SLR matching temperature, but the boundary layer of cooler gas will have some influence depending upon its thickness, temperature, and sodium vapor concentration. In Reference (41) the equations are derived and an example problem carried out for a similar evaluation of the effect of temperature gradients.

Three assumptions are made: 1) the temperature distribution corresponds to that of fully developed turbulent flow at the Reynolds number of the hot gases, 2) the sodium vapor concentration is even throughout the flame, and 3) the flame can be considered as two regions, a central core and a boundary layer, for this analysis. The first assumption is discussed later and evidence of its validity 13-1/2 inches from the flameholder is given then. The analysis, which is based on the emissivities of the two regions being proportional to their thickness, indicates the SLR reading is less than the central core temperature by 30°F to 50°F, depending on the temperature level. The higher temperature levels have the higher deviations. Because this analysis only places a limit on the effect of the boundary layer and does not prescribe a precise correction factor, no correction was made to the SLR readings and they are taken to represent the core temperature.

When all of these possible errors in the SLR measurement are combined, the limits for the uncertainty in the SLR core temperature are found to be -50°F to +90°F. Although these limits are wide, when it is considered how large the corrections and uncertainties are for thermocouple measurements of flame temperatures ranging up to 3300°F, and how non-ideal are conditions in the flame, then the relatively high accuracy of the SLR method may be appreciated.

Bulk Mean Gas Temperature

The bulk mean temperature of the gases is desired for the evaluation of combustion efficiencies and for the calculation of heat transfer coefficients. The feasibility of assuming that the velocity and temperature distributions could be represented by fully developed turbulent flow at the 4-inch level, or 13-1/2 inches from the flameholder, was investigated. Thermocouple and pitot-static tube traverses of the flame at the 4-inch level were taken at a low fuel-to-air ratio. The conduction and radiation corrections for the 16-gauge bare chromel-alumel thermocouple were made using the methods and charts of Scadron and Warshawsky.(68) The velocity and temperature distributions were flat, not falling off until within 1/4 inch of the wall, and so did not contradict the distributions for a fully developed turbulent flow.

The bulk mean temperature obtained for such a flow by a graphical integration is given by the relation

$$T_b = 0.82\ (T_{SLR} - T_s) + T_s \qquad (9)$$

Uncertainties in the interaction of the combustion and the flameholder on the flow pattern and temperature distribution are admittedly large; however, verification of the mean bulk temperature determined in this manner from the SLR flame temperature is given by the combustion efficiencies found independently through pressure-drop measurements. The combustion efficiencies determined by these two methods agree within 6 per cent for all of the stable combustion runs and the average of the two methods agrees within 2 per cent.

Justification of Microphone Position

In the chamber volume between the flameholder and sonic plate, the sound is believed to be uniformly distributed and of a random nature rather than of a resonating nature. Theory supports this belief. None of the frequencies generated in the combustion chamber correspond to possible primary or first harmonic resonant modes in this space where the microphone is located. The location of the microphone within this volume would have been critical if resonance existed; however, minor changes of an inch in the flameholder position around the 17-1/2 inch level as well as a major shift to the 13-1/2 inch level produced no irregularities in the measured sound intensities. Further verification of the lack of resonance is indicated by the fact that upstream changes, such as moving the sonic plate, had little if any effect on the intensity or frequency of the generated sound.

The accuracy of the sonic measuring equipment is presented in the Apparatus Section. A simple check was made with the Massa microphone by comparing its reading with the reading of the General Radio microphone which came with the sound level meter. The two microphones were placed next to each other for this test. Application of the correction factor determined by the relative impedances of the two microphones brought the two readings to within 2 db of each other for sound levels of 100 to 130 db.

Combustion Efficiency from Pressure Measurement

The combustion efficiency is determined independently by the SLR measurements and by pressure-drop measurements. The evaluation of

the bulk mean temperature from SLR measurements is discussed earlier in this section. The combustion efficiency is readily found, once the temperature of the gases is known, by use of Equation (14) below. An outline of the method and theory used to evaluate combustion efficiency from pressure-drop measurements is presented below.

For a thin discontinuity in flow, the general mass, momentum, and energy relations can be reduced to the following approximate one-dimensional equations.

$$\text{Mass:} \qquad \rho_1 u_1 A_1 = \rho_2 u_2 A_2 \tag{10}$$

$$\text{Momentum:} \quad \left(P_1 + \frac{\rho_1 u_1^2}{g_c}\right) A_1 = \left(P_2 + \frac{\rho_2 u_2^2}{g_c}\right) A_2 + F_D \tag{11}$$

$$\text{Energy:} \quad \overline{C_{p_1}} (T_1 - T_o) + \frac{u_1^2}{2g_c} + Q_r^{(T_o)} - Q_t = \overline{C_{p_2}} (T_2 - T_o) + \frac{u_2^2}{2g_c} \tag{12}$$

If no steep gradients exist at stations 1 or 2, the equations can be applied to a deflagration with negligible error.

The use of the ideal gas law and several simplifying assumptions leads to the following equations from which the flame temperature and then the combustion efficiency are calculated.

$$\frac{T_2}{T_1} = \frac{P_2}{P_1} \frac{\overline{M_2}}{\overline{M_1}} \frac{A_2}{A_1} \frac{g_c}{\rho_1 u_1^2} \left[P_1 - P_2 \frac{A_2}{A_1} - P_D + \frac{\rho_1 u_1^2}{g_c}\right] \tag{13}$$

$$E = \frac{Q_r^{(T_1)}}{Q_R^{(T_1)}} \times 100 = \frac{\overline{C_{p_2}}(T_2 - T_1) + Q_t}{Q_R^{(T_1)}} \times 100 \tag{14}$$

The derivation of these equations is presented in Appendix C. Subscripts 1 and 2 refer to conditions at the inlet and at the outlet, respectively, i.e., the 25-inch and 2-inch levels. The reference temperature is that of the inlet, i.e., $T_o = T_1$. $Q_R^{(T_1)}$ is the possible chemical heat release at T_1 for total combustion of the limiting reactant. All the inlet conditions are known as well as A_2. Integration of the local heat fluxes plus the heat absorbed by the flameholder yields Q_t, the total heat lost by the flame. The drag of the flameholder and walls, P_D, is estimated from cold flow data and from the calculated temperature profiles of the flame. The drag of the flameholder is assumed equal to its cold flow drag at the same inlet Reynolds number. The drag of the walls, which is a minor part of the total drag, is evaluated using the calculated temperature profile of the flame, an estimated exit composition, the ideal gas law, and the friction factor for smooth pipe and for the local Reynolds number. The estimated composition is revised if the calculated combustion efficiency disagrees with that assumed in the estimation of the composition. The calculations would then be repeated. Since the average molecular weight, $\overline{M}_2$, and the mean heat capacity from T_1 to T_2, $\overline{C}_{p_2}$, are first estimated on the basis of approximate values for T_2 and E, revisions of these estimates may also be necessary before the final T_2 and E are calculated.

Prediction of Resonant Frequencies

The wave equation in cylindrical coordinates is

$$a^2 \left[P_{rr} + \frac{1}{r} P_r + \frac{P_{\theta\theta}}{r^2}\right] + a^2 P_{xx} = P_{tt} \qquad (15)$$

The appropriate boundary conditions are

1. P is finite at all times
2. P is cyclic in θ
3. $P = 0$ at $\theta = \pi/2$
4. $dP/dt = 0$ at $t = 0$
5. P is finite at all positions
6. $dP/dr = 0$ at $r = R$
7. $dP/dx = 0$ at $x = 0$ (flameholder)
8. $P = 0$ at $x = L_e$ (open end)

The solution is readily obtained by the method of separation of variables and differs only slightly from the case presented by Morse[56] of a cylinder closed at both ends, instead of just at the one end, $x = 0$, in this study.

$$P = C \cos m\theta \cos \frac{(n_x + 1/2)}{L} \pi x \; J_m\left(\frac{\alpha_{mn}\, \pi}{R} r\right) e^{2i\pi ft} \tag{16}$$

where

$$n, n_x, m = 1, 2, 3, \ldots$$

are the wave numbers. Values of α_{mn}, which satisfy the requirement that $dJ_m/dr = 0$ at $r = R$ are given by Morse. The frequency, f, is given by the relation

$$f_{m,n,n_x} = \frac{a}{2} \sqrt{\left(\frac{n_x + 1/2}{L_e}\right)^2 + \left(\frac{\alpha_{mn}}{R}\right)^2} \tag{3}$$

The significance of the various wave numbers is given in the Literature Survey.

Theory of Acoustical Damping

The theory of the quarter-wave tube as a damping influence on longitudinal waves is simple. When the tube is placed at a pressure antinode, a pressure condensation will travel along the tube and be reflected as a condensation from the end of the quarter-wave tube and return to the main tube out of phase with the oscillation there. Thus damping is accomplished.

The theory of the spray muzzle as a damping influence on longitudinal oscillations is also readily explained. The spray quench when placed at a velocity antinode hinders the particle movement of the wave due to the large inertia of the water particles.

Accuracy of Flow Measurements

The propane, air, and water rotameters were calibrated by the manufacturer accurately to within 1 per cent of full scale reading. The propane and air rotameters were spot checked with a wet test meter and readings that agreed within 1 or 2 per cent were obtained. The water rotameters were checked with a bucket and a set of scales.

EXPERIMENTAL PROCEDURE

A typical run starts after the behavior of the combustion process has been investigated and the desired conditions for the run decided upon. The flameholder is positioned at the desired burning length and carefully centered in the combustion tube before ignition of the flame. After the air flow is set at a moderately high rate and the water streams to the chamber jacket and the flameholder are flowing, then the propane is turned on and slowly increased in rate as the spark plug is continuously being fired. Ignition of the propane and air is thus accomplished at as lean a mixture as possible.

If the spray-quench muzzle is attached to the end of the burner, the water spray is turned on immediately after ignition. The flow rates are now adjusted to the conditions for the run. Steady state, which is usually reached within five minutes, is checked by taking several readings of key thermocouples over several minutes' time.

Steady-State Measurements

After steady state is reached, the following data are read: pressure drop from the 25-inch level to the 2-inch level, flow rates of air, propane, flameholder-water, burner-water, thermocouple readings of the air, propane, and the combined gas streams, as well as of the inlet and outlet water streams to both the burner and flameholder, and the sound pressure level and frequencies. If any of the readings at the beginning and end disagree, the run is repeated. A complete set of readings of the thirteen operable embedded thermocouples is taken about midway through a run with over half of them being read twice to check the equilibrium.

Next the sodium-line-reversal measurements are made. The sodium bicarbonate duster is turned on immediately after all of the embedded thermocouples have been read, but the lamp is turned on about five minutes early to allow it to warm up. If any steam is condensing on the lenses, air jets are played on both sides of each lens while the SLR measurements are made. Two sodium-line-reversal measurements at one level in the burner are taken a few minutes apart to be certain that the lamp is at equilibrium at the flame temperature. Readings are taken at the 4-inch level for all runs and at both the 4-inch and 10-inch levels when the burning length is 17-1/2 inches or more. The sodium bicarbonate is dusted into the flame only during the SLR measurements, unless otherwise noted for a particular run.

The sound level is measured with the Massa microphone in the burner, and the frequency spectrum is scanned during every run with the sound analyzer. For a few runs the sound level outside of the burner is also measured. The Massa microphone is connected to the tape recorder for a few recordings of transverse and organ-pipe oscillations in the burner.

The heaters in the propane tank are adjusted at the beginning of a run to maintain the propane pressure at a fairly constant level. When the outdoor temperature is above 40°F, the heaters are adequate to maintain the propane pressure even at high propane rates, but when the outdoor temperature drops much below 30°F, adequate propane rates are not possible.

Cold Flow Measurements

For each series of runs cold flow measurements, i.e., measurements without combustion, are taken of pressure drops and of the heat transfer coefficients. The cold flow drag of the flameholder and tube walls is measured for air flowing at the same inlet Reynolds number as that of the run. Heat transfer rates and coefficients are evaluated at the average Reynolds number of the burned gases using air heated to about 170°F and two thermocouples at the 4-inch level to measure air temperatures. Integration of the local heat transfer rates along with an energy balance determines the air temperature at the other stations.

Since it is not feasible to insulate the burner's water jacket, some heat is transferred to the water stream from the room. A correction for this is evaluated by measuring the temperature rise of the water when there is no gas flow in the burner.

Control of the Flame-Generated Oscillations

The various flame-generated oscillations are studied and controlled by the use of different flameholders and by the use of different conditions at the end of the burner.

The flameholders with a free annulus are suitable for studying flame-generated longitudinal oscillations. The attenuation of this longitudinal oscillation can be varied considerably. The spray-quench muzzle with a screen placed below the spray damps out the organ-pipe completely, while without this screen a fairly intense longitudinal oscillation is possible, and without the muzzle the attenuation at the end of the burner is a minimum. The blockage of the flameholder also offers control over

the sound intensity because an increase in blockage increases the intensity of the longitudinal oscillations due to improved reflection of the oscillation at the flameholder.

The flameholders with the screen in the annulus are suitable for the study of a transverse mode of oscillation. The screen stabilizes the flame closer to the tube walls and thus brings a greater release of energy into the region where the pressure amplitude of the transverse wave is greatest and where the energy is most beneficially applied to drive this oscillation. The transverse mode is kept free from a separate organ-pipe oscillation by using the spray muzzle with its screen to damp the latter mode. The transverse oscillation may be damped out by making the annulus of the flameholder long and thus causing the unburned gases to jet through the annulus and sweep the area near the tube wall free from any active combustion.

Corrosion of the Burner

The burner walls and windows were regularly inspected and cleaned if necessary. No corrosion nor tarnishing of the inside tube wall occurred throughout the experiments. At the end of the project, the outer wall of the main tube, i.e., the cooling-water side, was found to be clean and about 95 per cent rust free.

EXPERIMENTAL RESULTS

The results of the heat transfer studies on propane-air flames are presented in graphical form. The main emphasis has been to study the effect of the dependent variable, sound level, on the local rates of heat transfer and on the local convective coefficients. The effect of process variables such as fuel-to-air ratio and Reynolds number are not of primary interest. In fact, the main interest in the process variables and in the geometry of the burner rests on their effect upon the flame-generated oscillations.

Range of Process Variables

The range of Reynolds numbers to be studied, 35,000 to 47,000, is limited because a large burner was required as determined by preliminary experiments to generate screeching combustion, i.e., transverse oscillations. The safe minimum flow rates to prevent flashbacks are approximately 25 per cent less than the maximum capacity of the air supply system. The study is limited to lean fuel-air mixtures not only because of limitations on the propane supply but also because this is the region of most practical interest and because the burning tends to become rough in rich fuel-air mixtures, particularly in a large burner. The burning lengths are also dictated by sonic considerations.

Form for Data Presentation

The effects of flame-generated oscillations and other variables such as burning length, Reynolds number, and fuel-to-air ratio on the profile of local rates of heat transfer along the tube are presented in

graphical comparisons. Temperature profiles are presented in a similar manner for a few runs. Coefficients for convective heat transfer are also presented along with a correlation for the coefficients as a function of sound level. At the end of this section, some heat transfer profiles for a quiet burner plus some miscellaneous curves are included.

For the profiles of both local heat flux and gas temperatures, the data are plotted as 1-inch wide lines rather than as points since the heat fluxes represent average values over the 1-inch long thermocouple sections. The calculation of the heat flux has been discussed, and the details of the calculations are in Appendix B. The flame temperature is measured at the 4-inch level for all runs and in addition at the 10-inch level for the runs with a 17-1/2-inch burning length. Therefore, to evaluate the gas temperatures closer to the flameholder and thus to obtain a temperature profile of the flame along the entire burner, the following procedure is employed. The heat transfer coefficient at the 4-inch level, h_4, determined by the measurement of the flame temperature is used to evaluate a multiplier, h_4/h'_4, by which the cold flow coefficients at the other four stations, h'_x, are multiplied.

$$h_x = \left(\frac{h_4}{h'_4}\right) h'_x \qquad (17)$$

The resulting coefficients, h_x, are then used in conjunction with the local heat fluxes and radiation corrections to calculate the flame temperatures closer to the flameholder.

A tabulation of the flameholders, denoted f.h. in the figures, is given in Appendix A. The complete listing of the data for all the runs is also in Appendix A.

Effects of Transverse Oscillations on Heat Transfer Profiles

The effect of a strong transverse oscillation on the local rates of heat transfer is depicted in Figures 8 and 9 at two different Reynolds numbers. The lower curve in each figure is the profile for the case where the screech has been damped by the long annulus flameholder, S-2. The sound level of 130 to 133 db is that of stable combustion or of a "quiet" burner, i.e., a burner in which no one frequency predominates nor is resonant. The sound level recorded for cold flow is around 124 db. This comparison is not entirely of screeching versus non-screeching combustion because the flameholders are different. However, the effect of the flameholders can be evaluated under non-oscillating or stable conditions, which is the case in Figure 10. Here the S-1 flameholder is seen to produce a 20 per cent higher peak and a 8 per cent greater amount of total heat transfer. A similar comparison with similar results can be made with Runs 14 and 50.

Intense screeching combustion, 151 to 154 db, thus causes a net increase in the peak of the heat transfer profile of 30 per cent and a net increase in total heat transferred to the tube of about 50 per cent instead of gross increases of 50 and 60 per cent, respectively.

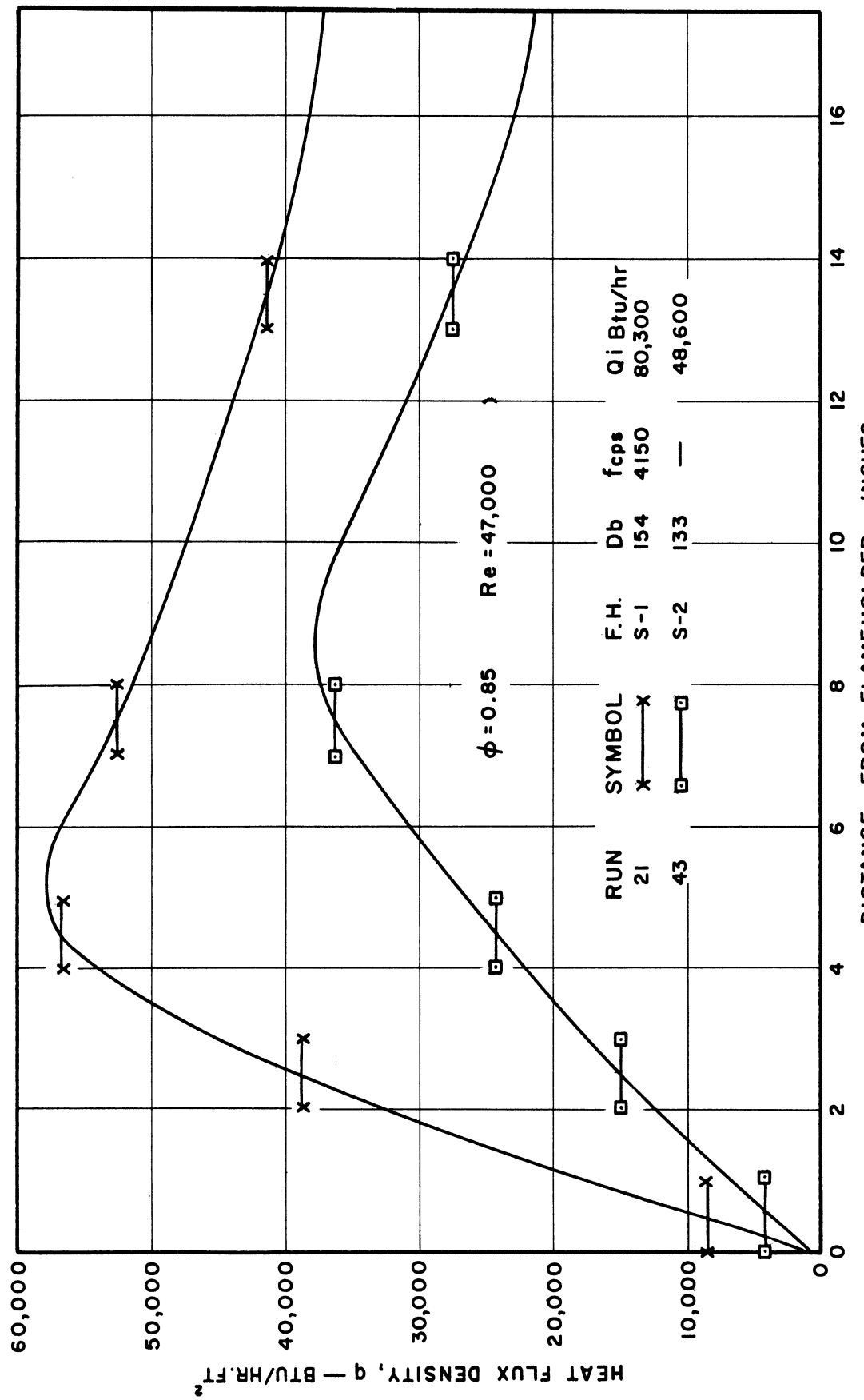

Figure 8. Profile of Heat Flux--Damped Versus Undamped Screech at Re = 47,000.

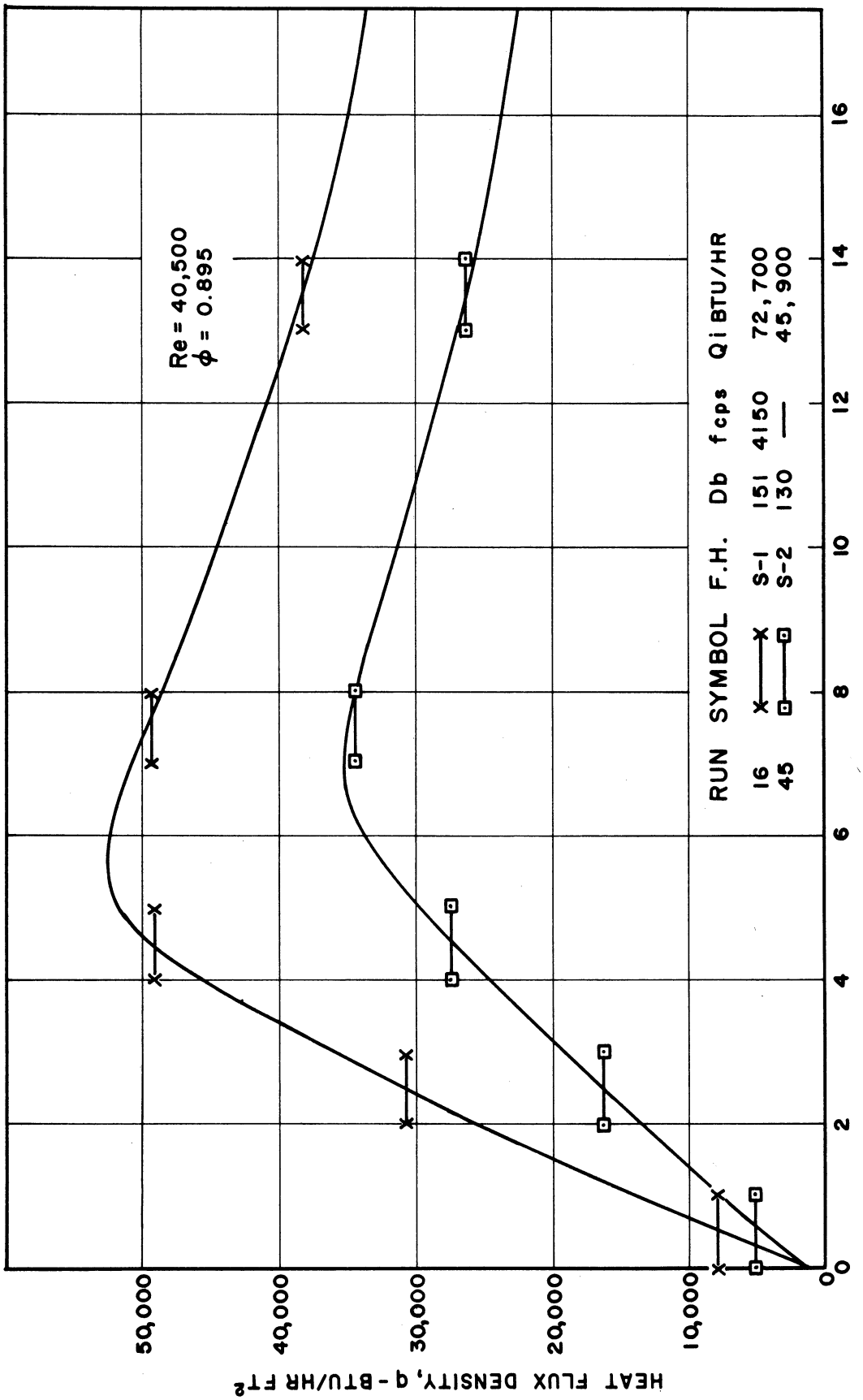

Figure 9. Profile of Heat Flux--Damped Versus Undamped Screech at Re = 40,500.

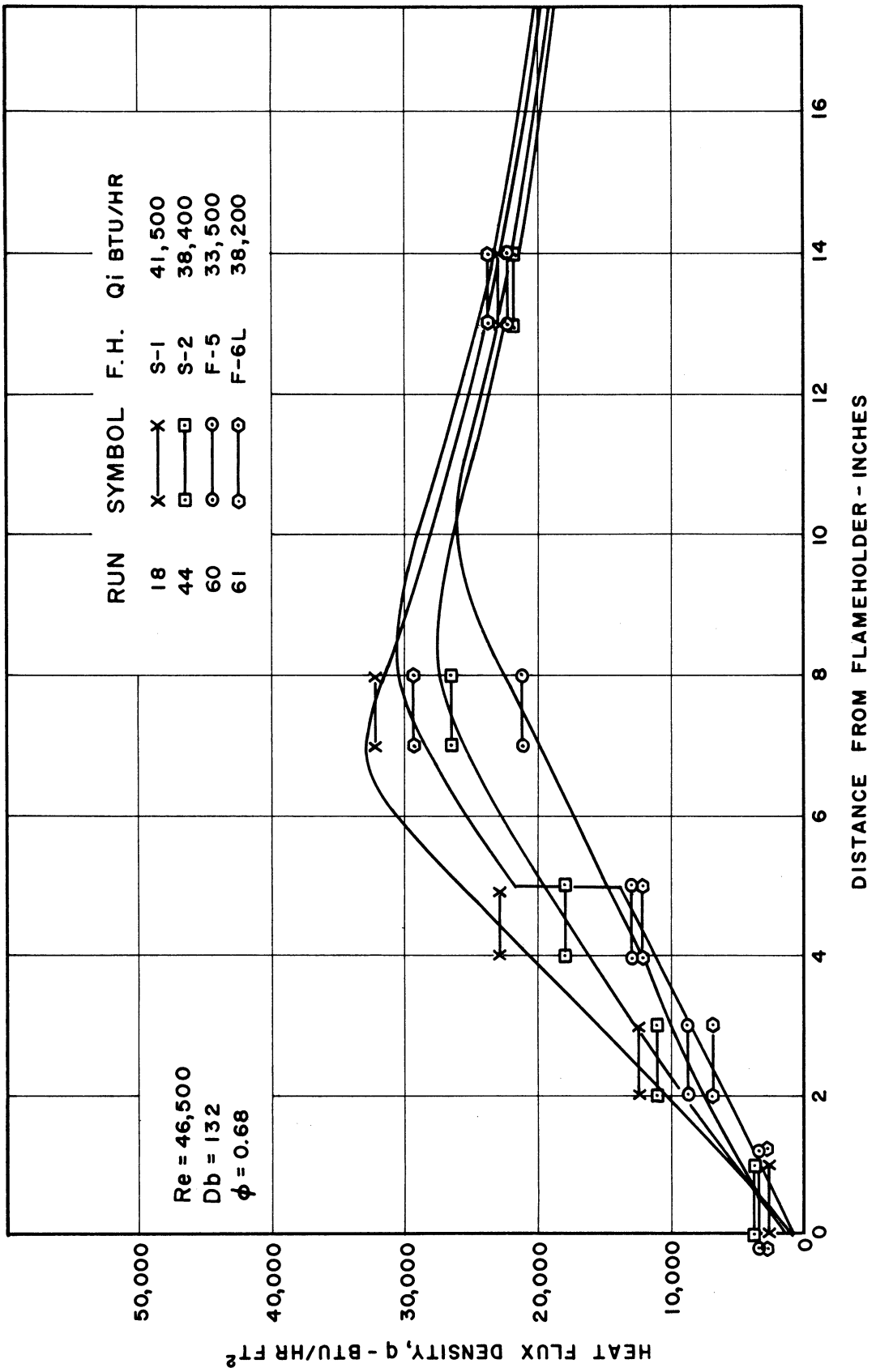

Figure 10. Profile of Heat Flux--Comparison of Flameholders Under Stable Conditions.

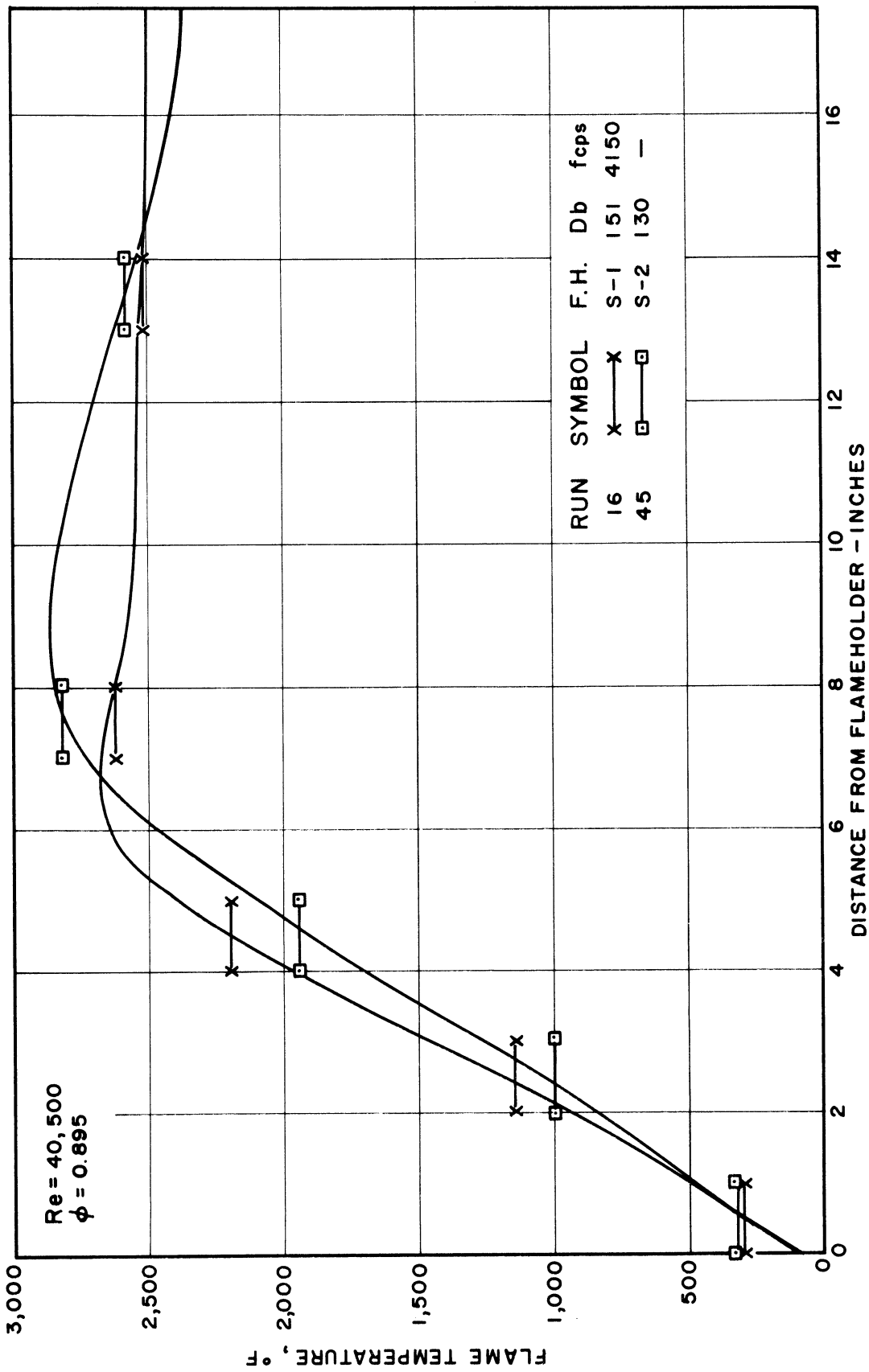

Figure 11. Temperature Profile--Damped Versus Undamped Screech at Re = 40,500.

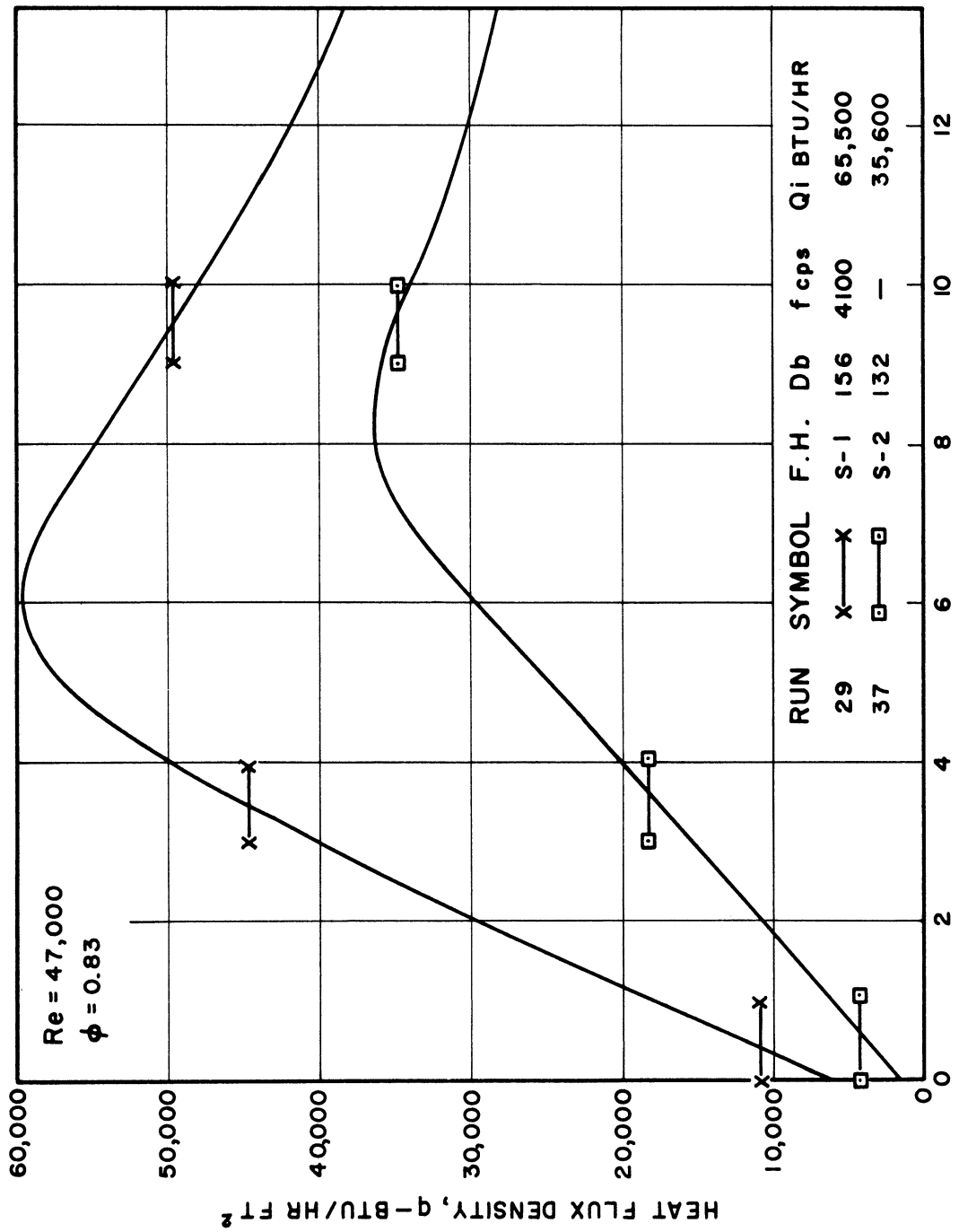

Figure 12. Profile of Heat Flux--Damped Versus Undamped Screech for L_b = 13-1/2 Inches.

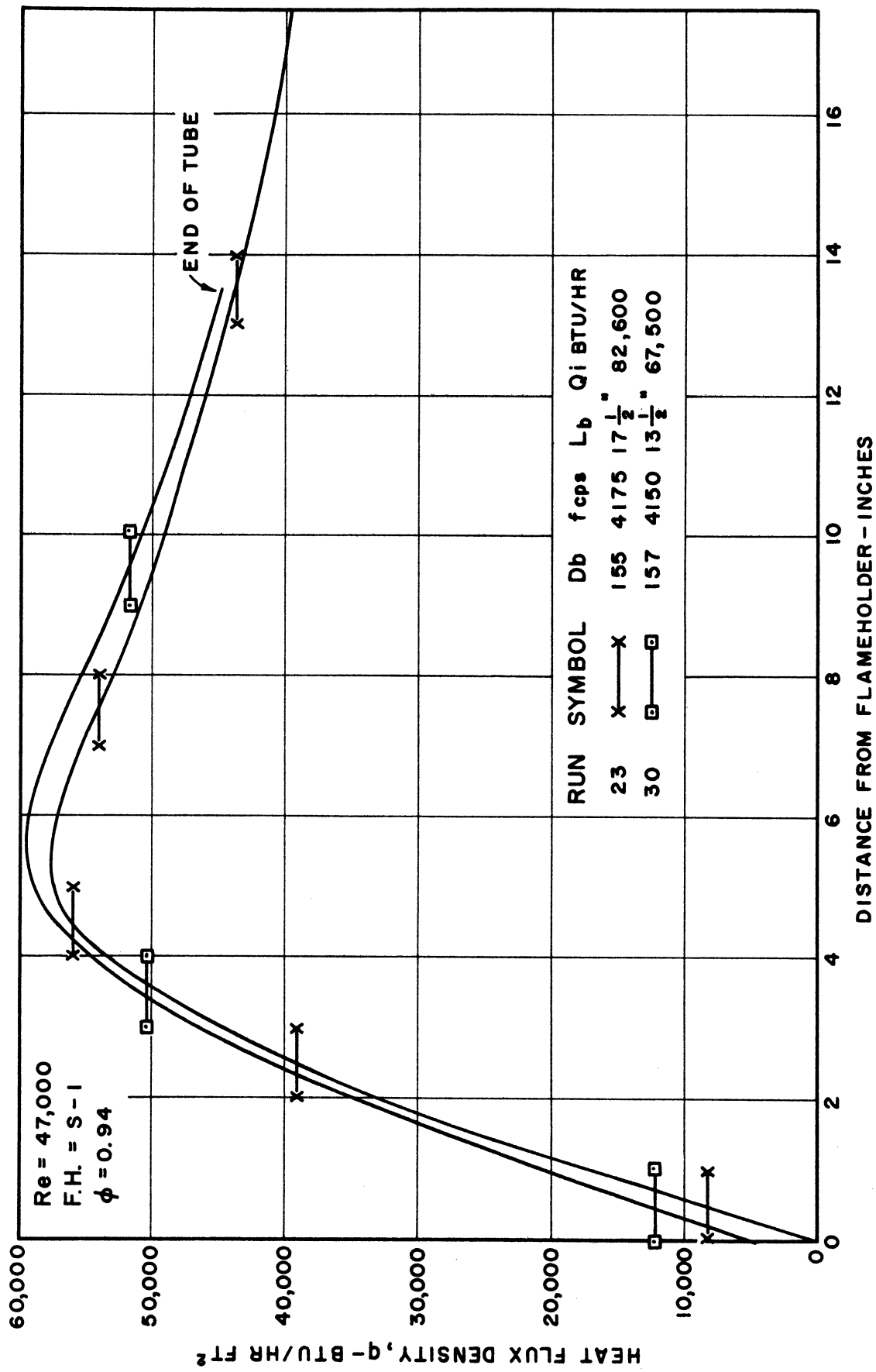

Figure 13. Profile of Heat Flux--Effect of Burning Length During Screeching.

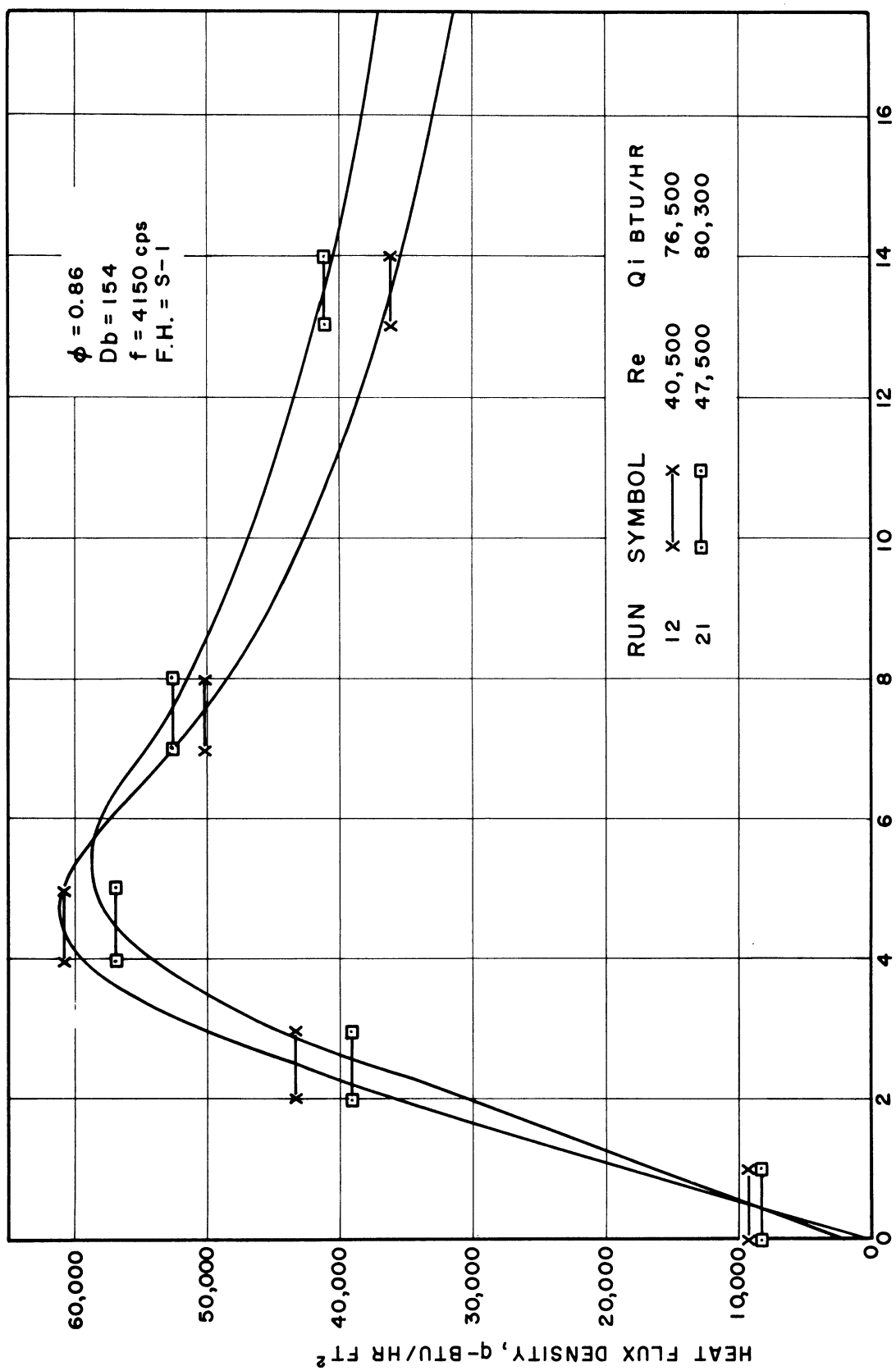

Figure 14. Profile of Heat Flux--Effect of Flow Rate During Screeching.

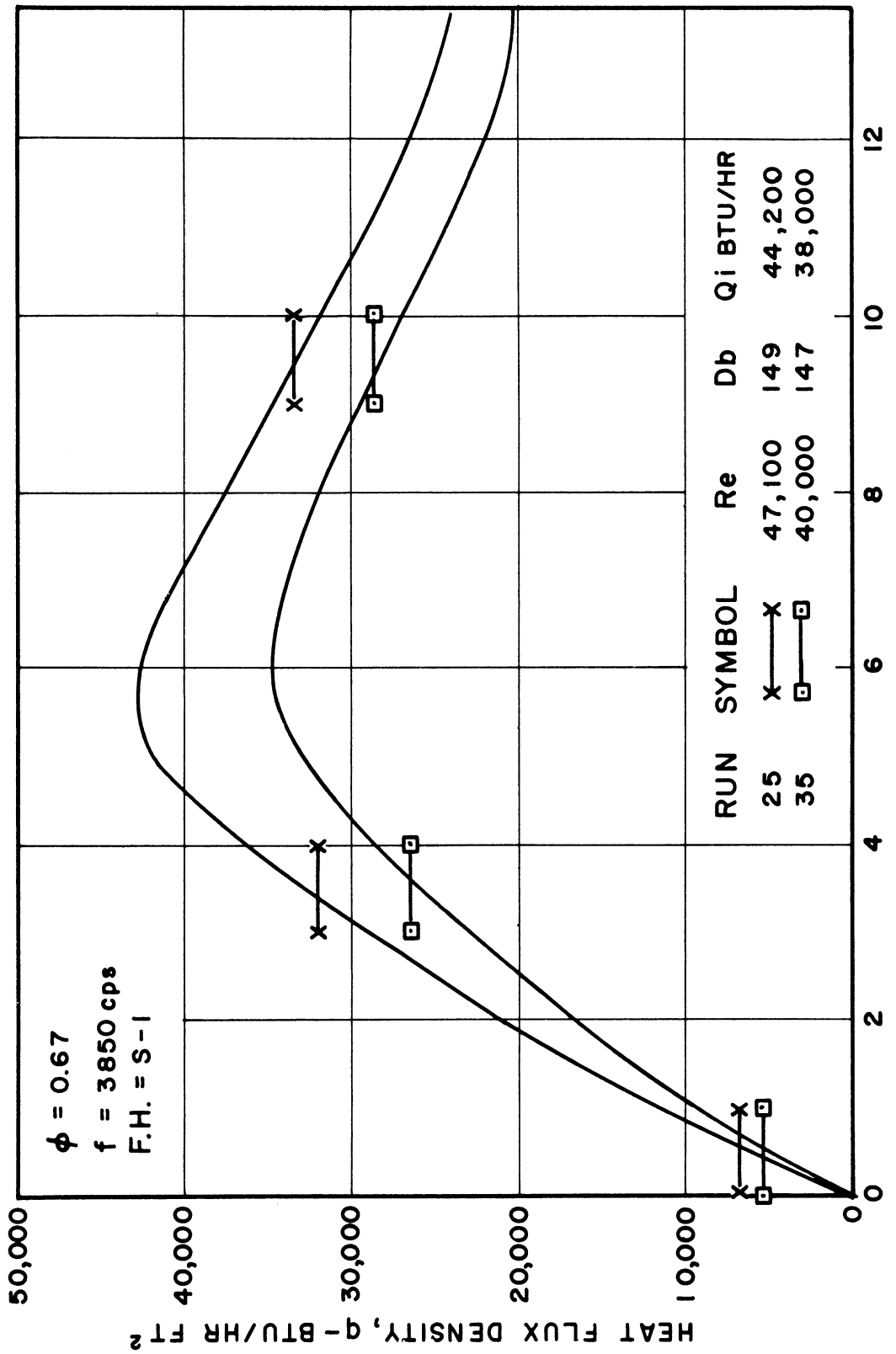

Figure 15. Profile of Heat Flux--Effect of Flow Rate and Slight Change in Sound Level.

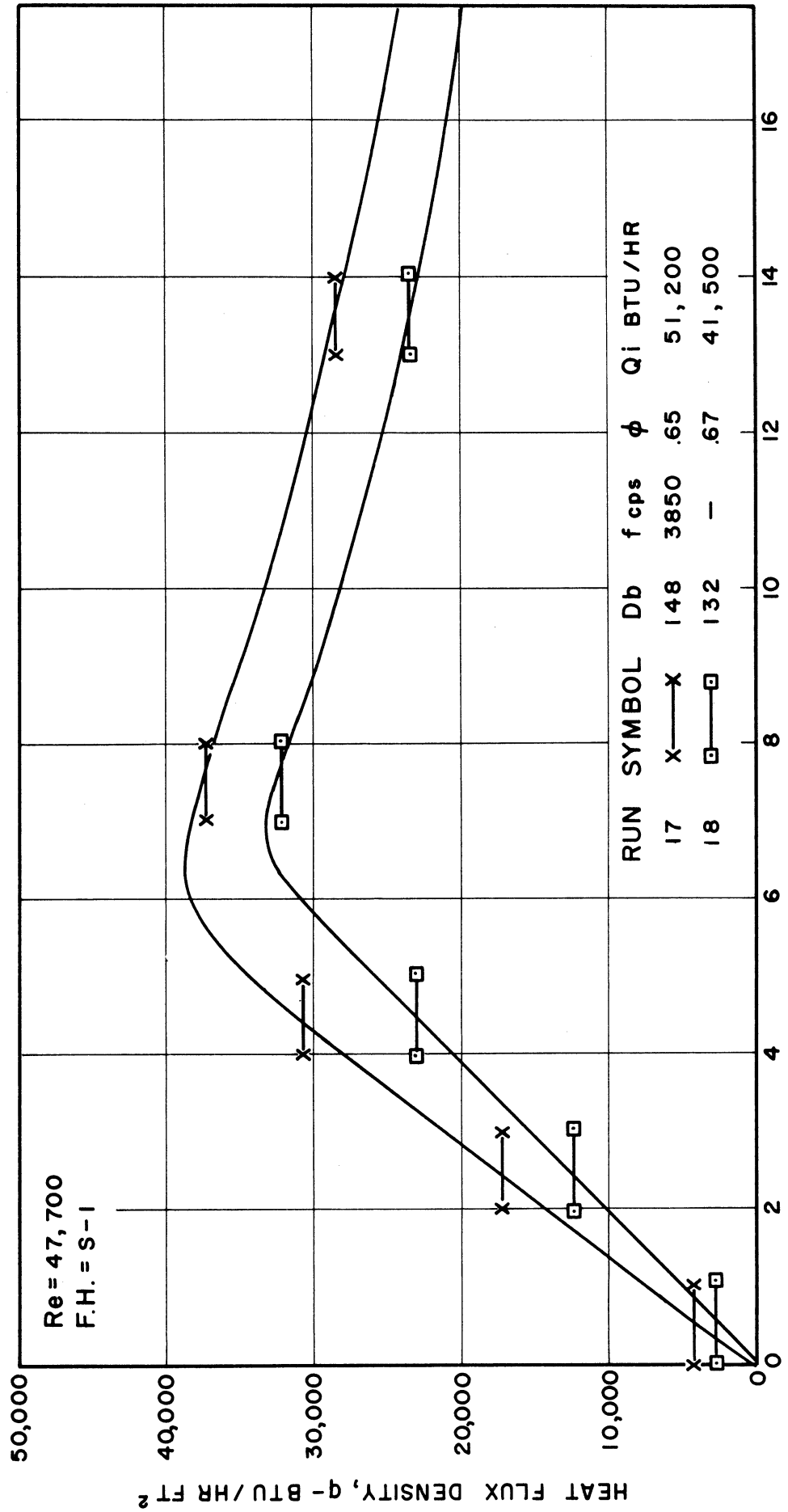

Figure 16. Profile of Heat Flux--Screeching Versus Stable Combustion at Re = 47,700.

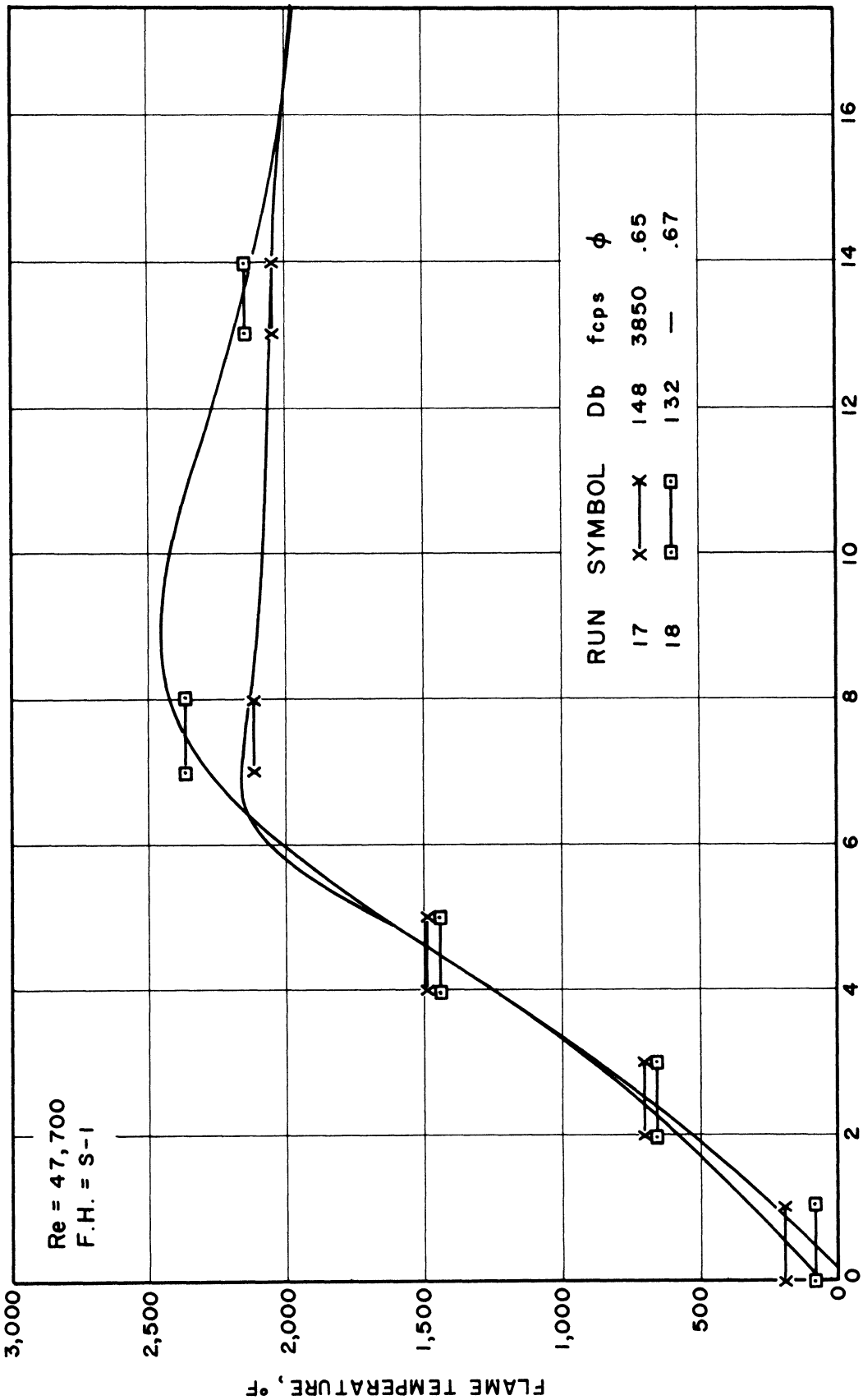

Figure 17. Temperature Profile--Screeching Versus Stable Combustion at Re = 47,700.

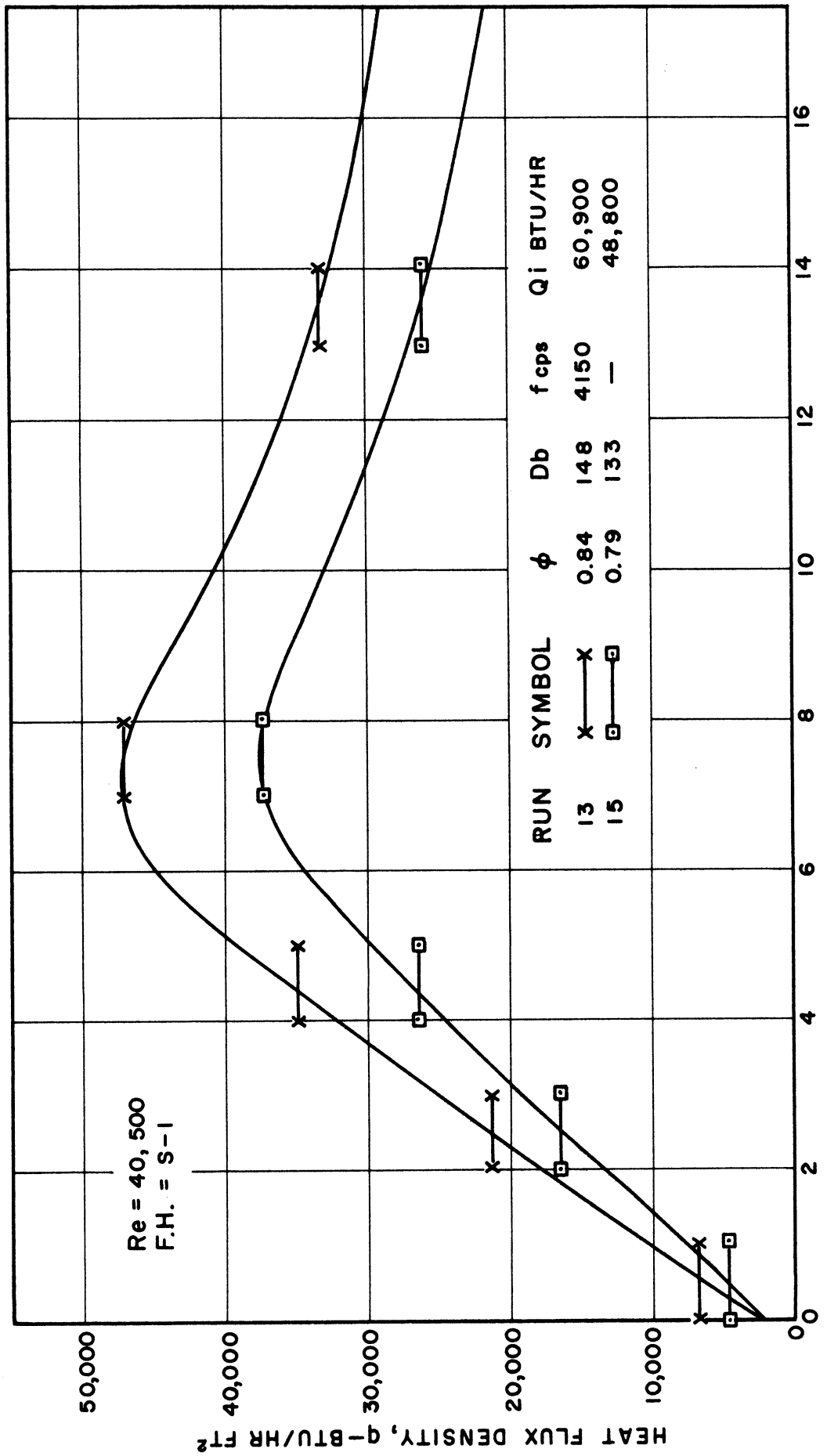

Figure 18. Profile of Heat Flux--Screeching Versus Stable Combustion at Re = 40,500.

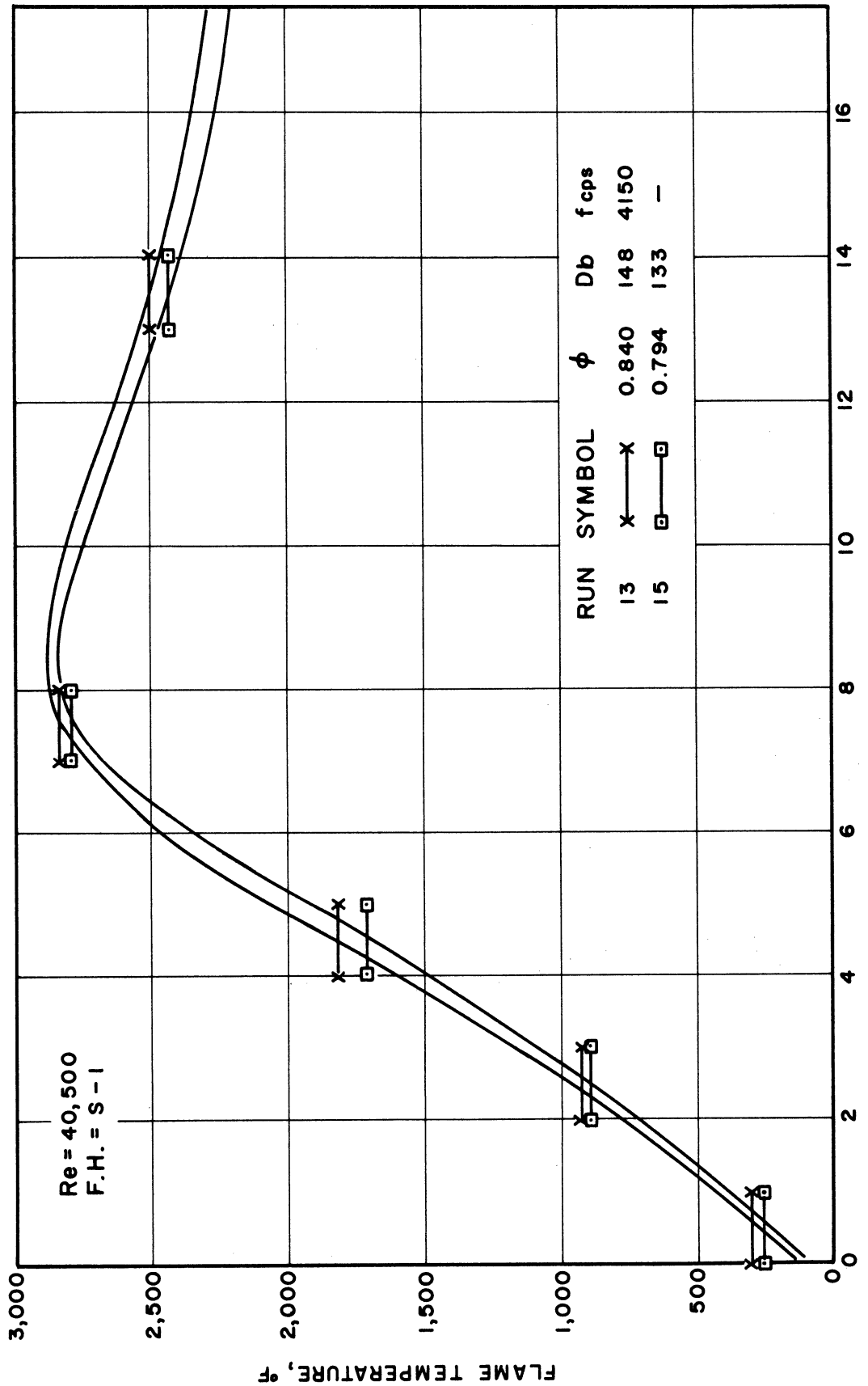

Figure 19. Temperature Profile--Screeching Versus Stable Combustion at Re = 40,500.

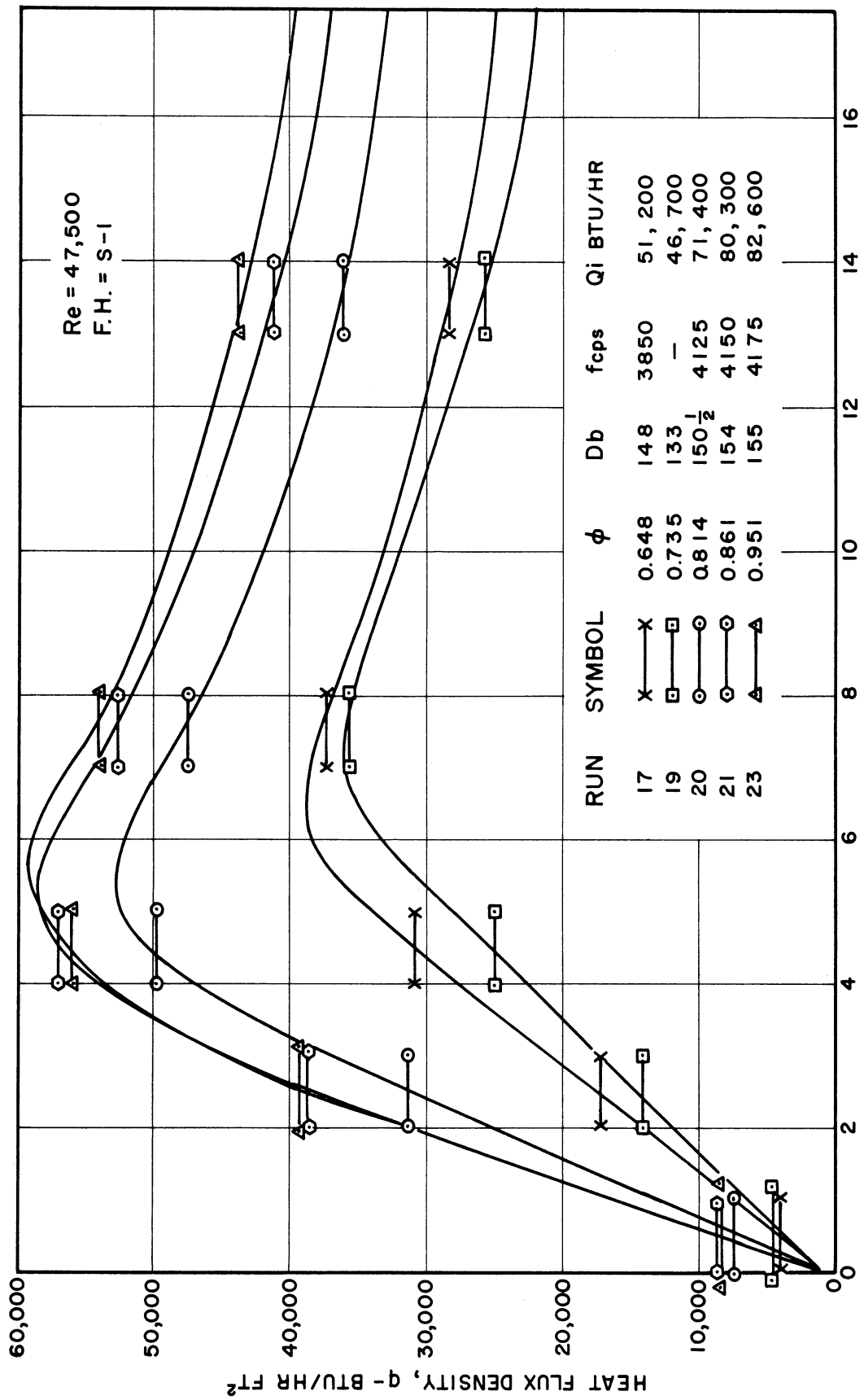

Figure 20. Profile of Heat Flux--Effect of Varying Fuel-to-Air Ratio with a Flameholder that is Prone to Screech.

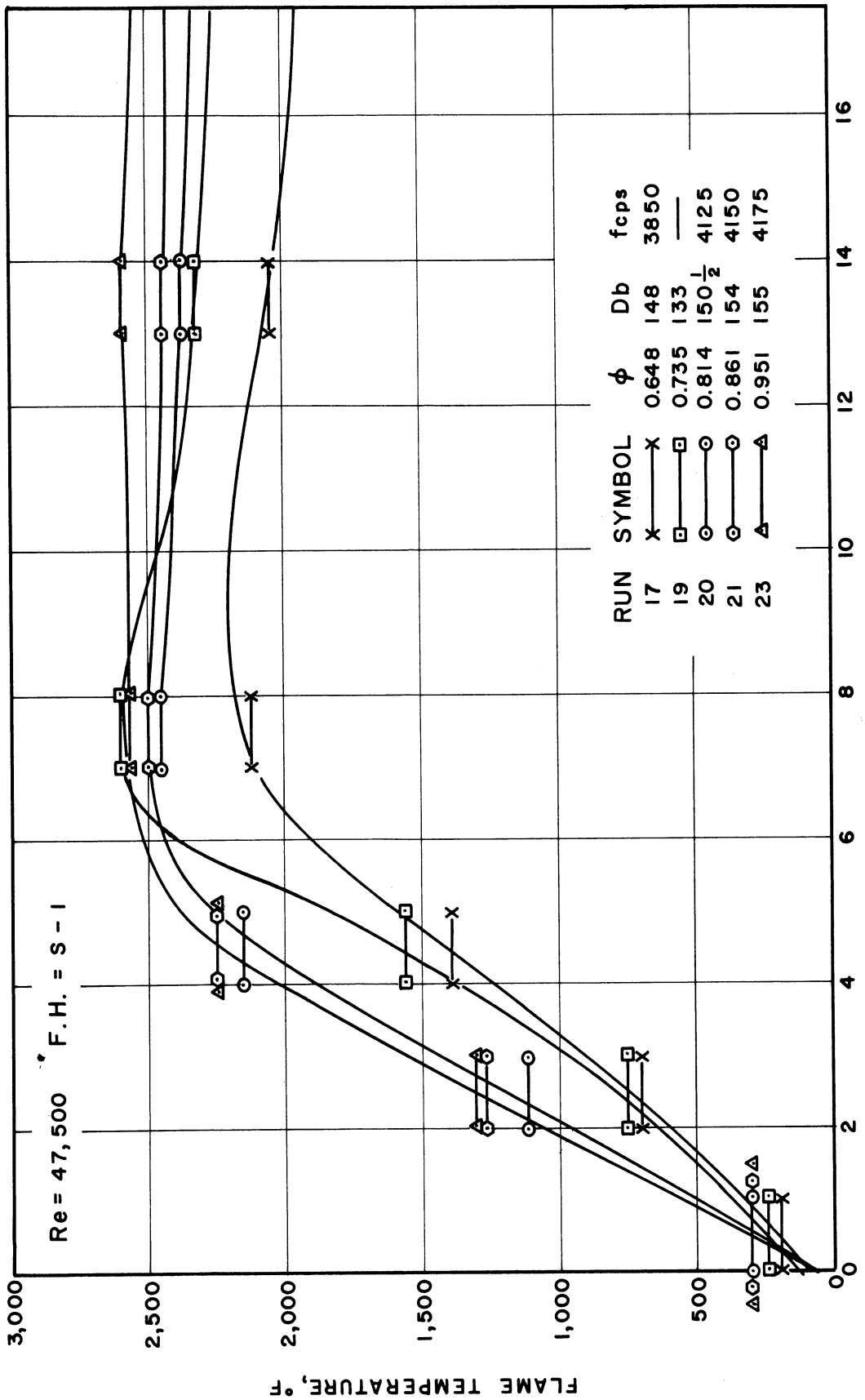

Figure 21. Temperature Profile--Effect of Varying Fuel-to-Air Ratio with a Flameholder that is Prone to Screech.

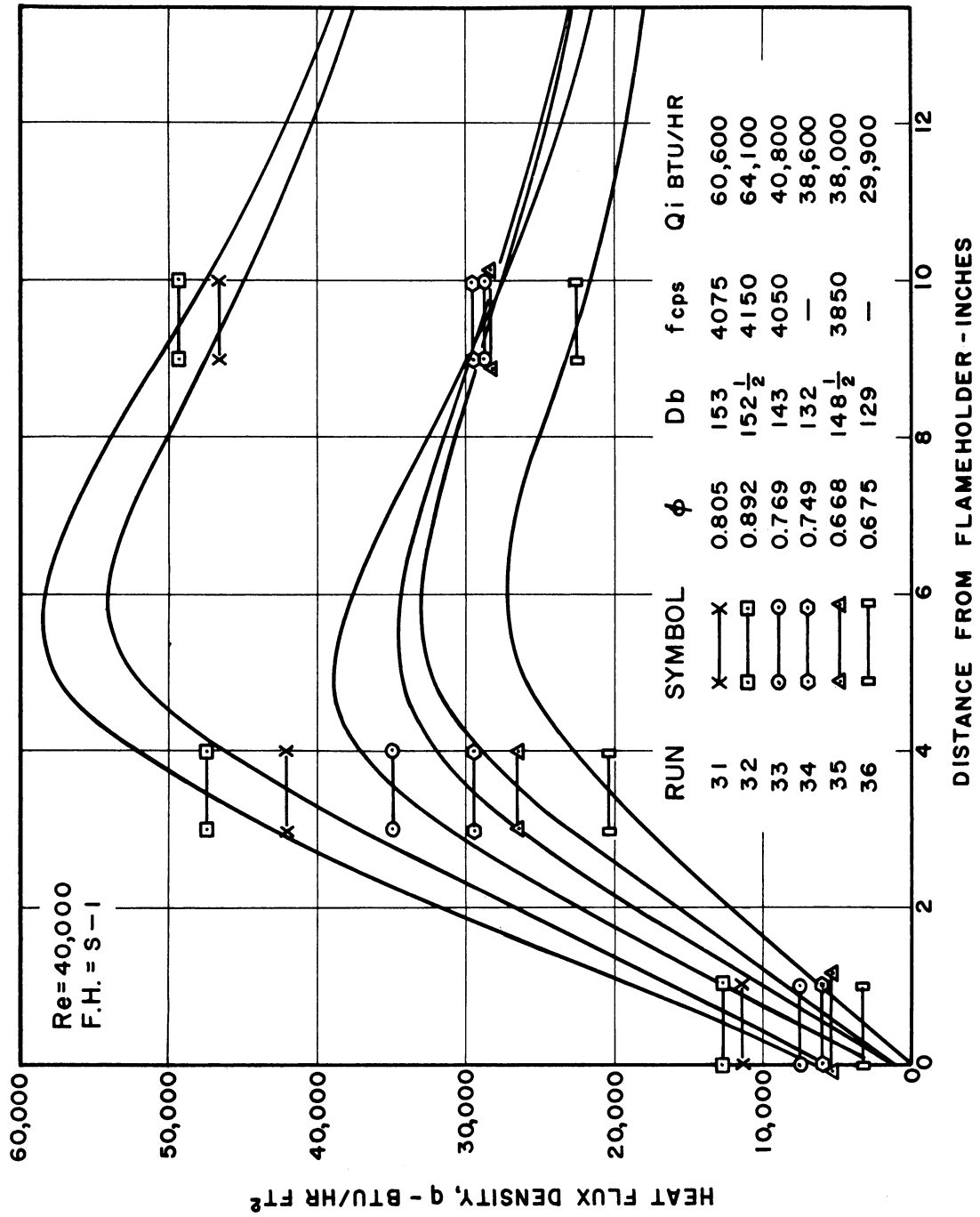

Figure 22. Profile of Heat Flux--Effect of Varying Fuel-to-Air Ratio with a Flameholder that is Prone to Screech with L_b = 13-1/2 Inches.

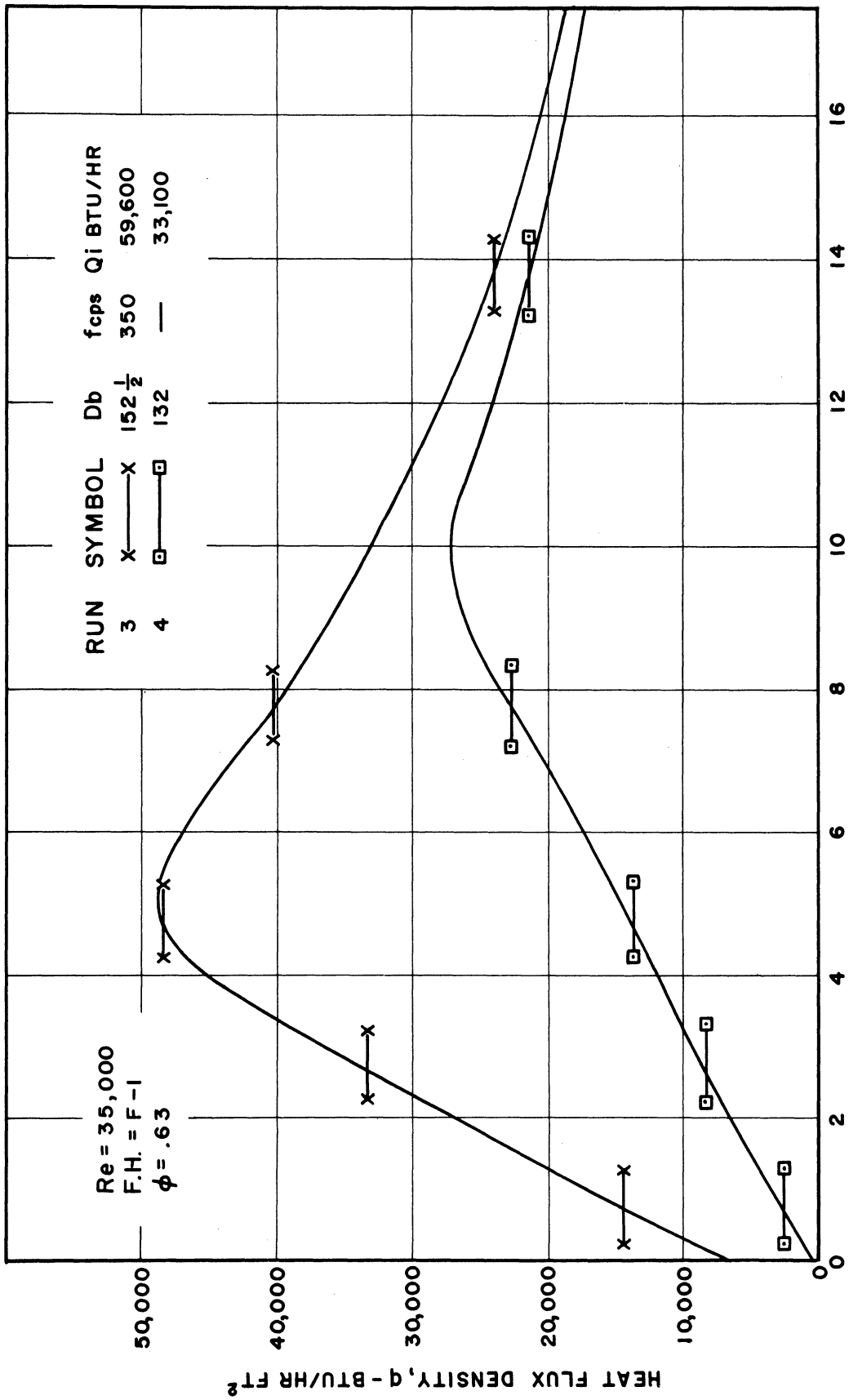

Figure 23. Profile of Heat Flux--Longitudinal-Oscillating Versus Stable Combustion at Re = 35,000.

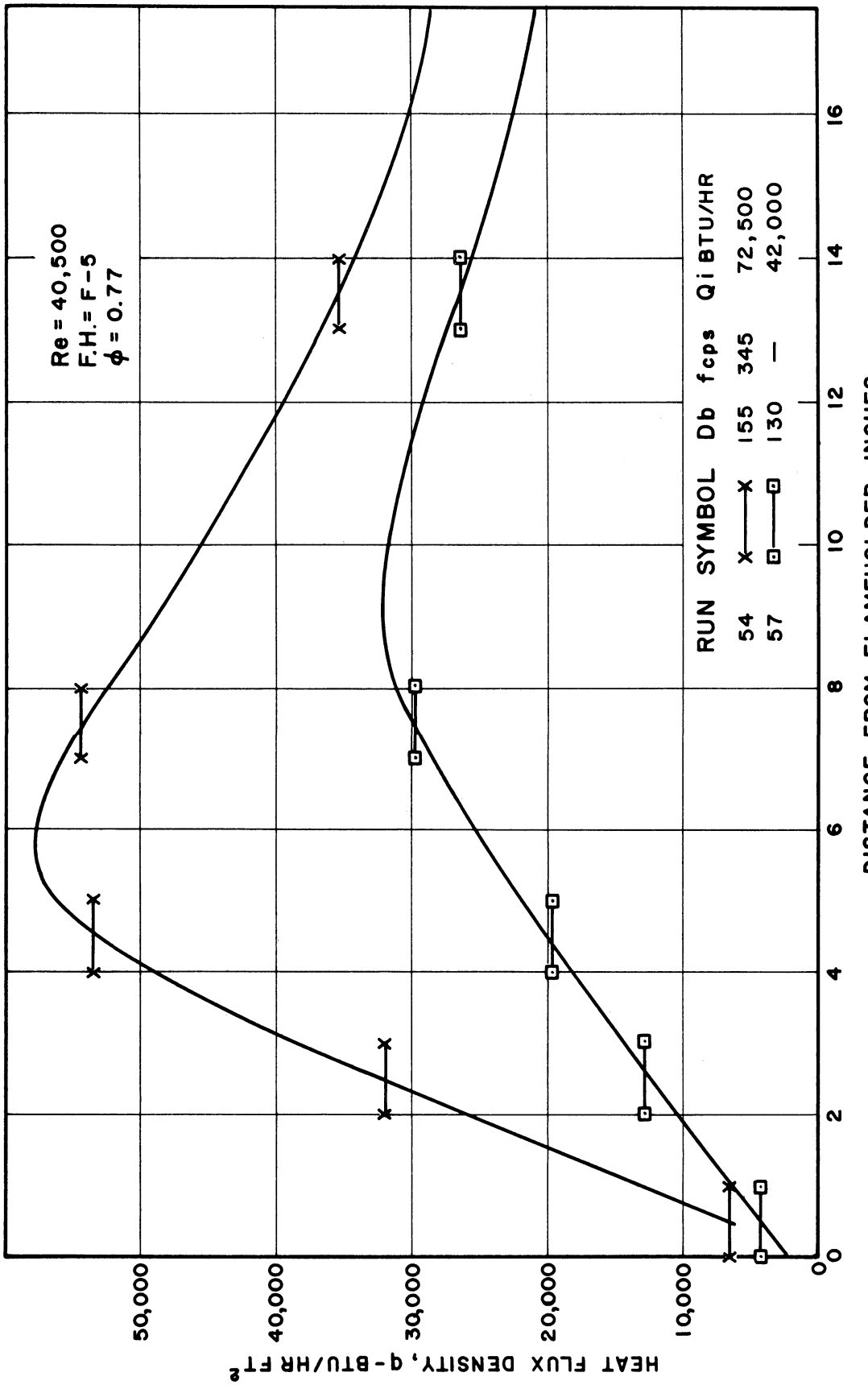

Figure 24. Profile of Heat Flux--Damped Versus Undamped Longitudinal Oscillations at Re = 40,500.

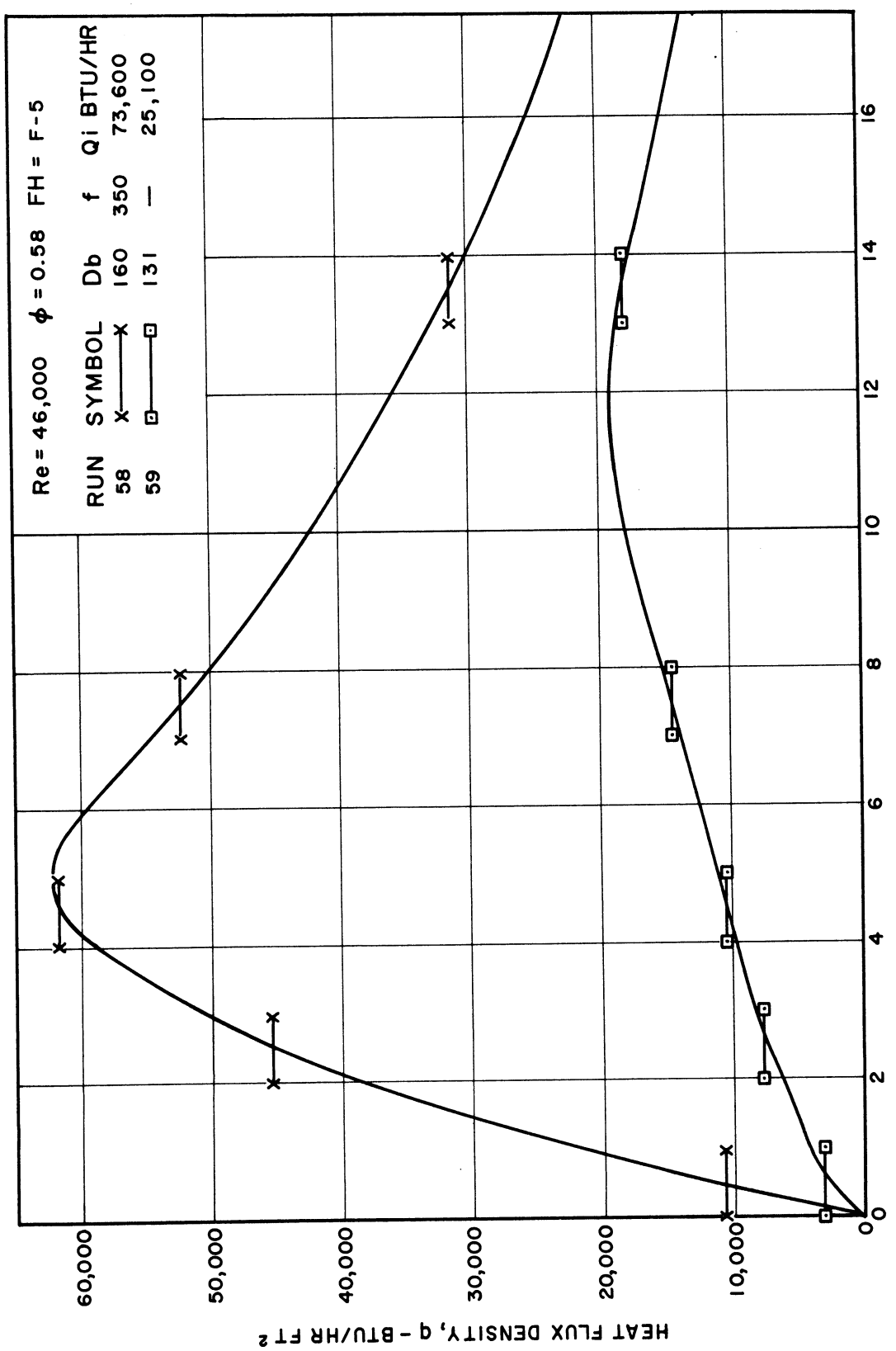

Figure 25. Profile of Heat Flux--Damped Versus Undamped Longitudinal Oscillations at Re = 46,000.

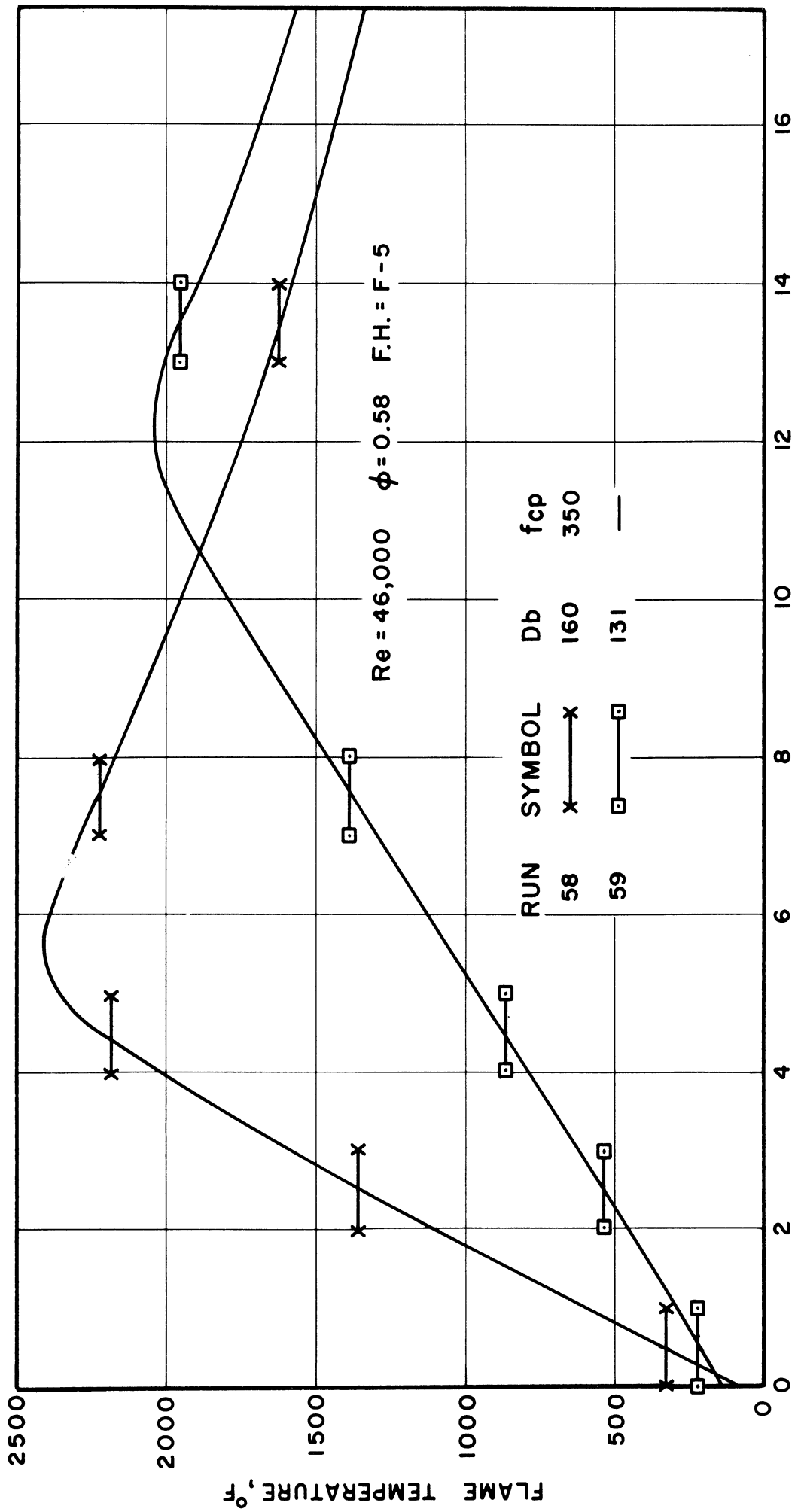

Figure 26. Temperature Profile--Damped Versus Undamped Longitudinal Oscillations at Re = 46,000.

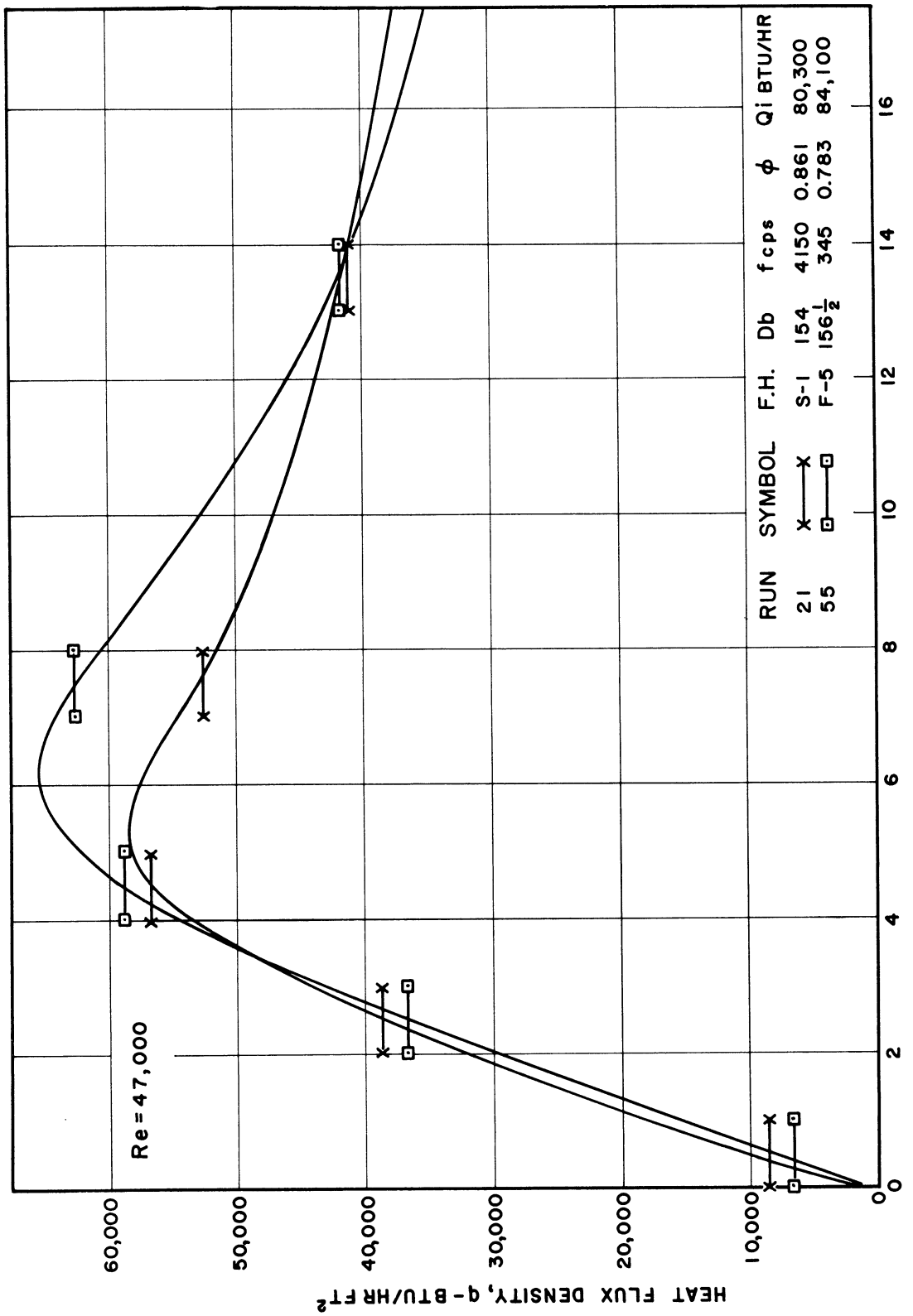

Figure 27. Profile of Heat Flux--Screeching Versus Longitudinal--Oscillating Combustion at Re = 47,000.

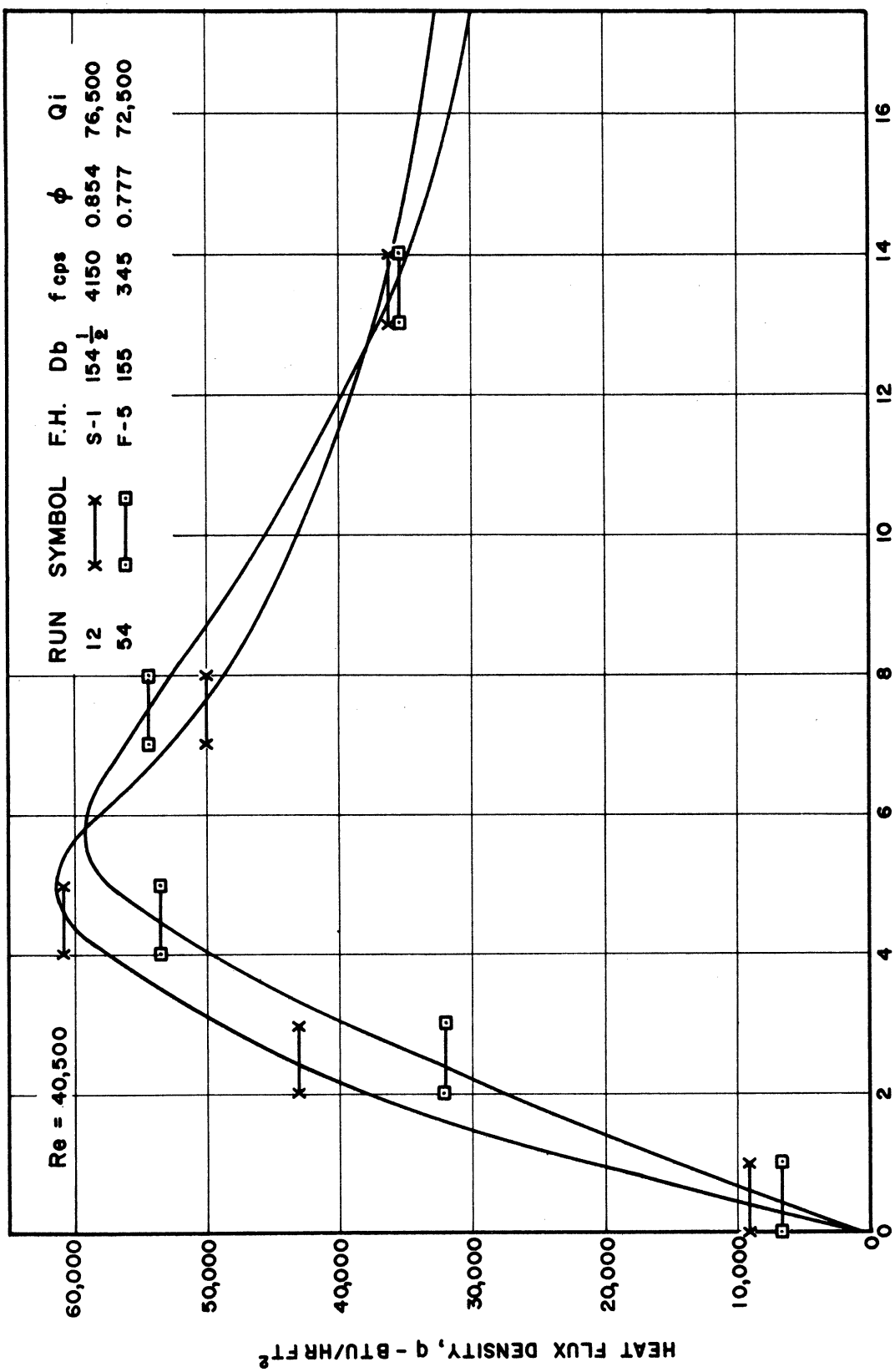

Figure 28. Profile of Heat Flux--Screeching Versus Longitudinal--Oscillating Combustion at Re = 40,500.

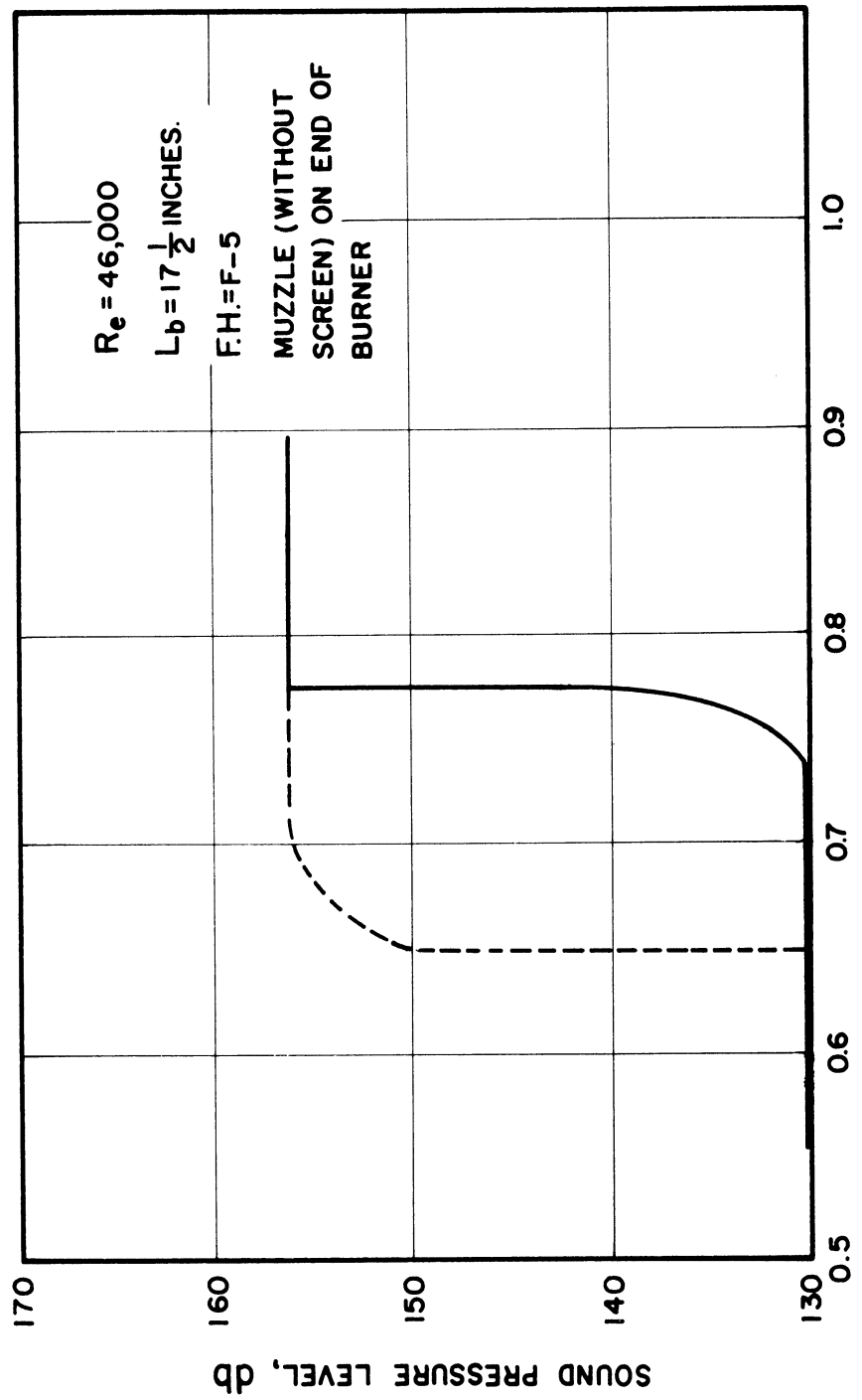

Figure 29. Hysterisis Behavior of the Longitudinal Oscillation with Fuel-to-Air Ratio.

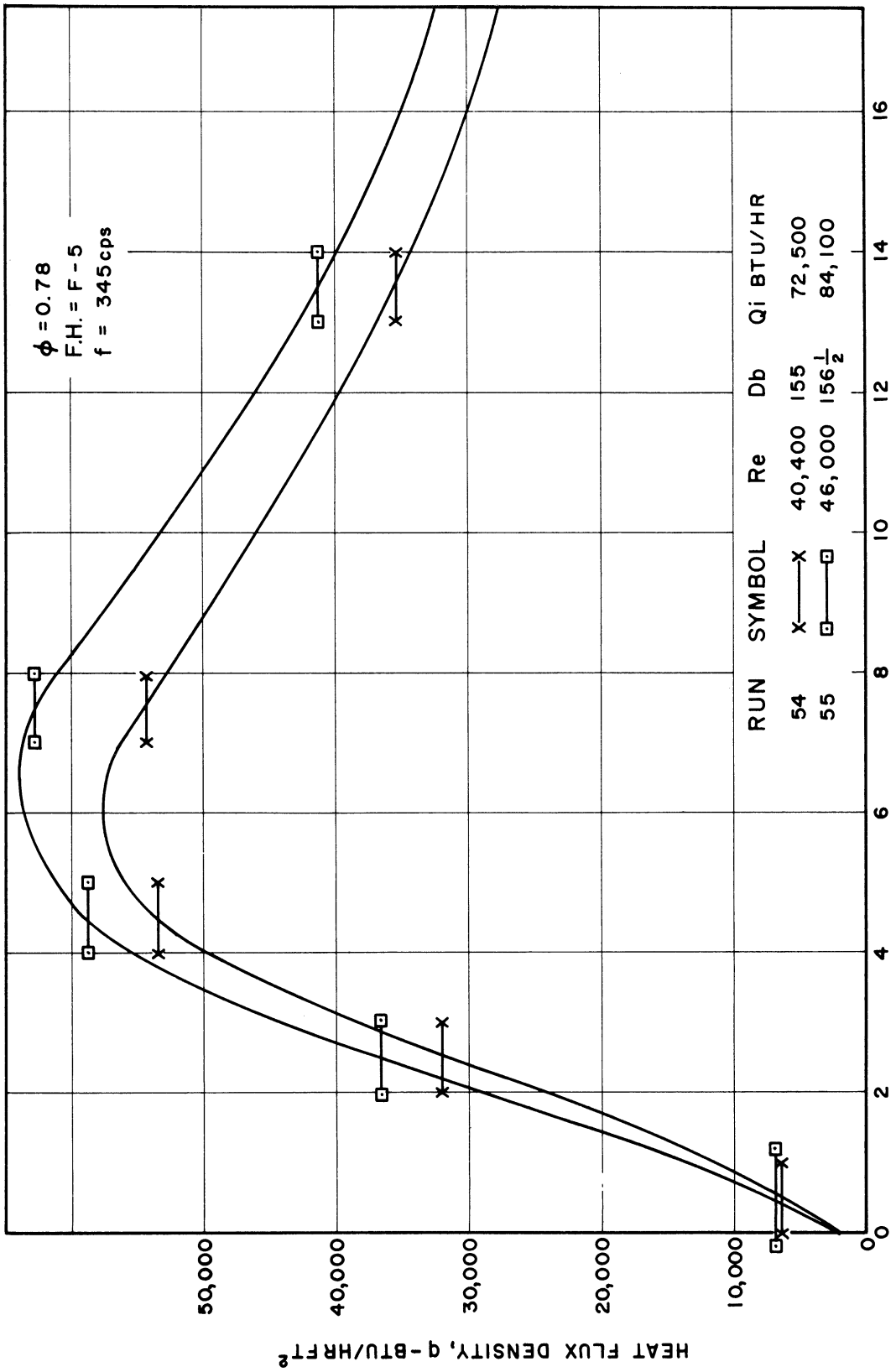

Figure 30. Profile of Heat Flux--Effect of Flow Rate During Longitudinal--Oscillating Combustion.

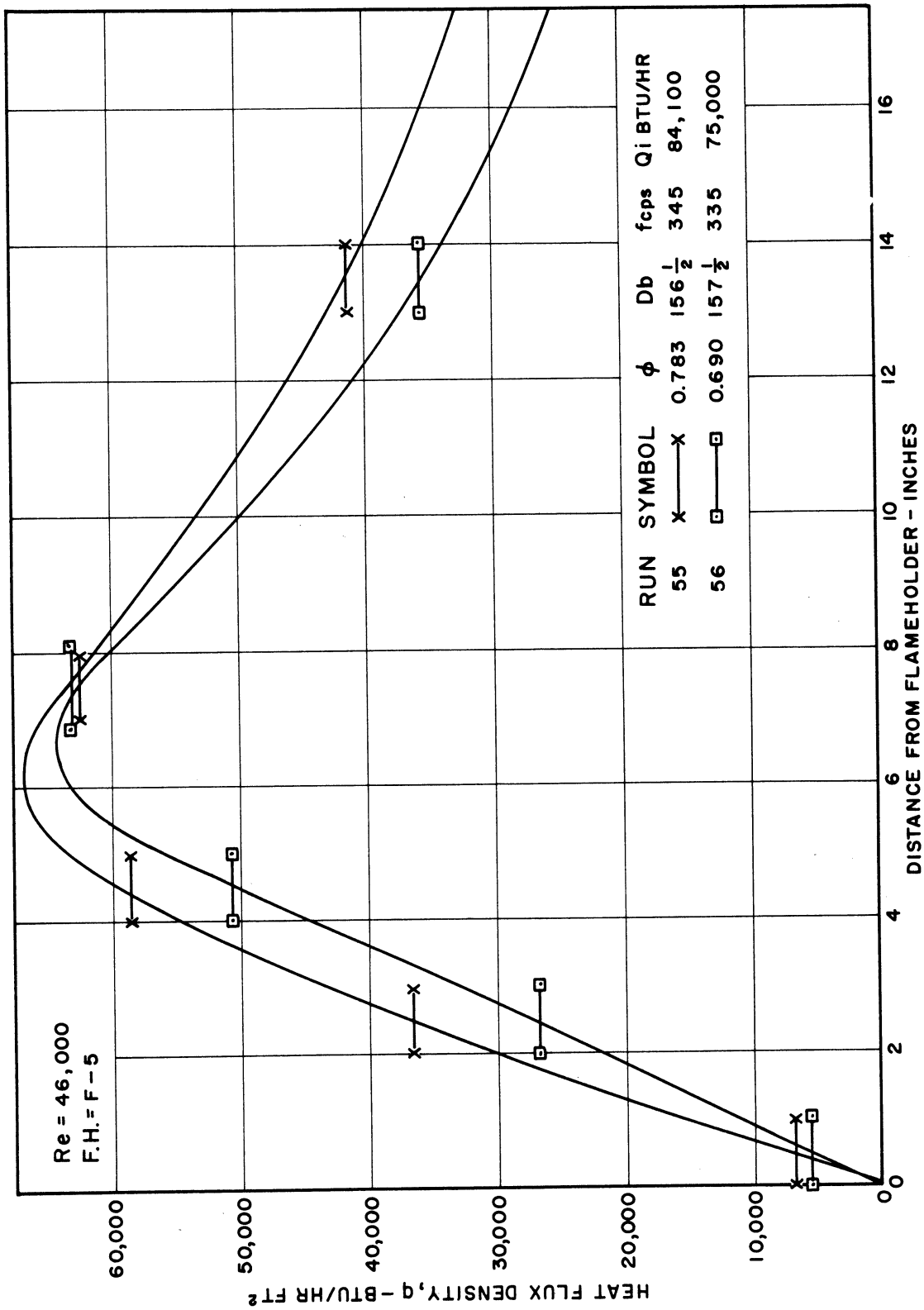

Figure 31. Profile of Heat Flux--Effect of Varying Fuel-to-Air Ratio During Longitudinal--Oscillating Combustion.

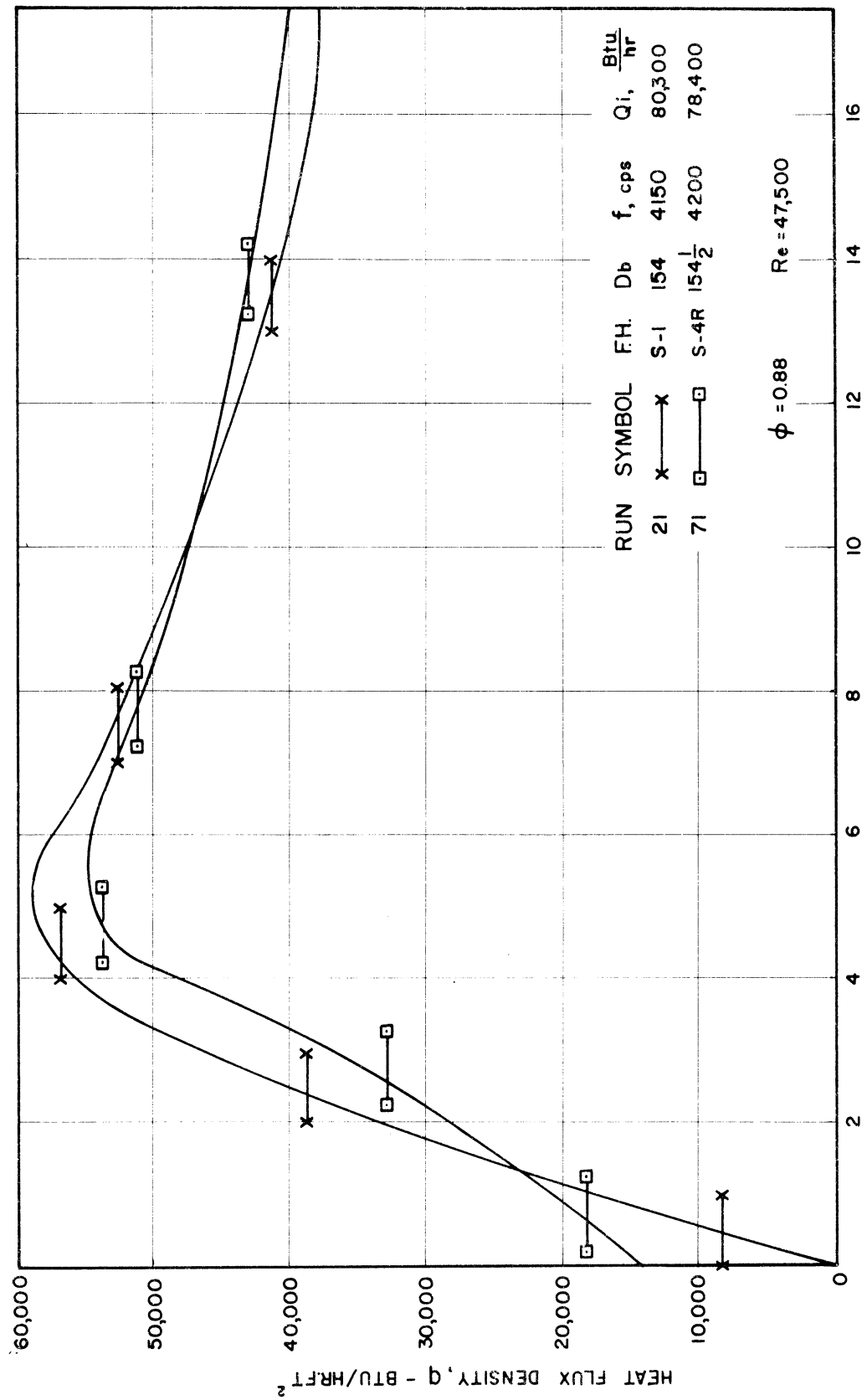

Figure 32. Profile of Heat Flux--Comparison of S-1 and S-4R Flameholders During Screeching Combustion.

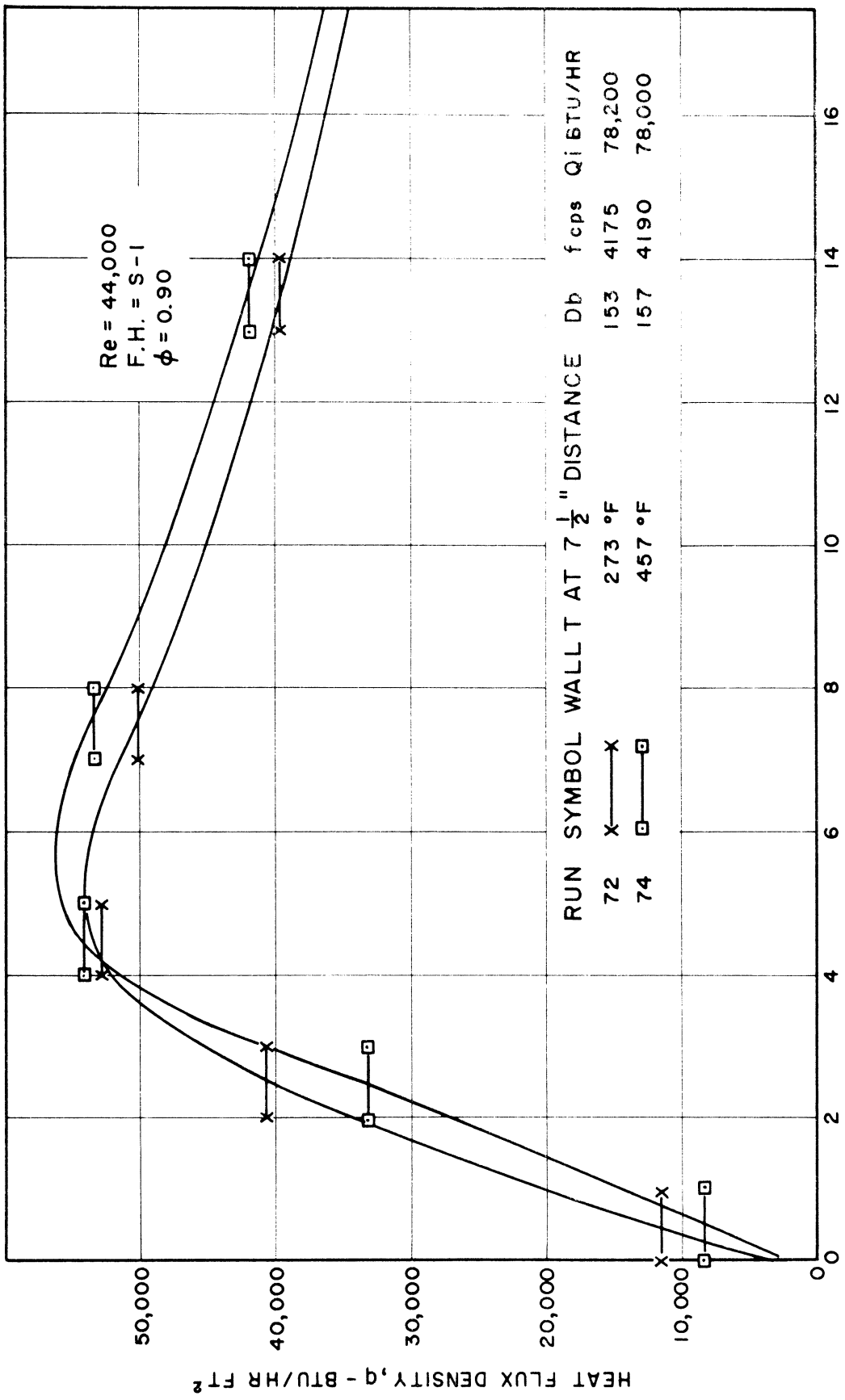

Figure 33. Profile of Heat Flux--Effect of an Approximately 200°F Rise in Wall Temperature During Screeching Combustion.

Temperature Profiles and Transverse Oscillations

The relative importance of changes in flame temperature compared to changes in heat transfer coefficient is indicated by the temperature profiles in Figure 11 for the runs of Figure 9. The two temperature profiles are similar.

Short Burning Lengths and Transverse Oscillations

Comparison of damped versus undamped transverse oscillations for a shorter burning length of 13-1/2 inches is similar to that for the 17-1/2-inch burning length. In Figure 12, the peak is raised over 60 per cent and the total heat transfer by over 80 per cent when the sound level is increased from 132 db to 156 db. A comparison of the two burning lengths during screeching combustion is shown in Figure 13 where it is seen that burning length has little effect on the profile. The flame-generated oscillation is slightly more intense for the shorter burning length.

Two runs, numbers 8 and 9, were conducted at a burning length of 8 inches although no profile of heat transfer rates could be determined. An increase in the propensity of the burner to screech was noted for this short burning length because not only was the screech more intense, but it was generated without the screen in the annulus of the flameholder to stabilize the flame closer to the wall. It is noted that the increase in total heat transferred to the tube due to an increase in sound level from 133 db to 159 db is about three-fold, judging from the heat absorbed by the tube's cooling water.

Flow Rates and Transverse Oscillations

The effect of flow rate during screeching on the local rates of heat transfer is shown in Figure 14. The higher flow rate tends to shift the peak downstream and to increase the rates downstream from the peak. A similar comparison of flow rates during screeching is made for the 13-1/2-inch burning length in Figure 15. However, in this case the sound levels are not identical, so that the higher flow of Run 25 together with its higher sound level is causing the general increase in its heat transfer profile.

Moderately Intense Screeching Combustion

The effect of a moderately intense transverse oscillation compared to a stable combustion with the same flameholder is shown in Figure 16 and is seen to be less than for the more intense screech. The temperature profiles in Figure 17 are similar except for a higher peak for the damped case. Another comparison of the effect of moderately intense screeching combustion at a lower flow rate is made in Figure 18. The peak is increased by 27 per cent and the total heat transfer by 25 per cent for Run 13 with the 148 db transverse oscillation compared with the stable Run 15. It should be noted that the flameholders are the same in this comparison, but the fuel-to-air ratio is lower by 6 per cent in the stable run. Temperature profiles are also presented for these two runs in Figure 19 and are seen to be very similar.

Fuel-to-Air Ratio and Heat Transfer Profiles

The general pattern in heat transfer profiles is portrayed by the five runs in Figure 20. Heat transfer rates are seen to increase with ϕ, i.e., fuel-to-air ratio as a fraction of stoichiometric, and with sound level. The corresponding set of temperature profiles follows in Figure 21. A similar pattern is obtained at the 13-1/2-inch burning length as seen in Figure 22.

Effects of Longitudinal Oscillations

The longitudinal oscillations have an effect on the heat transfer similar to that of the higher pitched transverse oscillations at the same sound level. Comparisons of the heat transfer profiles for damped and undamped longitudinal oscillations are presented in Figures 23, 24, and 25 at three different Reynolds numbers. The sound levels of the oscillation vary in each case, primarily because the degree of damping is varied. It is noted that the damping of the longitudinal oscillation is done with a spray-quench muzzle on the end of the burner and thus does not change the flow conditions in the burner.

In Figure 24, the peak for the case of an intense longitudinal oscillation is increased by over 75 per cent and the integrated heat transfer by almost 75 per cent. The increases due to the organ-pipe oscillation are similar in Figure 23. In the case of Run 58 with its counterpart, number 59, with damped oscillation, the increases for the longitudinal oscillation of 160 db are essentially three fold. No muzzle was on the

burner in Run 58 and one of the higher blockage flameholders was used. In all three comparisons the peak is moved closer to the flameholder by the oscillation. The temperature profile for Runs 58 and 59 is given in Figure 26. The temperature profiles are not as similar as in earlier cases; however, the maximum or peak temperatures are of the same order of magnitude. The biggest difference is their position.

Comparison of the Two Acoustic Modes

The transverse and longitudinal modes of acoustic oscillation appear to produce similar effects. A comparison of their profiles of local heat fluxes is made in Figures 27 and 28. In Figure 27 where the Reynolds number is 47,000, the longitudinal mode causes a 5 per cent greater heat transfer to the tube than the transverse mode. This increase is probably accounted for by the greater intensity of the longitudinal oscillation. In Figure 28 at a Reynolds number of 40,500, the intensities are approximately equal. Here the transverse mode causes a slightly greater rate of heat transfer as expected because the propane-air mixture is closer to stoichiometric, i.e., ϕ is closer to 1.0.

Hysterisis with Organ-Pipe Oscillations

A pronounced hysterisis effect exists in the case of longitudinal oscillations. When the fuel-to-air ratio has been increased high enough to bring the intense organ-pipe oscillation on, the fuel-to-air ratio can be decreased by as much as 10 to 20 per cent without any change in sound

level. This phenomenon is shown in Figure 29 for the case of the F-5 flameholder and the muzzle without its screen on the end of the burner. The solid line represents the sound level as ϕ is increased from a low value in a stable burner. The dotted line shows the sound pattern as ϕ is decreased after the intense longitudinal oscillation has set in.

Fuel-to-Air Ratio, Flow Rates, and Organ-Pipe Oscillations

The next two figures, numbers 30 and 31, depict the effect of varying flow rates and fuel-to-air ratio with intense longitudinal oscillations being generated. Increases in the profile occur with increases in either flow rates or fuel-to-air ratio as was true with the transverse oscillations.

Transverse Oscillations with Ring-type Flameholder

Some additional studies were made of the transverse oscillation with a different type of flameholder. In Figure 32, a comparison is given of the heat transfer profile with a ring-type flameholder to that with the previous screen-in-annulus flameholder. The difference is slight with a definite rate of heat exchange at the flameholder in the case of partial stabilization of the flame by an eighth-inch, asbestos ring cemented to the tube wall at the flameholder level.

Effect of Higher Wall Temperatures on Screech

The effect of higher wall temperatures on screeching combustion was tested to a limited extent, by slowing the flow rate of the tube's cooling-water enough so that it boiled through all but the first 4 inches of the burner length. Wall temperatures were thus raised by about 200°F.

The effect on the heat transfer profile is not large as shown in Figure 33; however, the sound level did increase by a significant amount, from 153 db to 157 db.

Local Heat Transfer Coefficients

The heat transfer coefficients to be presented are for convective heat transfer, with the radiation corrections to the local measured fluxes being estimated by the methods in McAdams.[48] Flame temperatures were measured at three distances from the flameholder by the SLR method. Local coefficients are calculated at these three points using the bulk gas temperatures determined by Equation (9) from the SLR measurements. The details of the calculations are included in Appendix B in conjunction with the sample calculations.

The effects of varying flow rates, varying gas temperatures and properties, and different flameholders on the coefficient, h, is removed by dividing it by h_∞ and h'/h'_∞. The quantity, h_∞, is the coefficient predicted for fully developed turbulent flow by the empirical correlation recommended by Zellnik[91] for heat transfer from high temperature gas streams to a cooled tube.

$$Nu_s = \frac{h_\infty D}{k_s} = 0.023\ Re_s^{0.8}\ Pr_s^{1/3}\ T_b/T_s^{0.33} \qquad (18)$$

The ratio, h'/h'_∞, is the local coefficient measured without combustion divided by the predicted coefficient without combustion. This ratio of local coefficients for cold flow is plotted against tube length in Figure 34 for the various flameholders.

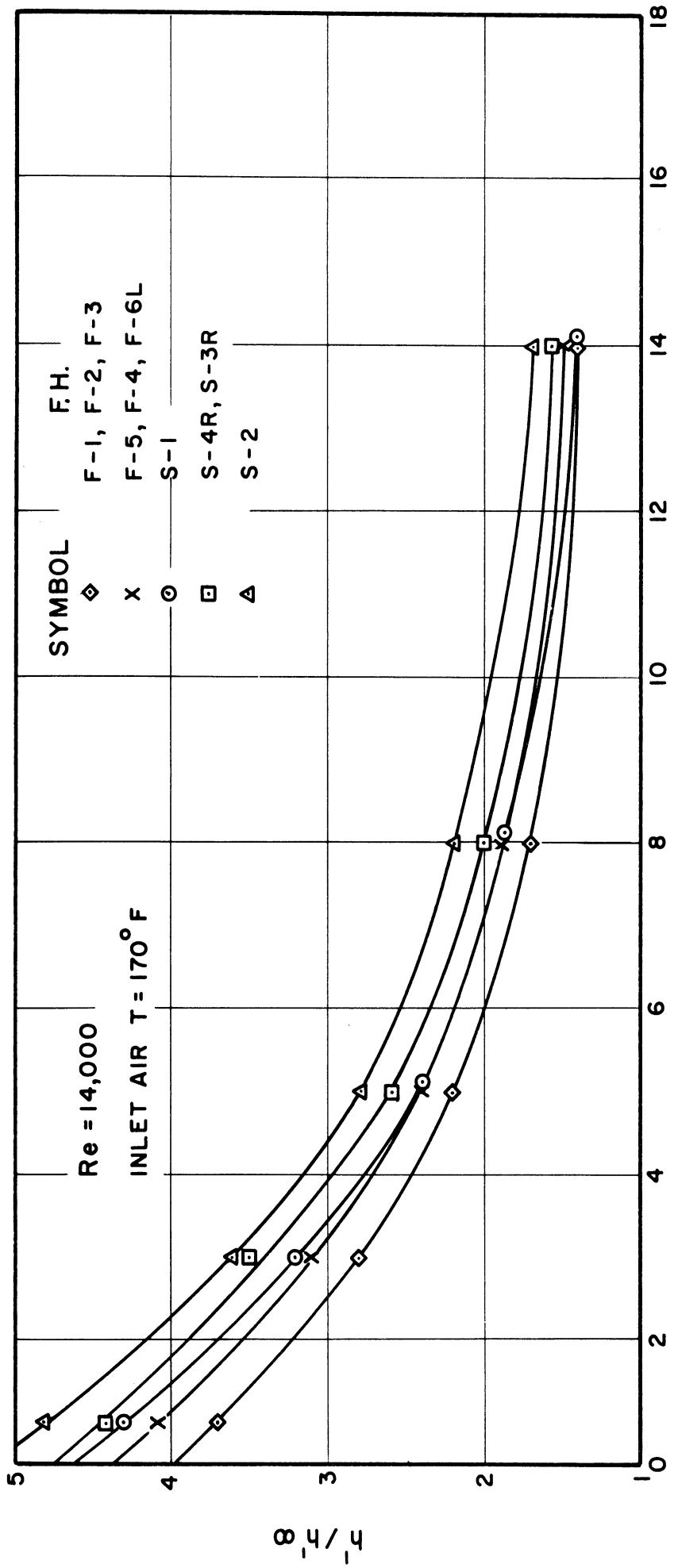

Figure 34. Coefficients Taken Without Combustion, h'/h'_{∞}, Versus Distance from Flameholder.

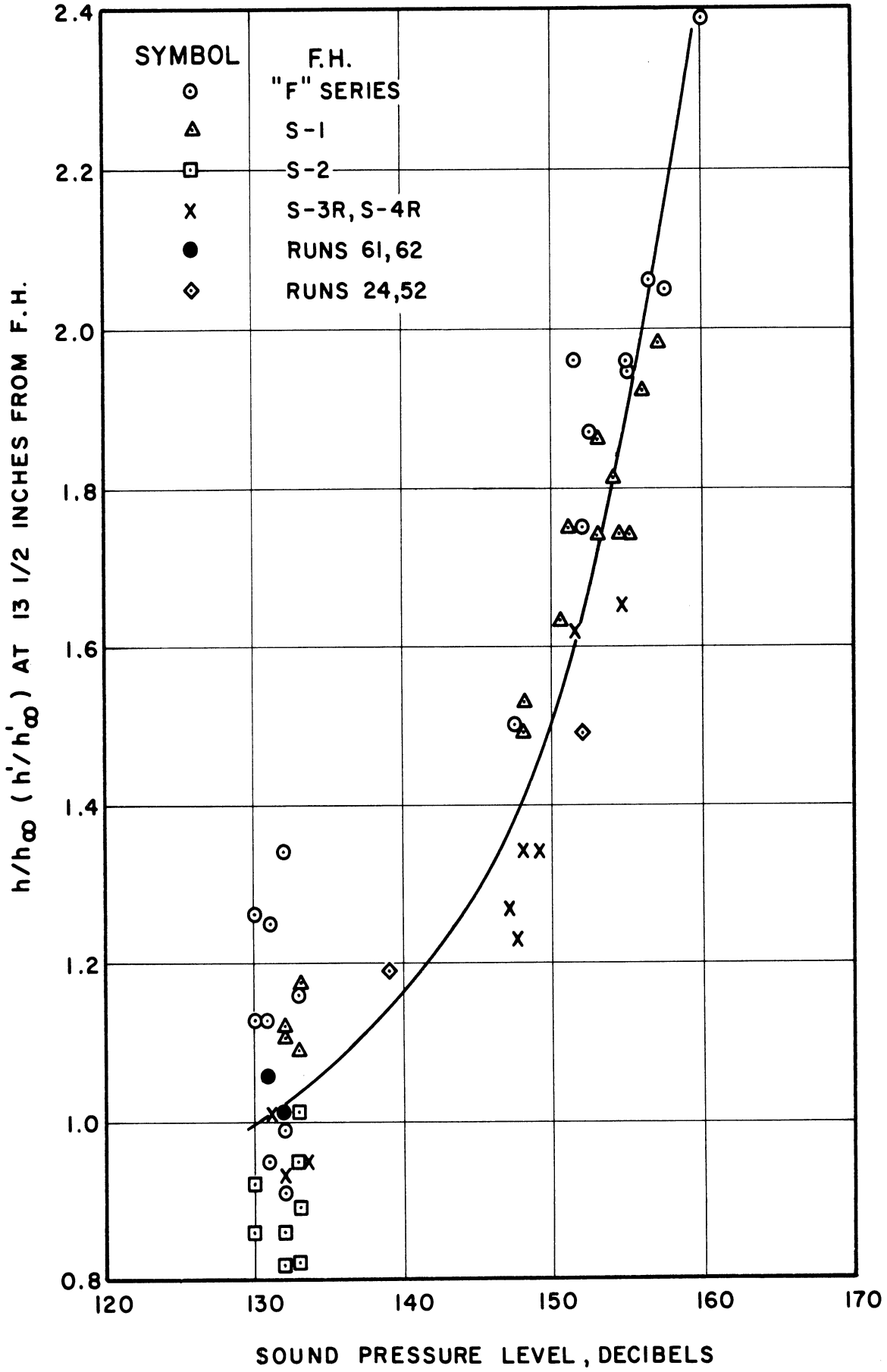

Figure 35. Local Coefficient for Convective Heat Transfer, 13-1/2 Inches from Flameholder, Versus Sound Level in db.

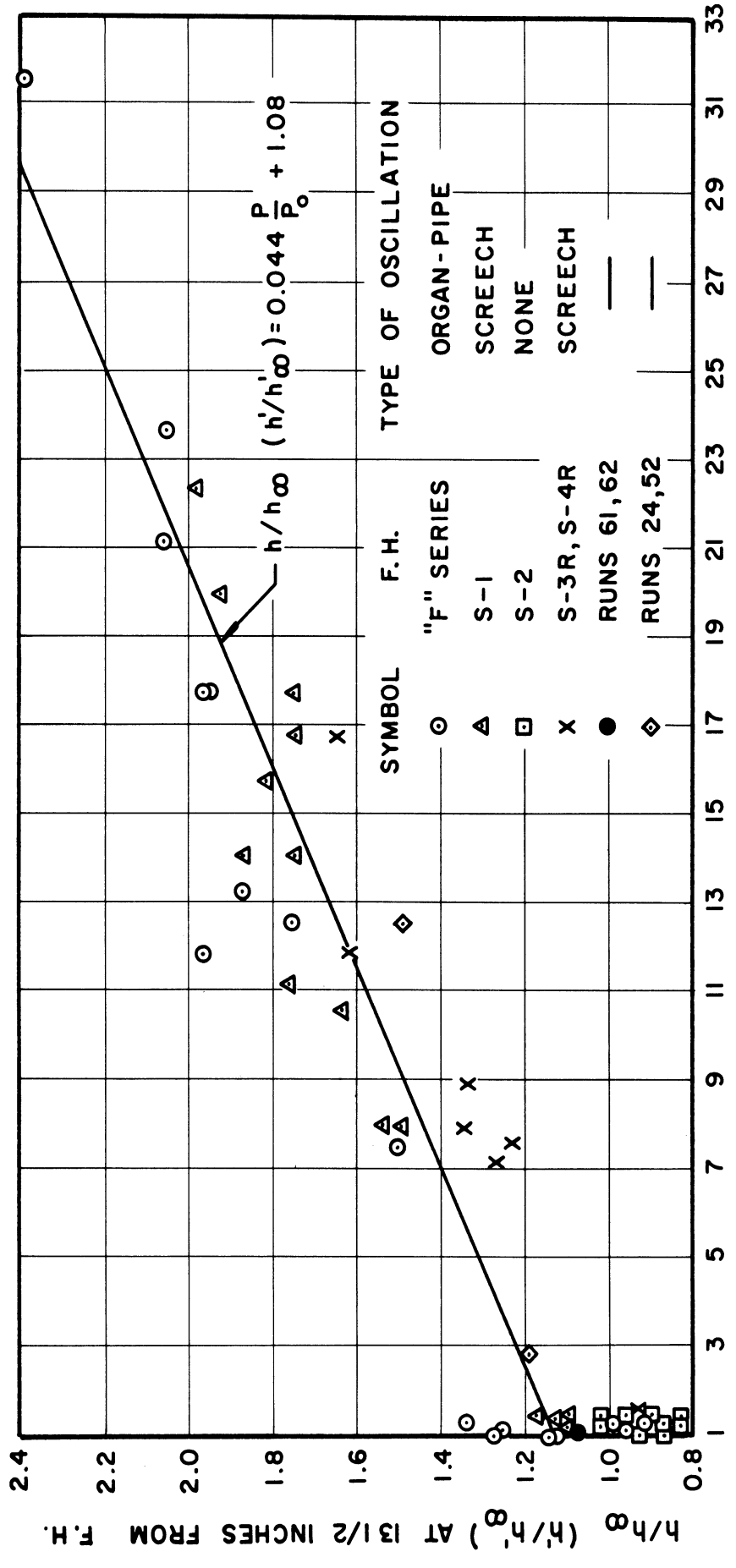

Figure 36. Local Coefficient for Convective Heat Transfer, 13-1/2 Inches from Flameholder, Versus Sound Pressure Amplitude.

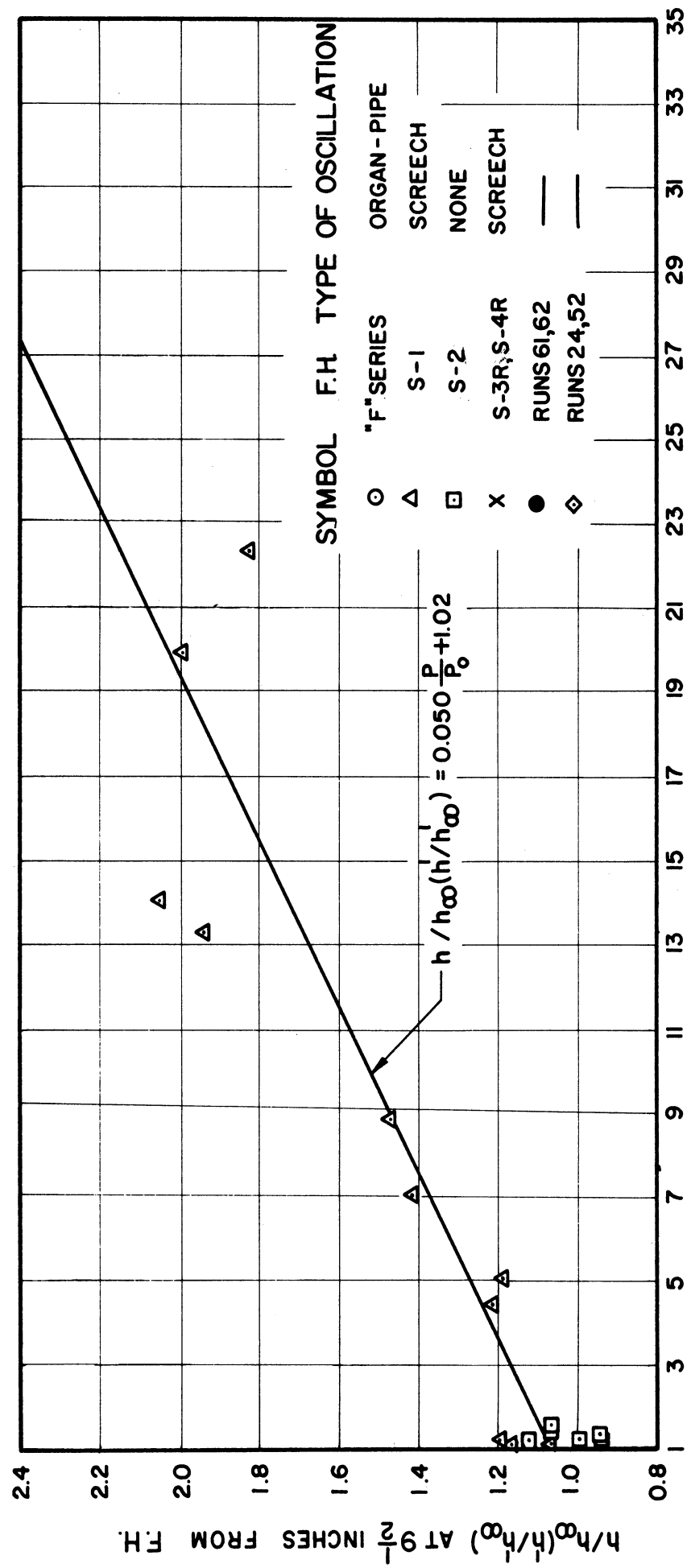

Figure 37. Local Coefficient for Convective Heat Transfer 9-1/2 Inches from Flameholder, Versus Sound Pressure Amplitude.

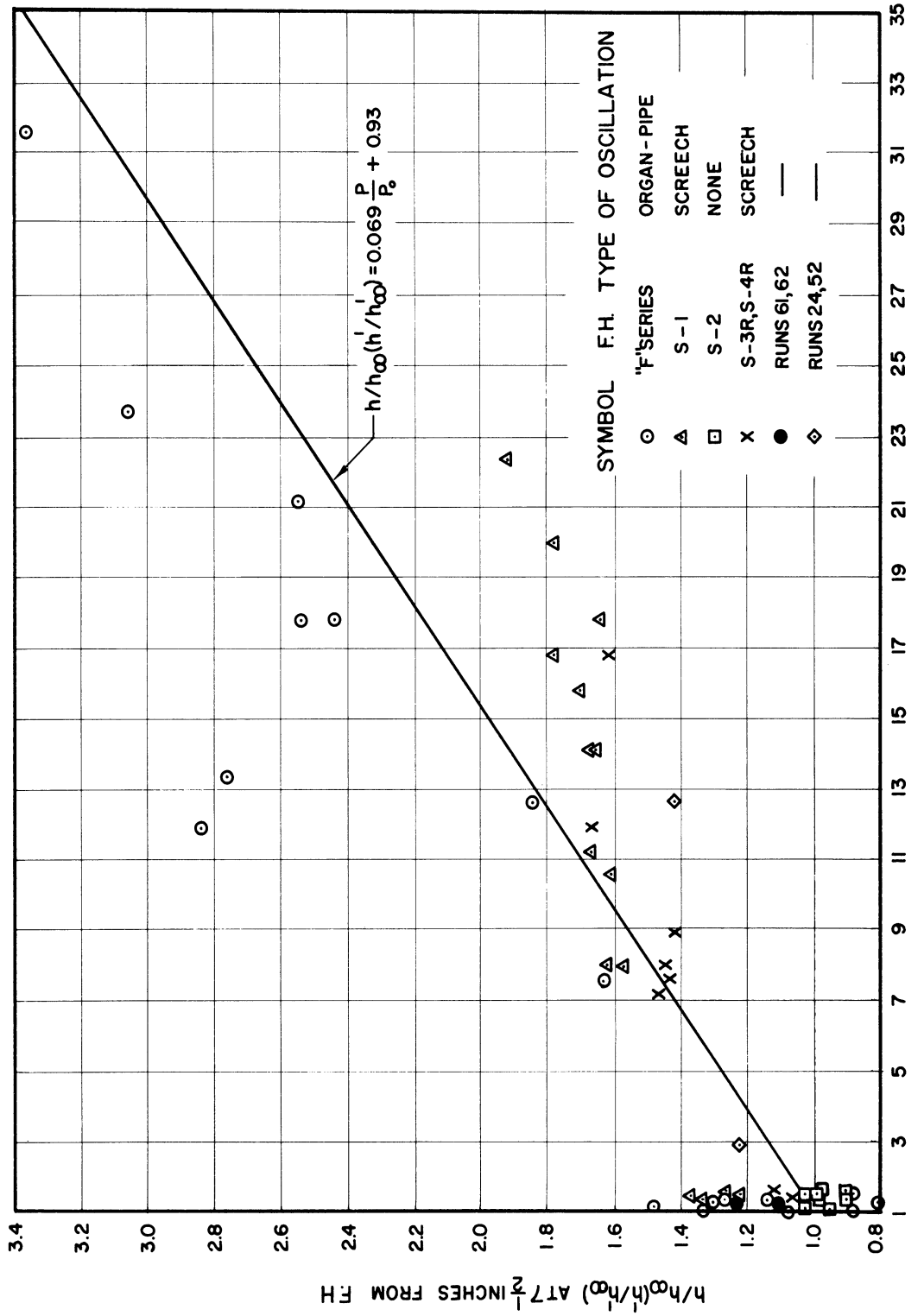

Figure 38. Local Coefficient for Convective Heat Transfer, 7-1/2 Inches from Flameholder, Versus Sound Pressure Amplitude.

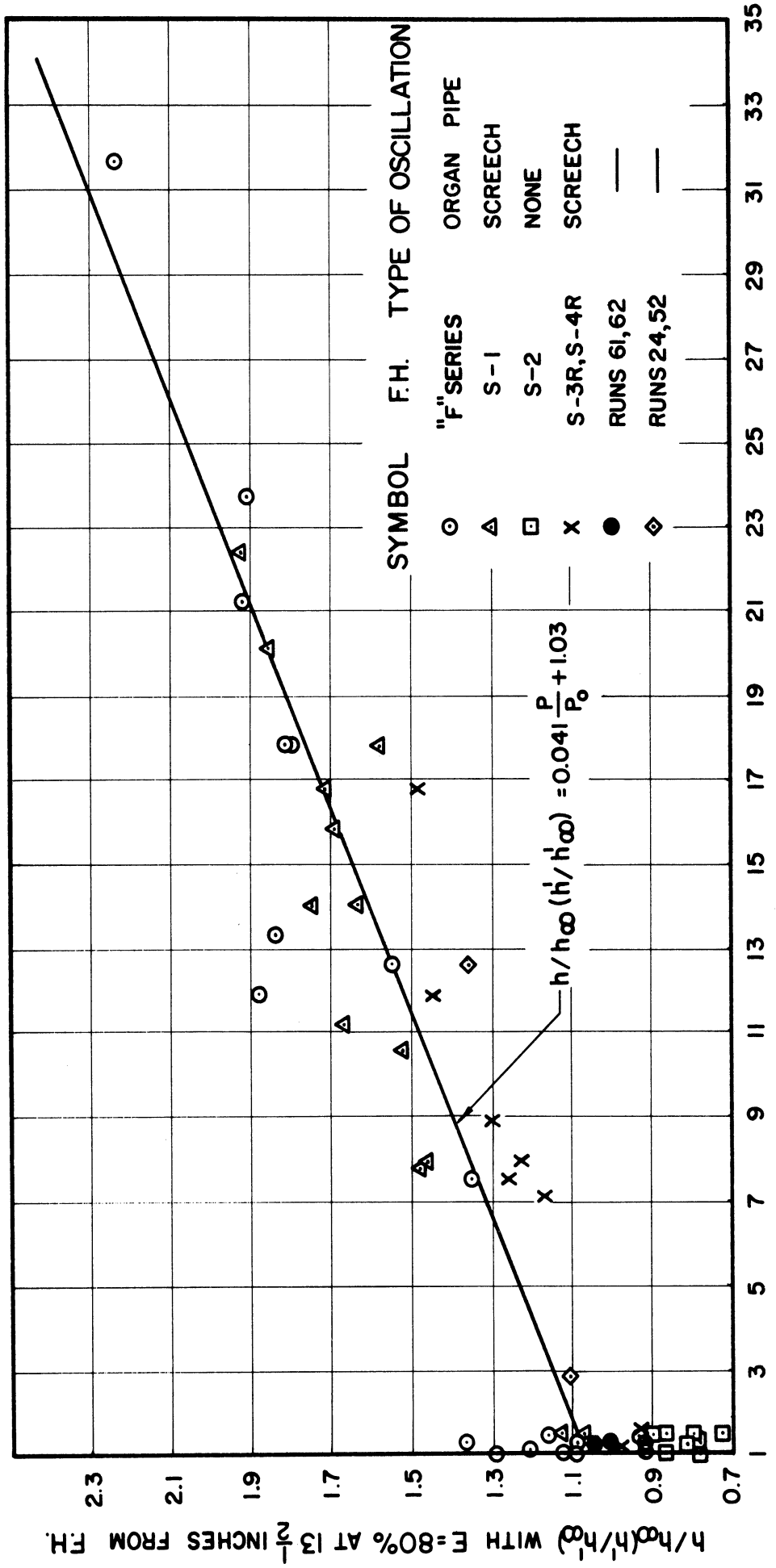

Figure 39. Local Coefficient for Convective Heat Transfer Based on E = 80 Per Cent, 13-1/2 Inches from Flameholder, Versus Sound Pressure Amplitude.

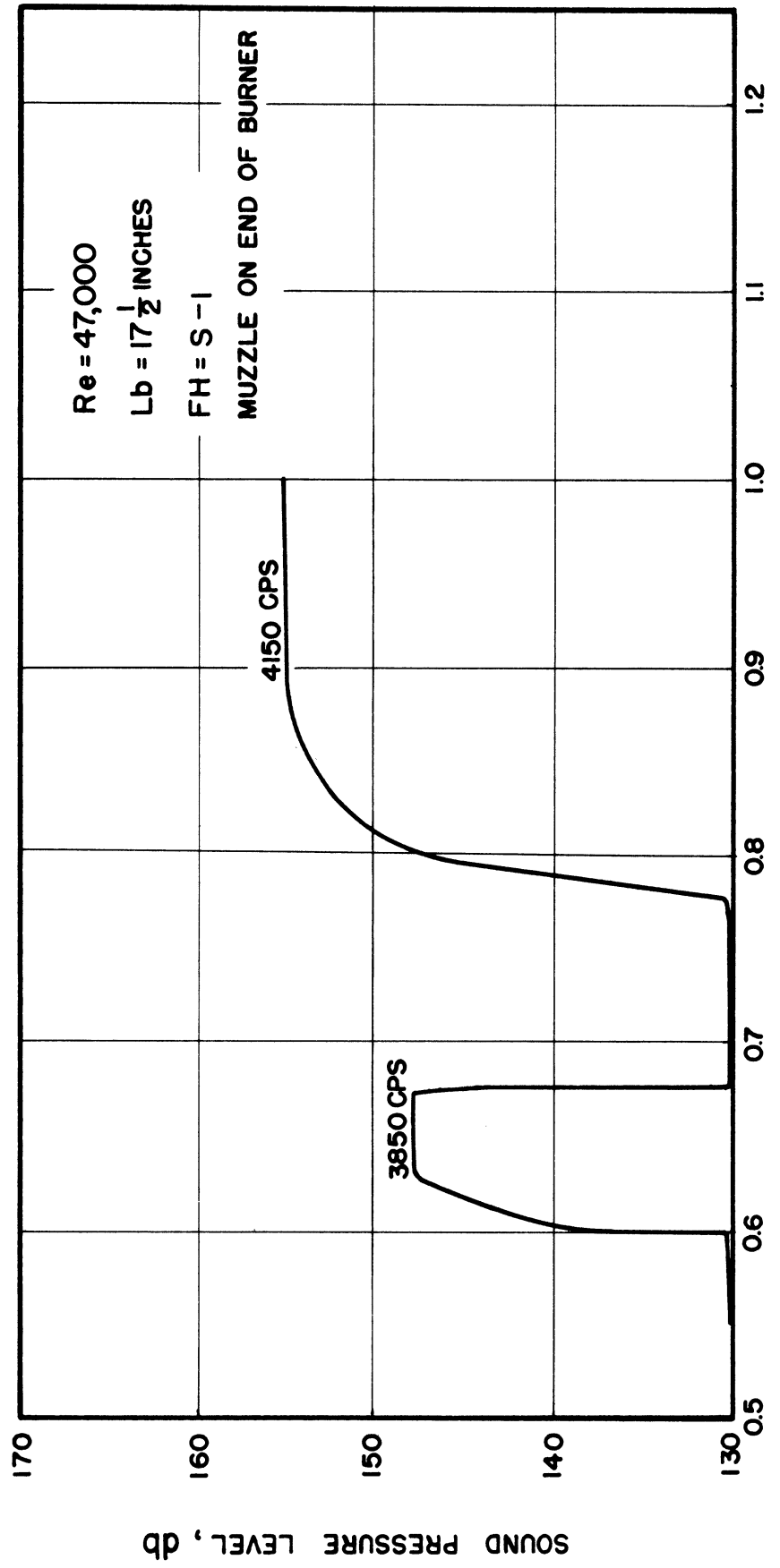

Figure 40. Behavior of Screeching Combustion with Fuel-to-Air Ratio.

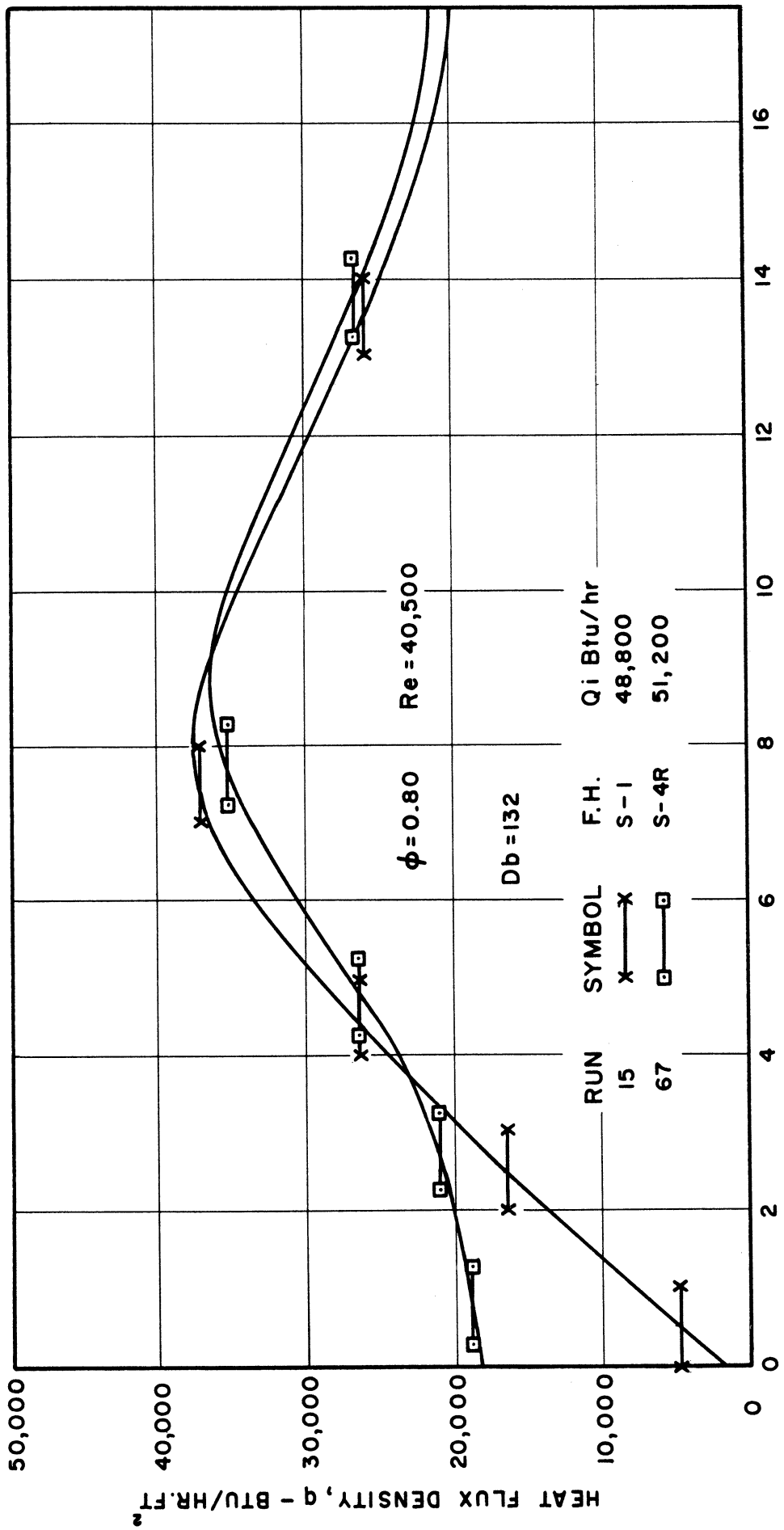

Figure 41. Profile of Heat Flux--Comparison of S-1 and S-4R Flameholders During Stable Combustion.

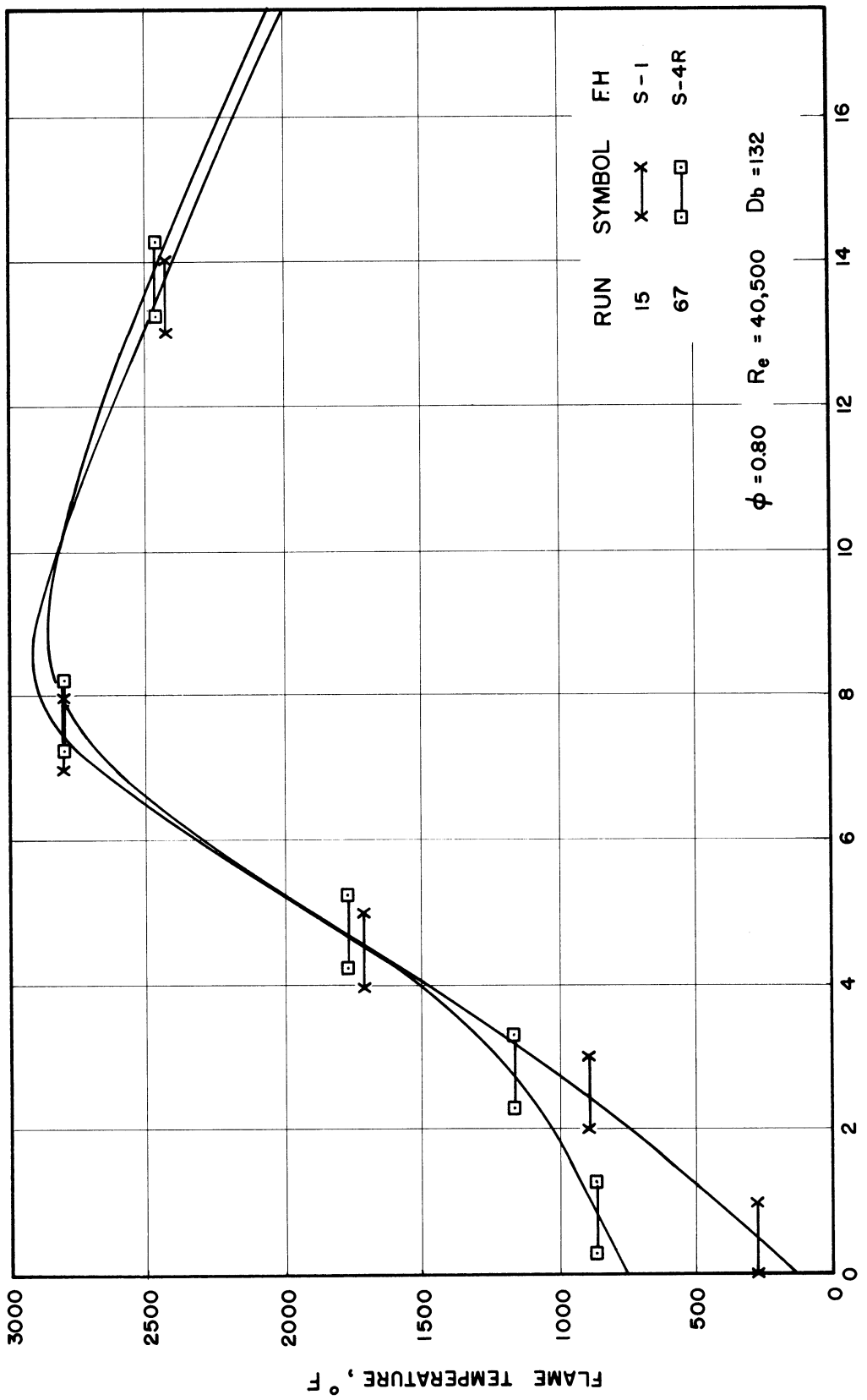

Figure 42. Temperature Profile--Comparison of S-1 and S-4R Flameholders During Stable Combustion.

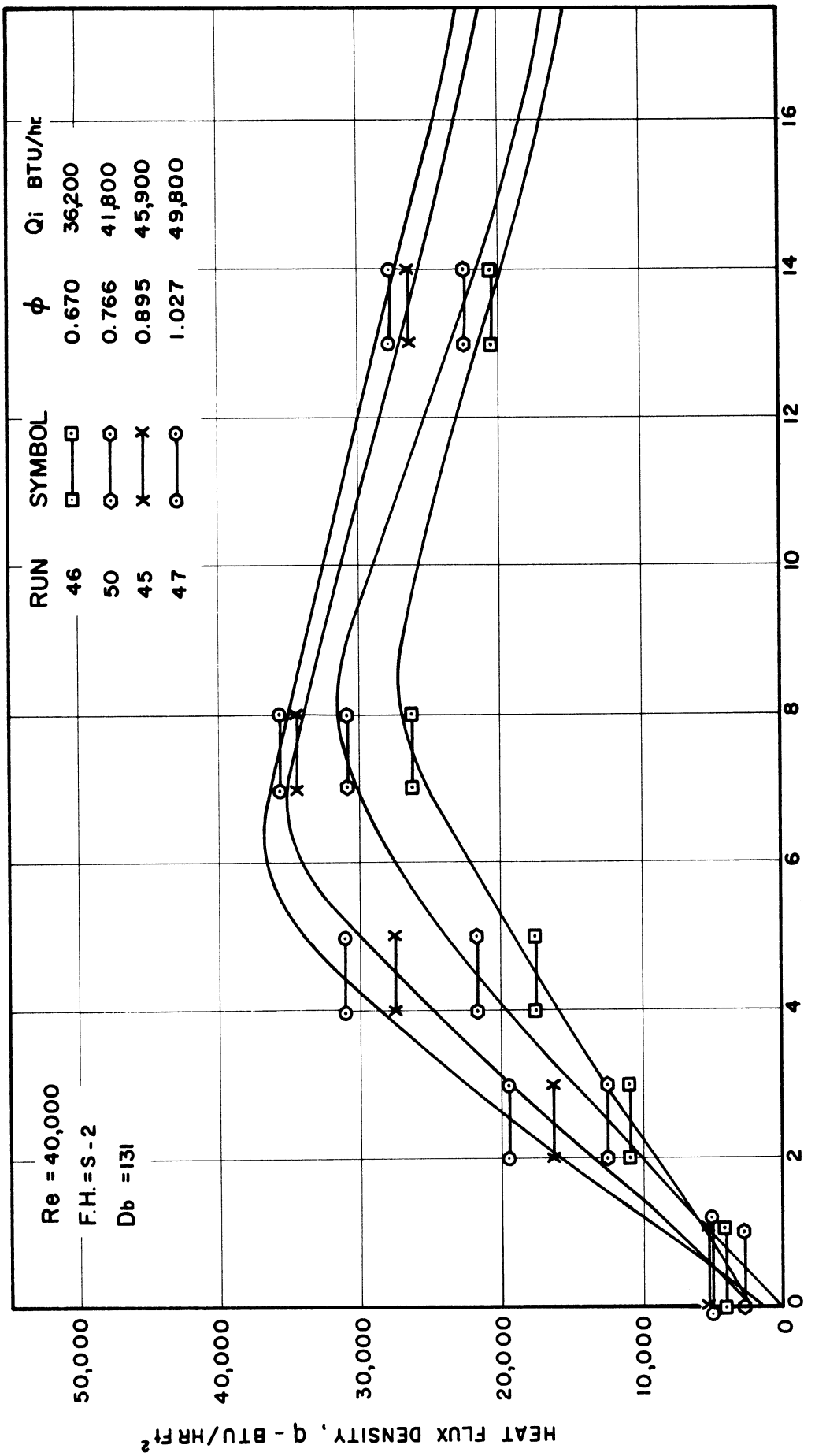

Figure 43. Profile of Heat Flux--Effect of Varying Fuel-to-Air Ratio During Stable Combustion.

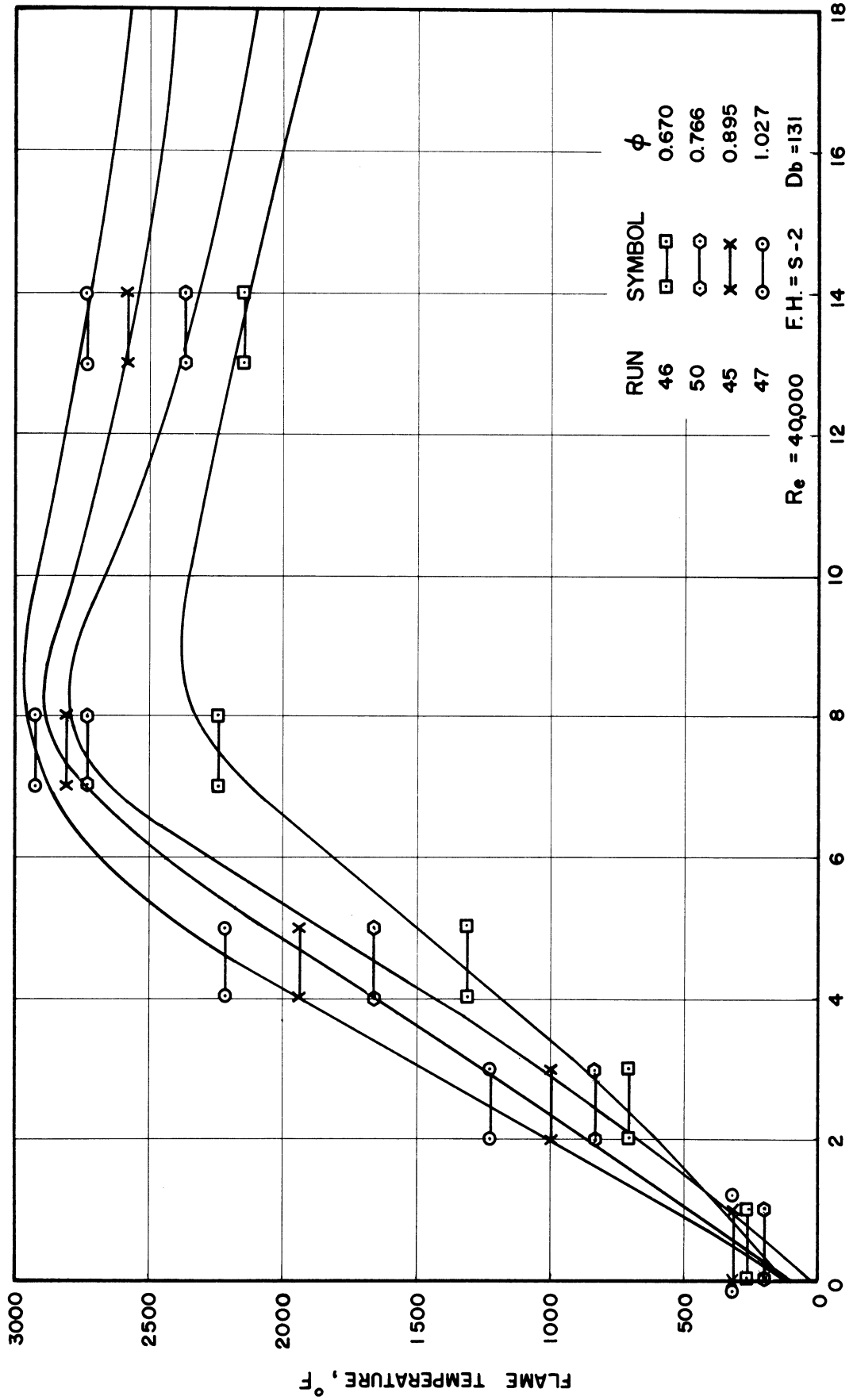

Figure 44. Temperature Profile--Effect of Varying Fuel-to-Air Ratio During Stable Combustion.

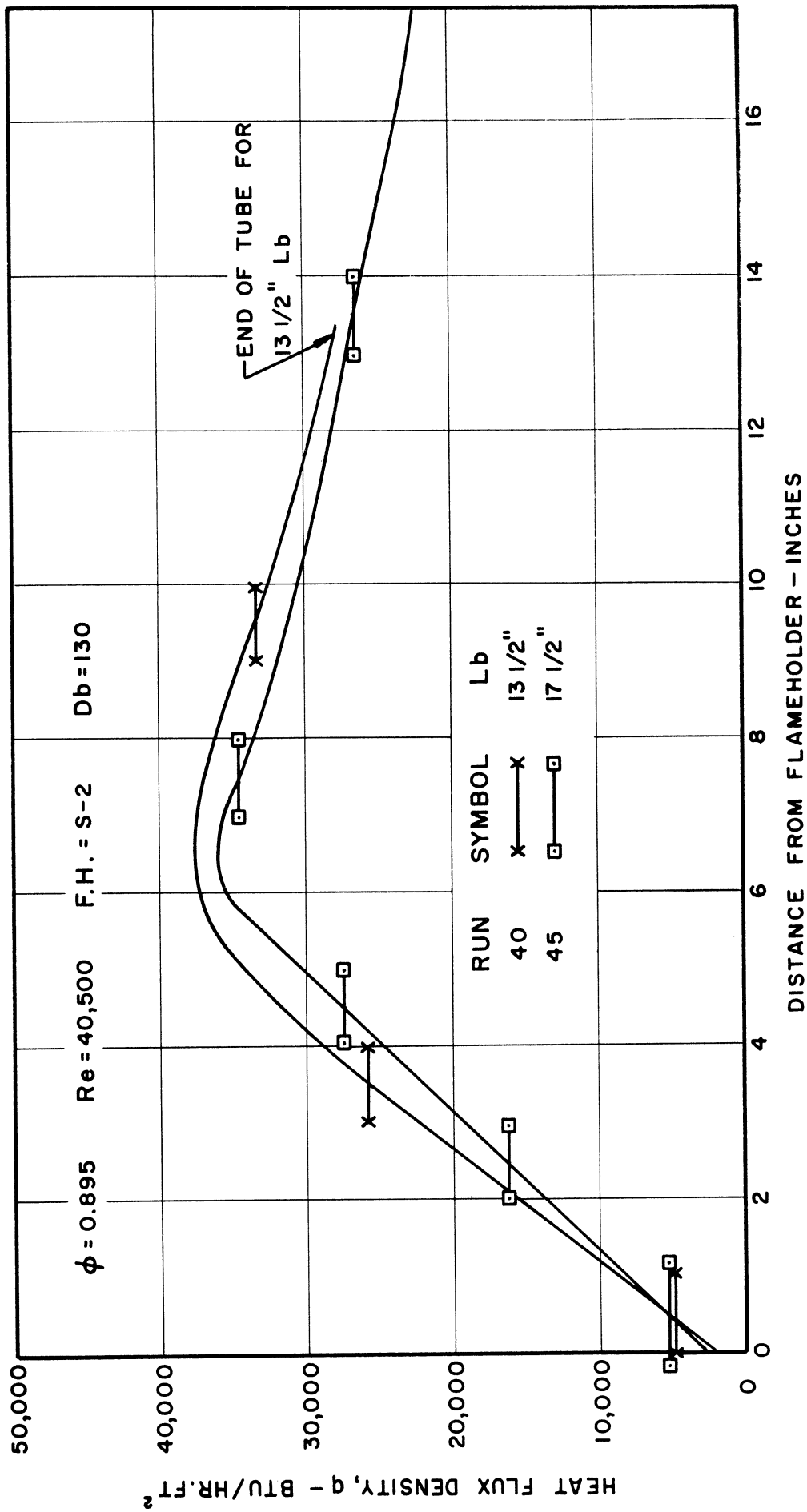

Figure 45. Profile of Heat Flux--Effect of Burning Length During Stable Combustion.

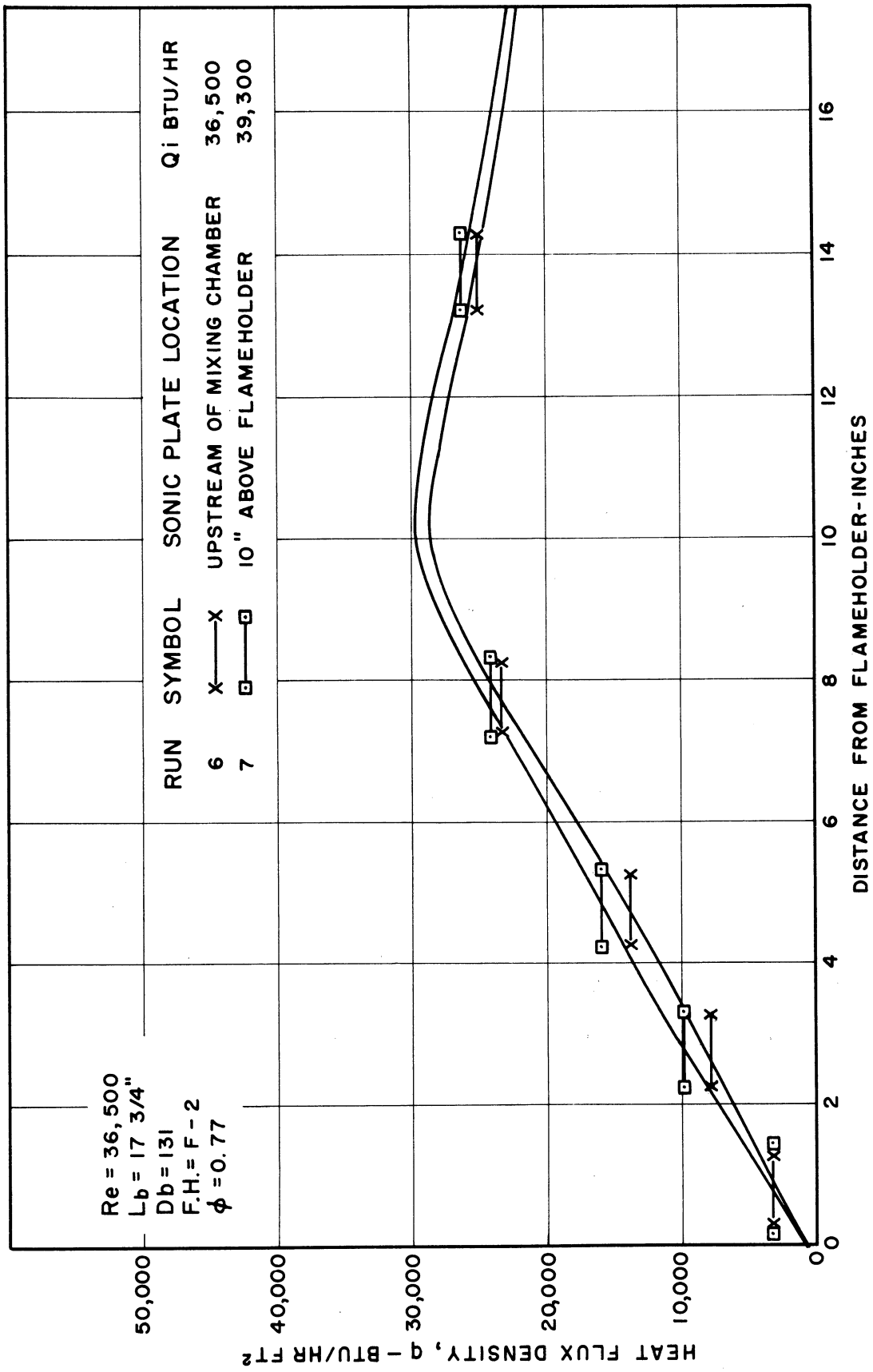

Figure 46. Profile of Heat Flux--Effect of Varying Inlet Turbulence Intensity by Moving Sonic Plate.

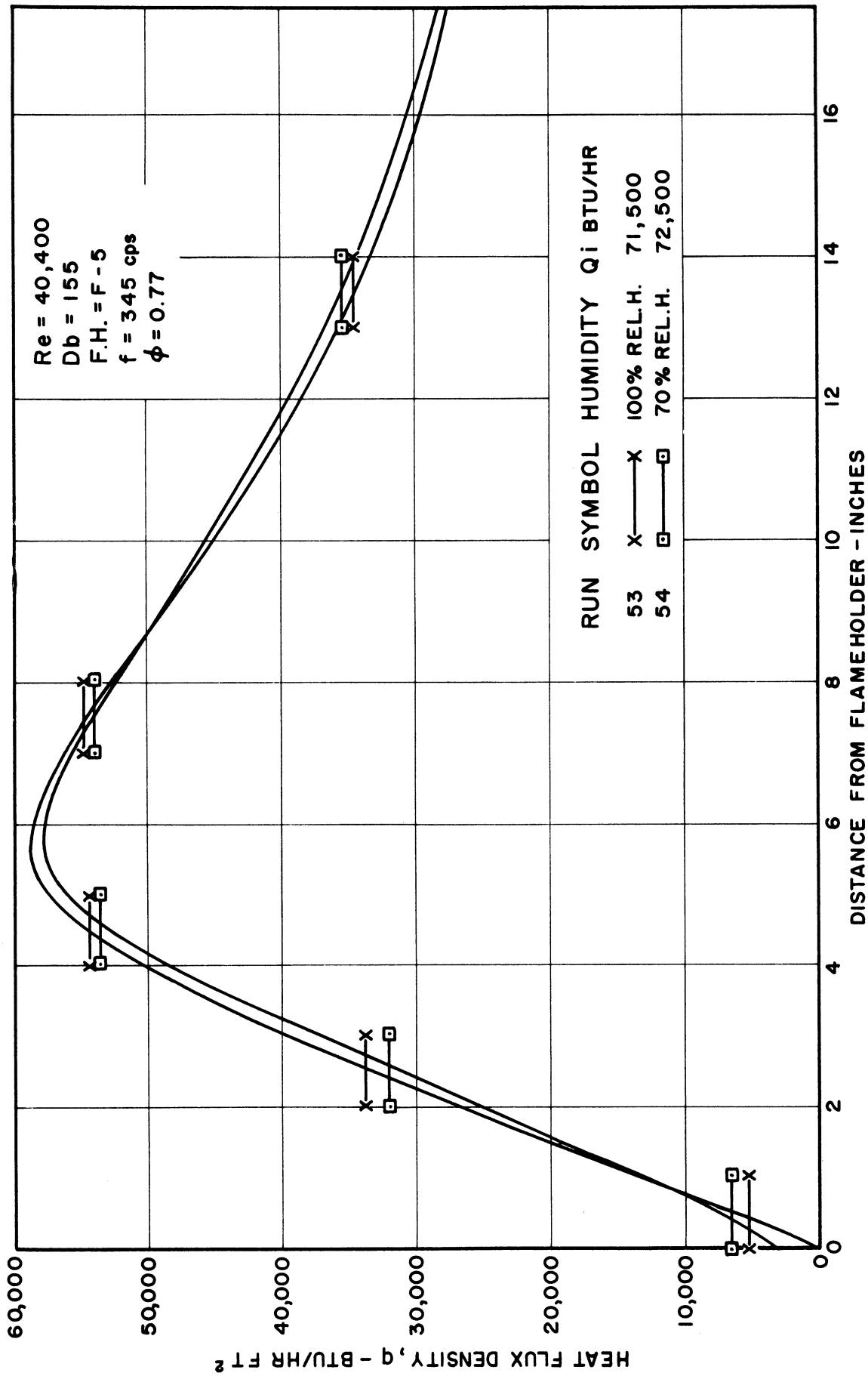

Figure 47. Profile of Heat Flux--Effect of Atmospheric Humidity.

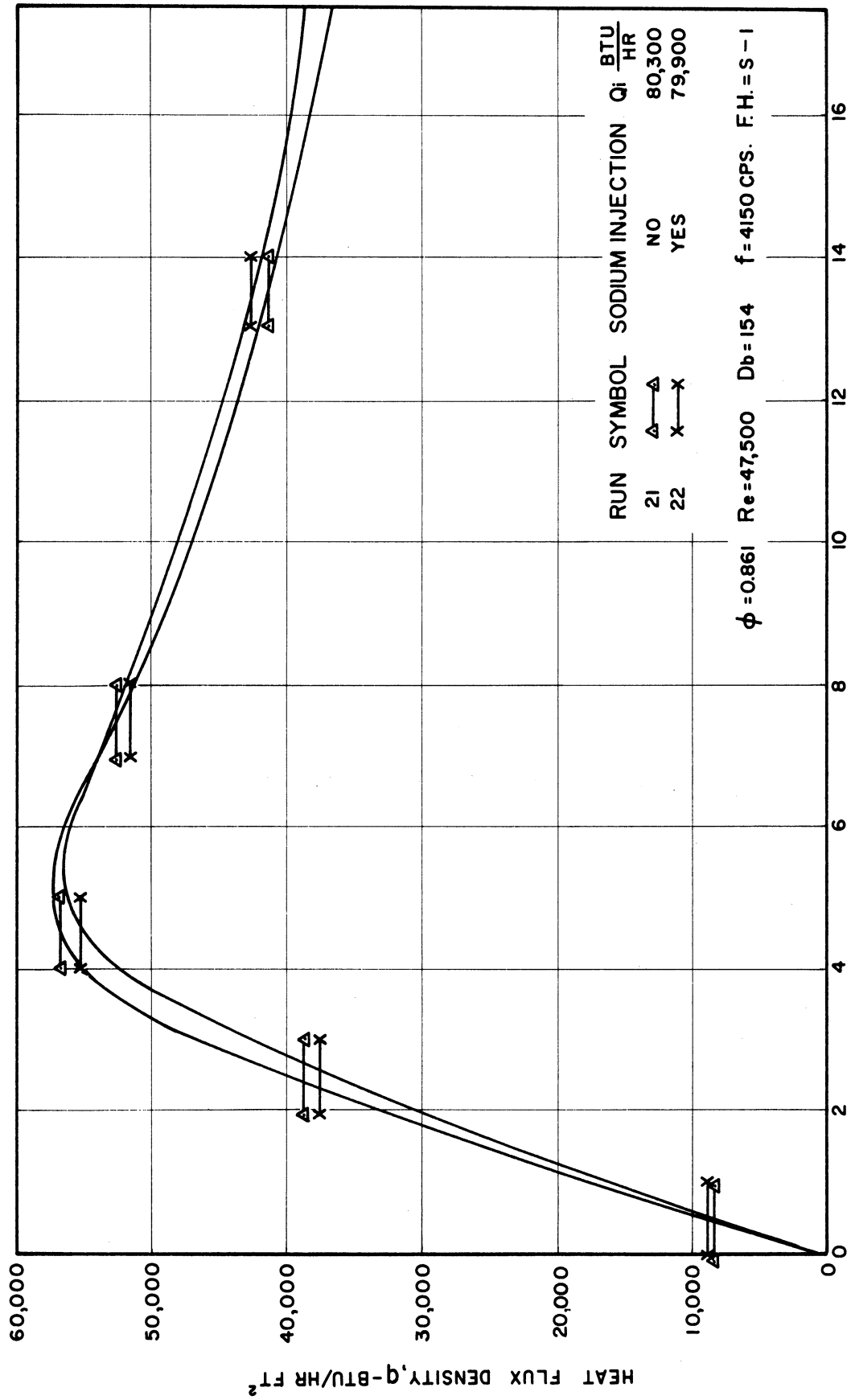

Figure 48. Profile of Heat Flux--Effect of the Injection of Sodium Salt.

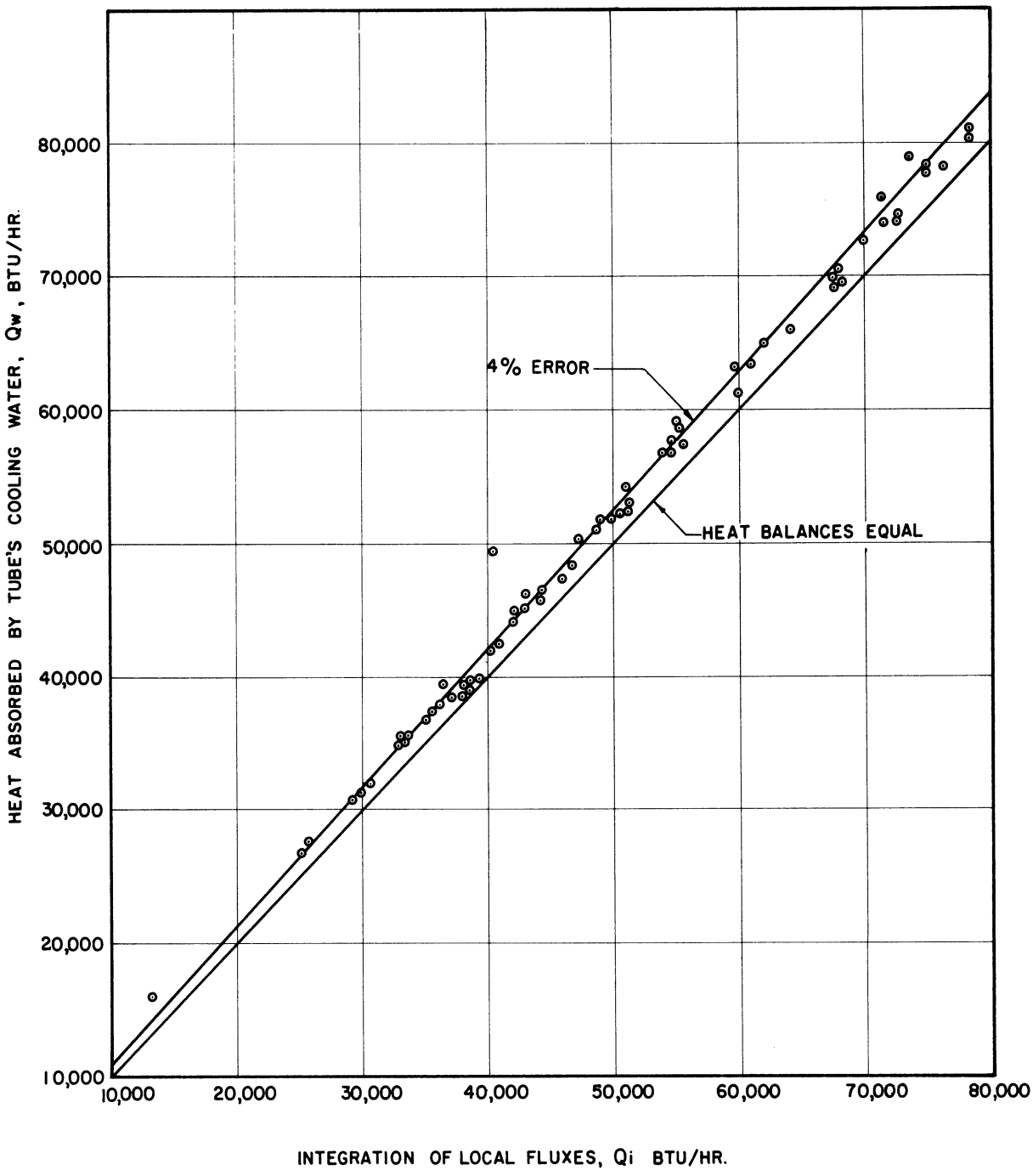

Figure 49. Summary of Heat Balances.

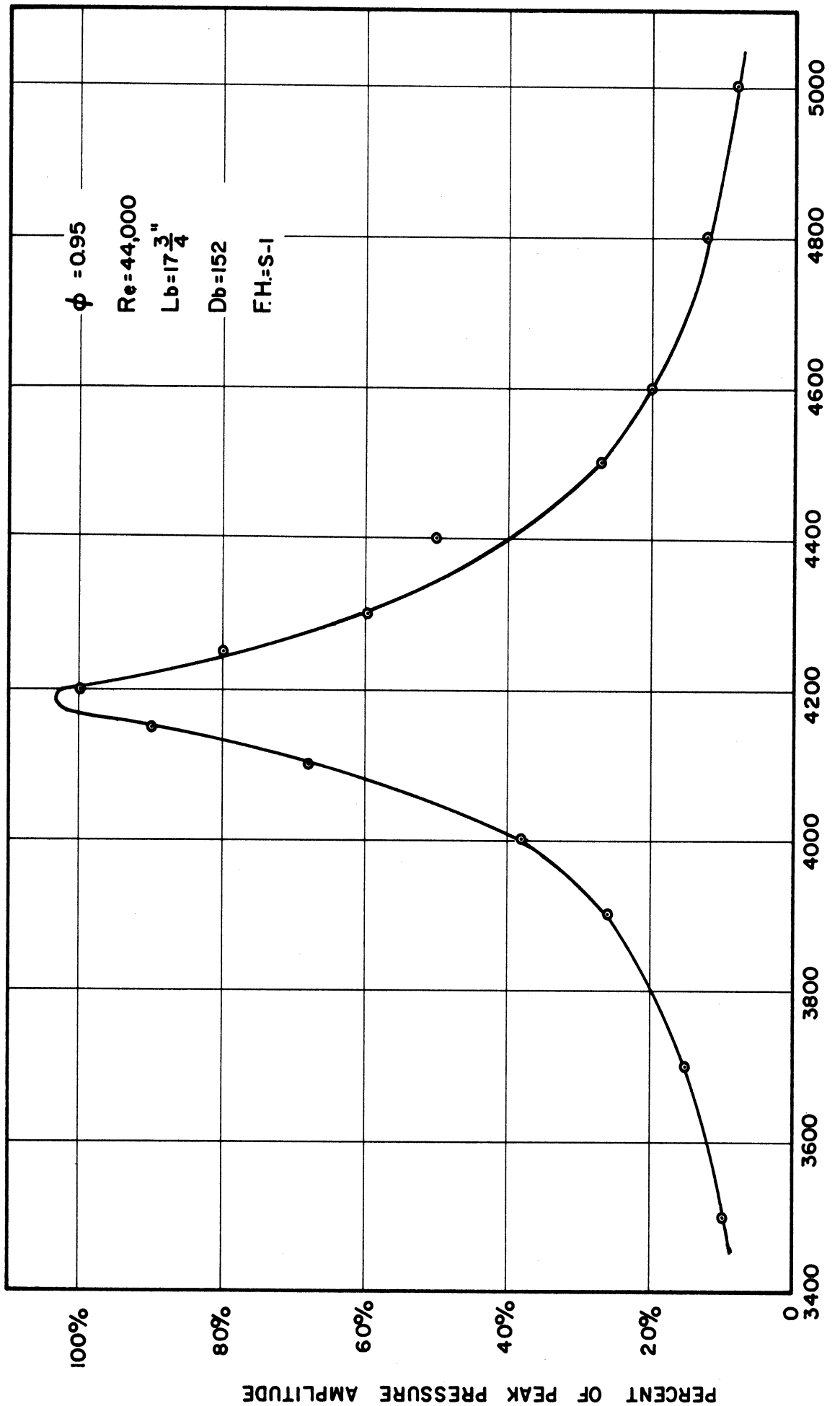

Figure 50. Typical Frequency Traverse During Screeching Combustion.

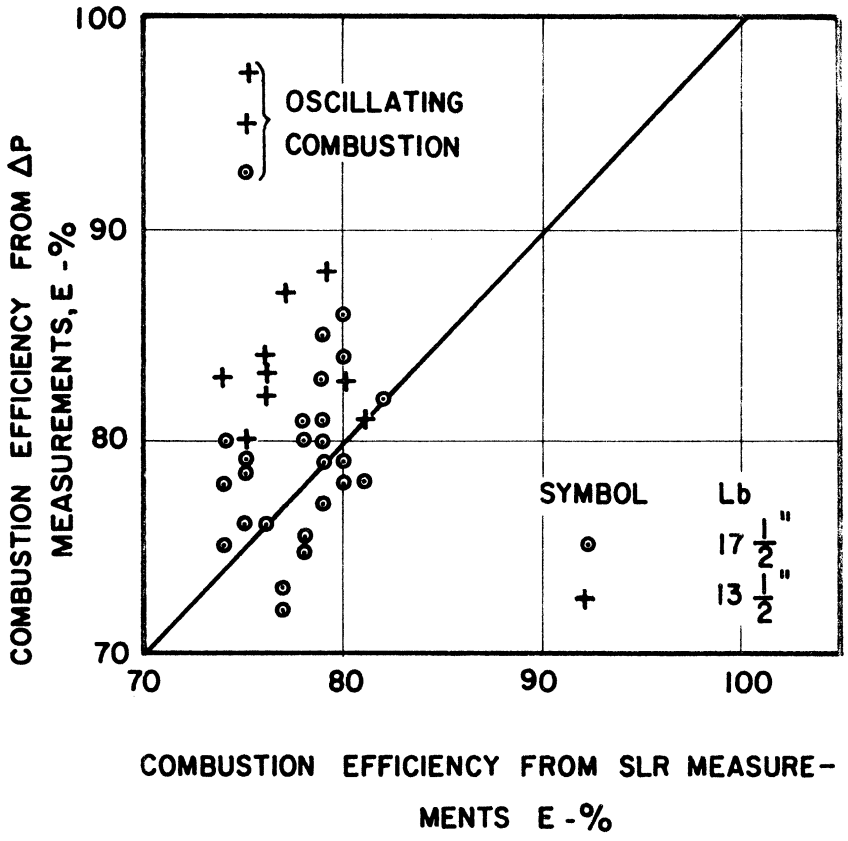

Figure 51. Comparison of Combustion Efficiencies Obtained by the SLR and Pressure-Drop Measurements.

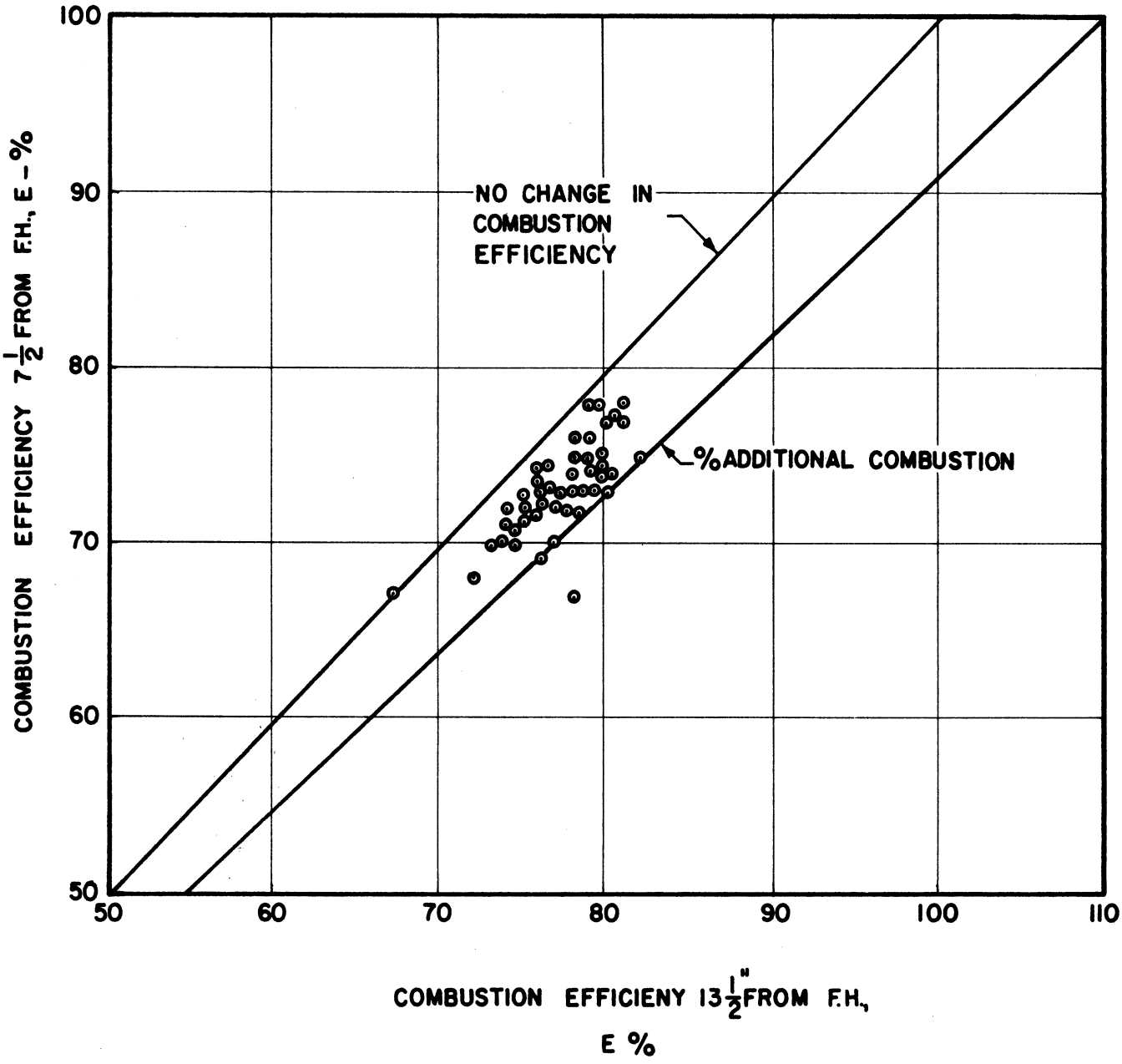

Figure 52. Difference in Combustion Efficiency at the 7-1/2 and 13-1/2 Inch Distances from Flameholder.

The local coefficients, 13-1/2-inches from the flameholder, for convective heat transfer from the flame divided by the above terms are presented in Figure 35 as a function of sound pressure level in decibels. This normalized coefficient doubles for an increase in sound level from stable conditions of 130 to 133 db to an intense oscillation of 155 to 157 db. The effect of the transverse and the longitudinal oscillation on the coefficient are seen to be very similar. The transverse oscillation is associated with the "S" series of flameholders, while the longitudinal oscillation is associated with the "F" series.

Correlation of Heat Transfer Coefficients

The extreme curvature in the correlation can be removed by changing the scale for the sound pressure level. Since the decibel scale is a logarithm of the ratio of pressure amplitudes, a logical scale is the linear one of the ratio of pressure amplitudes. The local coefficients at 7-1/2, 9-1/2, and 13-1/2 inches from the flameholder are plotted in Figures 36, 37, and 38 versus the sound pressure amplitude divided by the amplitude corresponding to 130 db.

A straight line correlation appears valid, particularly for the stations farthest from the flameholder. The correlation at 7-1/2 inches from the flameholder, where the combustion is more active and the effects of combustion more pronounced, is not clear.

In addition to the coefficients calculated from measurements of the flame temperature, heat transfer coefficients for the 13-1/2-inch distance were also calculated assuming the combustion efficiency at this

point was 80 per cent for all of the runs. The assumption of combustion efficiency determines flame temperatures at that point. These coefficients normalized as before are presented in Figure 39 and are in surprising agreement with those based on the measured flame temperature. The correlations for these coefficients at three distances from the flameholder are

$$\text{13-1/2-inches: } \frac{h}{h_\infty\, h'/h'_\infty} = 0.044\ P/P_o + 1.08 \tag{19}$$

$$\text{9-1/2-inches: } \frac{h}{h_\infty h'/h'_\infty} = 0.050\ P/P_o + 1.02 \tag{20}$$

$$\text{7-1/2-inches: } \frac{h}{h_\infty\, h'/h'_\infty} = 0.069\ P/P_o + 0.93 \tag{21}$$

$$E = 80\ \%,\ \text{13-1/2-inches: } \frac{h}{h_\infty\, h'/h'_\infty} = 0.041\ P/P_o + 1.03 \tag{22}$$

The accuracy limits are $\pm$ 10 per cent for all the correlations except at the 7-1/2-inch distance, where they are $\pm$ 20 per cent. The correlation at the 7-1/2-inch distance is justified by the existence of clear correlations at the other points.

Behavior of Burner with Increasing Fuel-to-Air Ratio

The pattern of the flame-generated transverse oscillations as a function of fuel-to-air ratio is represented in Figure 40 where sound pressure level is plotted against fuel-to-air ratio. As the fuel-to-air ratio is increased from a very low value, a 3850 cps note rapidly increases in amplitude beginning at a ϕ of about 0.6 and reaches a plateau of about 148 db. At a ϕ of about 0.68 the oscillation suddenly ceases; then beginning at a ϕ of about 0.77 a 4150 cps note rapidly increases in amplitude to a higher plateau of about 155 db.

Stable Burners

Some additional profiles of local rates of heat transfer are presented to show the effects of flameholders, flow rates, and fuel-to-air ratio in a stable burner. Also runs taken to check possible sources of error are presented.

In Figures 41 and 42, the ring-type flameholder in compared with the screen-in-annulus type with regard to the heat transfer and temperature profiles. The effect of increasing the fuel-to-air ratio with the oscillations damped is shown in Figures 43 and 44. It is noted that the temperature profiles increase in a general fashion like the heat transfer profiles. The effect of burning length is compared in Figure 45 for stable combustion.

In a previous figure, number 10, the effect of four flameholders on the heat transfer profile is shown. The curve for Run 61 shows a step increase 5 inches from the flameholder because a 1/32-inch asbestos sheet lined the inside of the tube from 5 inches above to 5 inches below the flameholder for this run. The purpose of this liner was to increase the inside surface temperature to intensify screech as was done earlier by a decrease in the cooling of the tube. However, its acoustical impedance was low and so actually proved to be an effective damper of screech.

Effect of Inlet Flow Conditions

The effect of changing the inlet flow turbulence is shown in Figure 46, where in Run 7 the sonic plate is 10 inches above the flameholder and in Run 6 it is upstream of the entire mixing chamber. Negligible

effects are also shown by a similar comparison, using Runs 2 and 4. The humidity of the air did not vary much due to its compression to 105 psia, which lowered its humidity to 0.003 lbs/lb, or below the lowest atmospheric humidity encountered. The effect of running on a rainy day compared to a day of low humidity is shown in Figure 47. Since in most runs the sodium salt was injected only during the SLR measurements, there is the question of what change occurred in the heat transfer profile. In Figure 48, a comparison of Runs 21 and 22 shows a negligible effect. Other similar comparisons may be made with Runs 26 and 28 or 48 and 49.

Heat Balances

The difference between the total heat transfer through the tube as determined from the tube's cooling water and that determined from the integration of the local heat flux is shown for each run in Figure 49. The heat transfer determined by the cooling water is consistently high, averaging about 4 per cent above the integrated value.

Pureness of Flame-Generated Notes

When the frequency spectrum is scanned during a resonating oscillation, a typical bell-shaped curve is obtained, such as presented in Figure 50. The band width of a pure note measured by the sound analyzer is 2 per cent of the measured frequency. The band width of the flame-generated transverse oscillations averaged 3.7 per cent and that of the organ pipe 3.3 per cent. Only in Runs 24 and 52 did more than one note register greater than 10 per cent on the sound analyzer. In these runs a relatively weak organ pipe note was present along with the strong transverse note.

Comparison of Combustion Efficiencies

The combustion efficiencies determined by the two independent methods, that of pressure-drop and SLR measurement of flame temperature, are compared in Figure 51. The averages of the two methods for a 17-1/2-inch burning length and a stable burner are within 2 per cent of each other. The pressure-drop combustion efficiencies, when the burning length is 13-1/2-inches, are consistently higher than those determined from flame temperature measurements. When the sound level increases due to a resonating note, the pressure-drop combustion efficiencies become meaningless, being over 100 per cent except for the three runs with low resonating intensities, the points for which are circled in the figure.

Additional Combustion After 7-1/2-Inches

The combustion efficiencies for the 17-1/2-inch burning length are evaluated at both 7-1/2-inches and 13-1/2-inches from the flameholder based on the SLR measurements at these points. The plot of one against the other in Figure 52 reveals that additional combustion occurred in every run between the 7-1/2-inch distance and the 13-1/2-inch distance. On the average this increase was 5 per cent.

DISCUSSION

A significant result of this study is the correlation of forced convective heat transfer with sound pressure level. Also of importance is the finding that a transverse oscillation is just as influential on the heat transfer process as a longitudinal oscillation of the same intensity. The reported failures of burners in the literature due to screeching combustion are, therefore, probably connected with rising wall temperatures and subsequent increases in the intensity of the oscillation. The evidence that the acoustic oscillations cause greater hydrodynamic changes than changes in the combustion phenomena is presented as well as explanations for the various results and identification of the modes of oscillation.

The measurement of the local heat fluxes is the primary objective of this study, with the measurement of flame temperature being a secondary objective. Whereas the measurements of heat flux have been covered previously and their accuracy shown to be high, the accuracy of the measurement of flame temperature needs further discussion.

Flame Temperatures

In this combustion study, the average gas temperatures determined from sodium-line-reversal measurements are substantiated by the temperatures determined from pressure-drop measurements in the case of stable combustion. Accurate determinination of heat transfer coefficients does not require temperature measurements accurate to the nearest degree

or even ten degrees because the temperature differences are large, approximately 2000°F. The accuracy of the coefficient is not altered by more than 5 per cent even if the flame temperatures are in error by 100°F. The limits of the SLR inaccuracy are estimated in the section, Experimental Theory and Accuracy, to be - 50°F to + 90°F. Since the bulk mean temperature is given by the relation

$$T_b = 0.82\ (T_{SLR} - T_s) + T_s, \qquad (9)$$

the inaccuracy limits on the average temperature are only 82 per cent as large or approximately - 40°F to + 75°F, which corresponds to a 3.7 per cent error in a 2000°F difference.

If the distribution factor of 0.82 is in error, it is probably a consistent error and would result in a consistent error in the coefficients and thus not disturb the correlation. However, this factor is not only corroborated by the pressure-drop measurements, but also by the thermocouple and pitot-static tube traverses as discussed in the section, Experimental Theory and Accuracy. Good evidence of how uncritical the gas temperature is in determining the correlation of heat transfer coeffients is given by those coefficients at the 13-1/2-inch distance which were determined from the assumption of a combustion efficiency of 80 per cent at that point.

Temperature Profiles

It is recalled that the temperature profiles depended on the scaling of the cold flow coefficients for heat transfer in such a way

that at the 4-inch level they are equal to the measured value during combustion. This method of evaluating the coefficients does not assume that the combustion process or the oscillation does not have any effect on the coefficients, but rather assumes that the effect of the combustion and oscillations is the same along the entire tube. This assumption is reasonable since the combustion chamber is only slightly more than three diameters long. This method of employing cold flow data is reasonable since there is evidence in the literature that convective heat transfer from high temperature combustion products can be approximated from empirical data for non-burning gases.[35][82] However, possible errors in the cold flow data plus the possibly large change in flow pattern caused by combustion mean that the temperature profiles have some degree of uncertainty.

Physical Versus Combustion Effects of the Oscillations

Several indications exist that the sonic oscillations affect the hydrodynamic conditions such as turbulence intensity and boundary layer thickness to a greater extent than the combustion phenomena, such as efficiency and flame speed. The correlation of the heat transfer coefficients with sound level is strong evidence that changes in the hydrodynamic phenomena are primary effects of the oscillations. The studies of several investigators[3][33][67] have indicated that a change in the flow pattern is associated with the flame-generated oscillations, particularly the periodic formation of vortices at the flameholder lip.

The similarity of the temperature profiles and the rather constant values of combustion efficiency for a damped versus an intense oscillation are two good indications of the relative insensitivity on the part of the combustion process to the oscillations. However, visual observations indicate an increase in flame speed, since a marked shortening of the flame is observed when oscillations, transverse or longitudinal, set in. Kippenham[36] and Markstein[50] concluded in their studies on the effect of oscillations on flames that apparent changes in flame velocity should be ascribed to changes in the flame area caused by the oscillations.

Corroboration by Other Investigations

Corroborations of the proposed correlation for the heat transfer coefficients as a function of sound pressure level are given by the works of Jackson[28] and Harrje.[22] They both found that the heat transfer coefficient increases with the sound pressure level independent of frequency. Harrje in his study of fully developed turbulent pipe flow found that the heat flux increase was linearly proportional to the amplitude of the oscillation. Jackson found a critical sound level of 118 db below which the imposed sonic oscillations had little effect.

A Reference Sound Pressure Level

It appears that the critical sound pressure level is a relative value. This is the main reason for choosing the sound level in the stable burner as the reference level and thus setting the ratio of pressure amplitudes equal to one there. In future studies this reference level may be different but will probably be the sound level for the flow, free of an applied or generated sonic field.

Effect of Frequency

One interesting result is the fact that the frequency or mode of oscillation has very little effect as long as the intensity is constant. At 13-1/2-inches from the flameholder very little difference exists in the coefficients for transverse or longitudinal oscillations; however, at 7-1/2-inches from the flameholder, the two modes of oscillation produce different coefficients with the longitudinal mode producing larger coefficients than the transverse oscillations.

The following explanation is offered. The longitudinal oscillation has a pressure antinode at the flameholder. The periodic increase in pressure at the flameholder periodically slows the flow of the unburned gases past the flameholder. During a period of slow flow, the flame in the region of most active combustion propagates closer to the tube wall causing higher rates of heat transfer and a pronounced peak in the heat transfer profile. The transverse oscillation also causes periodic fluctuations in the flow, but since they are at a much higher rate the flame has less time to propagate to the wall.

Sundstrom[78] found a flattening of the peak in the heat transfer profile with the longitudinal oscillation, and he states that the movement of gas particles back and forth is causing this flattening. However, in his case the longitudinal oscillation was resonating between the exhaust end and a plenum chamber, which acted as an open end several feet upstream from his low blockage flameholder. The pressure antinode was well upstream from his flameholder, so that instead of large pressure fluctuations downstream from the flameholder there was considerable gas particle movement.

Agreement with the Literature

The general similarity in the effects of the two different frequencies is substantiated by the literature. Jackson, Harrison, and Boteler[28] in their study of convective heat transfer with sonic fields imposed were not able to draw any conclusions as to the effect of frequency, although they varied the frequency from 125 cps to 2400 cps. In his heat transfer study, Havemann[23] found the frequency effects minor compared to the sound level. However, Tailby, in a study imposing sonic fields on a diffusion flame, found the 600 cps note to be more effective in promoting mixing and heat transfer than the 1700 cps note. Harrje[22] found the frequency was not the important variable but rather the amplitude of the unsteady velocity component.

In the present study, not only are the frequencies different but the entire mode of acoustical oscillation, so that the direction of particle movement is completely changed. The transverse oscillation causes particle movement around the tube's circumference and the longitudinal oscillation in the direction of the tube's axis. It also is worth noting that particle displacement in a sound field is reciprocally related to frequency for a given sound pressure, so that the lower frequency note might be expected to cause the greatest changes.

Further comparison of this study with Sundstrom's study[78] of longitudinal oscillations in a one-inch diameter burner reveals one other major difference. The organ-pipe oscillations in his study did not cause as great an increase in the total heat transfer to the tube as they did in

this study. The explanation rests mainly on the fact that the heat transferred to the tube in his study averaged approximately 25 per cent of the total heat released by the combustion process compared to about 10 per cent in this study. Thus the temperature of the gas fell twice as rapidly in the small tube with its greater surface area per unit volume than in the large tube.

Difference in Correlations

The variation in the correlation for the three distances from the flameholder may be caused by the influence of the combustion process. The positions closer to the flameholder are in general closer to the region of most active combustion. The turbulence intensity and the temperature and velocity profiles may be influenced by the combustion. By the 13-1/2-inch distance the flame had in general terminated except for the stable runs of very low fuel-to-air ratio. Therefore, the correlation at this position is probably the most free of combustion influences.

Explanation of Burner Failures

The increase in intensity of screech with higher wall temperatures is a significant finding. It leads to an explanation for the burner failures reported in the literature.(83) If the cooling of the combustion chamber were inadequate and an unexpected screeching combustion set in, the wall temperature would increase due to the increased heat transfer associated with the oscillation. Furthermore, the higher wall temperature would cause an increase in the screech intensity, and thus the amplitude of the oscillation and the wall temperature could reach very large values.

Determination of Resonance for Longitudinal Oscillation

Much evidence has been acquired to support the statement that the longitudinal oscillation is a primary mode, resonating between the flameholder as a closed end and the exhaust end. The frequency determined by the wave equation for a primary mode of longitudinal oscillation in a cylinder with one end open and one closed agrees with the measured frequency, i.e., the 350 cps note. The frequency calculated for the case of resonance occurring between the exhaust end and the sonic plate did not agree with the measured one. The method of Jost[30] was used in this calculation to account for the column of gas being hot gas between the end of the burner and flameholder and cold gas from there to the sonic plate. As unquestionable proof that the flameholder is acting as a closed end, the sonic plate was placed at several positions from 2 inches to 3 feet above the flameholder with no effect on the frequency.

Designation of the Acoustical Mode for Screech

The high pitched note can be identified on the basis of its frequency as a primary transverse oscillation because of previous investigations[8][21] that have shown screeching to be an acoustically resonant phenomenon and because the second mode of transverse oscillation and the first mode of radial oscillation have frequencies approximately 6300 cps and 7800 cps, respectively. The primary mode of transverse oscillation has a predicted frequency of 3800 cps at a mean gas temperature of 3000°R, compared to the measured frequency of 3850 to 4250 cps.

The primary mode is also the most probable one as pointed out by Tischler[83] and Maslen.[54] Thus a 4000 ± 300 cps note has the wave numbers m = 1 and n = 0 with the n_x wave numbers not clearly determined by frequency measurement since their effect on the frequencies is about two hundred cycles per second. However, the fact that the frequency of the screeching combustion does not change significantly when the burning length is varied from 8 inches to 17-1/2-inches gives good evidence that there is no counterpart resonance in the longitudinal direction; thus $n_x = 0$, and the screech is a pure primary transverse mode of oscillation. The change in frequency from 3850 cps to about 4150 cps with an increase in fuel-to-air ratio from a $\phi = 0.65$ to 0.9 can be accounted for by the increase in gas temperature and the accompanying increase in sonic velocity.

The possibility exists, however, that the mode of oscillation shifts as the fuel-to-air ratio is increased from a pure transverse mode with wave numbers, m = 1, n = 0, $n_x = 0$, to a transverse mode resonating in the longitudinal direction also, with wave numbers, m = 1, n = 0, $n_x = 1$. This change in mode would also explain the change in frequency and is suggested by the behavior of the transverse oscillation with increasing fuel-to-air ratio as shown in Figure 40. A definite answer to this question of the exact mode of oscillation can only be obtained by detailed probing of the flame with a microphone.

Failure of Pressure-Drop Method at High Sound Pressures

The pressure-drop determinations of the combustion efficiency are a good corroboration for the combustion efficiency determined by the

SLR measurements in a stable burner. However, at high sound levels the pressure-drop method appears to have little value. This failure at high sound levels is probably caused by the failure of two of the assumptions employed in this method to remain true during unstable combustion, but it may possibly be due to sonic waves in the manometer leads causing erroneous readings. The two key assumptions made in reducing the pressure measurements to combustion efficiencies are 1) that the pressure drop across the flameholder is unaffected by the combustion process or sonic oscillations, and 2) that the flow is one-dimensional with no gradients at the points of pressure measurement.

Either of these conditions can be disturbed by a flame-generated oscillation because, as pointed out by Rogers,[67] Kaskan,[33] and Barker,[3] there are definite changes in the flow pattern associated with the oscillation, particularly at the flameholder. Evidence that oscillations do cause increases in the pressure drop is given by Bayley,[5] who studied pulsating flow and found the pressure loss coefficient to increase proportionately to the amplitude of the oscillation.

The assumptions are evidently reasonable in a quiet burner. Sundstrom,[78] in fact, obtained good values with both quiet and oscillating flames. The pressure drop across the flameholder, however, is a higher proportion of the total pressure drop in the present study, but the drag due to the wall is larger in Sundstrom's small diameter tube. It might be recalled that the drag of the flameholder and wall as determined in cold flow are subtracted from the measured pressure drop to arrive at the pressure drop due to momentum changes.

Importance of Inlet Turbulence

The fact that the turbulence level upstream from the flameholder has little effect on the phenomena downstream from the flameholder is not surprising because the blockages of the flameholders are 90 per cent or more of the free stream area. Thus contraction of the stream in passing through the annulus between flameholder and tube wall is dominant in setting the flow pattern and conditions downstream from the flameholder. Changes in the contraction process caused by a long-annulus flameholder or by a screen in the annulus naturally can have a strong influence downstream. The long-annulus flameholder is believed to cause the unburned gas to jet through the annulus, sweeping the area near the tube wall free of combustion and thus preventing screech. Also the formation of vortices may be deceased due to the more streamlined annulus. The screen-in-annulus flameholder increases the stabilization of the flame near the wall and thus helps the generation of screeching combustion.

Explanation for Slight Difference in Heat Balances

The consistently 4 per cent higher heat absorption by the tube's cooling water compared to the integrated local fluxes may be explained by the fact that the room is warmer when the flame is burning, particularly near the burner; thus the correction, obtained from the cooling water temperature rise without combustion, is expectantly low.

CONCLUSIONS

1) Local coefficients for convective heat transfer can be correlated as a function of sound pressure level. The correlation approximately three tube diameters downstream from the flameholder is

$$\frac{h}{h_\infty \; h'/h'_\infty} = 0.044 \; \frac{P}{P_o} + 1.08 \qquad (19)$$

2) Transverse oscillations in a ramjet-type burner are just as influential in promoting heat transfer to the wall as longitudinal oscillations.

3) The hydrodynamic changes brought about by the sonic oscillations are the primary effects, while changes in the combustion phenomena are secondary.

4) The burning length has little effect on the heat transfer rates unless a change occurs in the intensity of the flame-generated oscillations. The shorter burning lengths promote screeching combustion.

5) The tendency of the flame to generate transverse oscillations in a ramjet-type burner can be promoted by increased flame stabilization near the tube wall.

6) Longitudinal oscillations can be damped by a spray-quench muzzle at the end of the burner.

7) Maximum rates of heat transfer in a stable burner are observed near stoichiometric inlet mixtures.

APPENDIX A

ORIGINAL AND PROCESSED DATA

APPENDIX A

ORIGINAL AND PROCESSED DATA

Run No.	1[a,b]	2[a,b]	3[b]	4[b]	5[b]	6[a,b]	7[b]	8[b]	9[b]	10	11	12	13	14[c]	15	16	17	18	19
G lb/hrft^2	3730	3710	3650	3670	3580	3780	3790	5010	5000	4130	4140	4200	4220	4150	4170	4180	4940	4940	4830
Re	36,000	35,900	35,200	35,500	34,700	36,500	36,600	48,500	48,400	40,000	40,000	40,500	40,700	40,100	40,300	40,500	47,800	47,700	47,600
ϕ	0.772	0.635	0.632	0.628	0.606	0.763	0.776	0.920	0.863	0.810	0.869	0.854	0.840	0.785	0.794	0.895	0.648	0.674	0.735
Flameholder	F-1	F-1	F-1	F-1	F-1	F-2	F-2	F-3	F-3	F-3	F-3	S-1	S-1	S-1	S-1	S-1	S-1	S-1	S-1
L_b, in.	17-3/4	17-3/4	17-3/4	17-3/4	17-3/4	17-3/4	17-3/4	8	8	18-1/2	18-1/2	17-1/2	17-1/2	17-1/2	17-1/2	17-1/2	17-1/2	17-1/2	17-1/2
SPL, db	131	130	152-1/2	132	151-1/2	130	133	159	133	147-1/2	152	154-1/2	148	132	133	151	148	132	133
f, cps	-	-	350	-	345	-	-	4250	-	4150	340	4150	4150	-	-	4150	3850	-	-
T_{SLR}°F, 4 in. l.	2840	2510	2210	2485	2110	2910	2960	-	-	2725	2750	2920	3010	2895	2930	3030	2460	2575	2805
T_{SLR}°F, 10 in. l.	2825	2420	2260	2360	2130	2820	2880	-	-	2800	2880	3070	3120	2910	2925	3155	2440	2525	2780
T_b°F, 4 in. l.	2355	2090	1840	2060	1755	2415	2460	-	-	2265	2295	2430	2500	2405	2430	2525	2050	2145	2330
T_b°F, 10 in. l.	2355	2020	1900	1970	1785	2345	2390	-	-	2340	2410	2570	2610	2430	2445	2640	2045	2105	2325
E_{SLR}%, 4 in. l.	78	82	79	81	78	80	80	-	-	74	74	79	79	79	79	78	78	78	79
E_{SLR}%, 10 in. l.	73	75	76	77	73	74	74	-	-	72	72	78	78	75	75	76	74	73	75
$E_{\Delta P}$ %, 2 in. l.	75	82	-	78	-	84	79	-	-	-	-	-	-	85	81	-	-	75	80
h, 4 in. l. Btu/hrft^2°F	9.4	9.2	12.9	9.7	13.1	9.3	9.6	-	-	12.9	15.0	14.3	12.4	9.2	9.6	14.5	13.8	10.2	10.2
h, 10 in. l. Btu/hrft^2°F	13.3	11.6	22.9	11.2	22.9	9.0	9.1	-	-	17.6	19.9	19.8	18.1	14.7	15.0	18.8	19.0	15.5	15.4
$h/(h_\infty\, h'/h'_\infty)$, 4 in. l.	1.25	1.26	1.87	1.34	1.96	1.13	1.16	-	-	1.50	1.75	1.74	1.49	1.12	1.16	1.75	1.53	1.11	1.09
$h/(h_\infty\, h'/h'_\infty)$, 10 in. l.	1.48	1.33	2.76	1.30	2.84	0.88	0.88	-	-	1.63	1.84	1.78	1.62	1.34	1.37	1.67	1.57	1.27	1.24
T_i°F	72	75	77	76	81	76	82	78	78	75	77	78	74	74	76	82	79	80	79
Q_{water} Btu/hr	45,000	35,400	63,200	35,500	58,900	39,300	39,900	49,300	15,800	61,100	81,000	78,100	63,400	50,100	51,600	74,500	52,900	43,100	48,300
Q_i Btu/hr	42,100	33,600	59,600	33,100	55,100	36,500	39,300	40,500	13,100	59,800	78,300	76,500	60,900	47,200	48,800	72,700	51,200	41,500	46,700
Q_{fh} Btu/hr	5,600	8,900	9,200	9,100	8,100	5,200	5,600	13,100	5,100	7,800	8,500	9,400	6,500	4,700	4,900	9,100	6,000	4,400	5,100
Local Heat Fluxes[g]																			
q, 17 in. l. Btu/hrft^2	4,100	2,600	14,400	2,500	13,000	3,100	3,000	-	-	10,700	24,800	9,100	6,900	3,900	4,700	7,800	4,100	2,700	4,400
q, 15 in. l. Btu/hrft^2	12,000	8,800	33,200	8,400	32,700	7,800	9,800	-	-	27,100	49,200	43,200	21,300	15,100	16,500	30,700	17,200	12,500	14,100
q, 13 in. l. Btu/hrft^2	21,200	14,500	48,400	13,700	47,300	13,700	15,900	-	-	42,500	58,400	60,800	35,000	25,600	26,300	49,100	30,800	23,000	24,900
q, 10 in. l. Btu/hrft^2	32,300	24,200	40,200	22,700	37,500	23,500	24,100	-	-	40,700	46,800	50,100	47,100	36,300	37,100	49,500	37,400	32,300	35,800
q, 4 in. l. Btu/hrft^2	24,600	20,800	24,000	21,400	23,000	25,100	26,200	58,300	16,400	30,600	35,300	36,200	33,200	24,700	26,000	38,300	28,500	23,400	25,900
Surface Temp.																			
T_s°F, 17 in. l.	99	91	157	90	150	94	93	-	-	138	210	126	113	97	104	123	101	93	102
T_s°F, 15 in. l.	134	116	239	113	237	113	124	-	-	212	320	291	182	150	156	228	159	136	144
T_s°F, 13 in. l.	171	139	299	133	294	132	143	-	-	272	348	365	236	190	193	308	217	181	190
T_s°F, 10 in. l.	215	179	251	170	235	177	179	-	-	247	271	292	281	245	256	279	225	214	237
T_s°F, 4 in. l.	163	148	161	152	156	165	172	293	128	185	206	211	198	167	169	214	179	166	172

Run No.	20	21	22[d]	23	24	25	26	27	28[d]	29	30	31	32	33	34	35	36	37	38
G lb/hrft^2	4810	4820	4810	4810	4210	4860	4860	4860	4860	4890	4840	4170	4190	4170	4130	4130	4130	4830	4830
Re	47,500	47,500	47,500	47,500	40,700	47,100	47,000	47,000	47,000	47,300	46,900	40,400	40.600	40,300	40,000	40,000	40,000	46,900	46,800
ϕ	0.814	0.861	0.861	0.951	0.955	0.666	0.676	0.745	0.679	0.829	0.932	0.805	0.892	0.769	0.749	0.668	0.675	0.834	0.746
Flameholder	S-1	S-1	S-1	S-1	S-1	S-1	S-1	S-1	S-1	S-1	S-1	S-1	S-1	S-1	S-1	S-1	S-1	S-2	S-2
L_b, in.	17-1/2	17-1/2	17-1/2	17-1/2	17-1/2	13-1/2	13-1/2	13-1/2	13-1/2	13-1/2	13-1/2	13-1/2	13-1/2	13-1/2	13-1/2	13-1/2	13-1/2	13-1/2	13-1/2
SPL, db	150-1/2	154	153	155	152	149	131	144	131	156	157	153	152-1/2	143	132	147	129	132	131
f, cps	4125	4150	4150	4175	70% 4175 30% 340	3850	-	4050	-	4100	4150	4075	4150	4050	-	3850	-	-	-
T_{SLR} °F, 4 in. l.	2815	2905	2920	3100	3150	2570	2710	2710	2730	2870	3135	2890	3120	2795	2850	2545	2590	3135	2850
T_{SLR} °F, 10 in. l.	2900	3030	3050	3160	3190	-	-	-	-	-	-	-	-	-	-	-	-	-	-
T_b °F, 4. in. l.	2350	2425	2440	2585	2620	2140	2255	2255	2275	2405	2620	2415	2605	2320	2370	2120	2155	2605	2375
T_b °F, 10 in. l.	2425	2535	2550	2650	2665	-	-	-	-	-	-	-	-	-	-	-	-	-	-
E_{SLR}%, 4 in.l.	76	76	76	74	74	78	80	75	81	75	74	78	78	75	79	77	76	77	76
E_{SLR}%, 10 in. l.	74	74	74	71	71	-	-	-	-	-	-	-	-	-	-	-	-	-	-
$E_{\Delta P}$%, 2 in. l.	-	-	-	-	-	-	83	96	81	-	-	-	-	93	88	-	83	87	82
h, 4 in. l. Btu/hrft^2°F	15.1	16.8	17.3	16.5	12.6	15.6	11.6	12.9	12.6	21.3	19.9	19.5	18.8	11.6	11.5	13.1	9.7	12.4	13.7
h, 10 in. l. Btu/hrft^2°F	20.1	21.4	20.8	20.8	16.1	-	-	-	-	-	-	-	-	-	-	-	-	-	-
$h/(h_m\ h'/h'_m)$, 4 in. l.	1.63	1.81	1.86	1.74	1.49	1.47	1.07	1.19	1.17	1.98	1.82	2.04	1.93	1.21	1.20	1.41	1.02	0.94	1.07
$h/(h_m\ h'/h'_m)$, 10 in. l.	1.61	1.70	1.65	1.64	1.42	-	-	-	-	-	-	-	-	-	-	-	-	-	-
T_i °F	81	81	84	79	86	79	79	80	80	76	77	80	80	80	81	83	80	80	81
Q_{water} Btu/hr	75,700	83,100	83,500	84,700	69,400	46,400	36,600	45,600	38,500	68,700	69,900	62,700	65,900	42,300	39,600	38,500	31,100	37,300	34,900
Q_i Btu/hr	71,400	80,300	79,900	82,600	68,300	44,200	35,100	44,200	37,200	65,500	67,500	60,600	64,100	40,800	38,600	38,000	29,900	35,600	32,800
Q_{fh} Btu/hr	8,800	9,100	8,700	9,300	7,800	6,200	4,200	5,900	4,400	9,000	9,200	8,400	8,600	6,100	4,400	5,300	3,900	5,400	4,800
Local Heat Fluxes[g]																			
q, 17 in. l. Btu/hrft^2	7,600	8,400	8,600	8,300	7,300	-	-	-	-	-	-	-	-	-	-	-	-	-	-
q, 15 in. l. Btu/hrft^2	31,300	38,800	37,500	39,100	37,600	-	-	-	-	-	-	-	-	-	-	-	-	-	-
q, 13 in. l. Btu/hrft^2	49,700	56,700	55,200	56,000	50,500	6,300	3,800	7,200	4,900	11,000	12,300	11,300	12,500	7,500	5,700	5,400	3,100	4,200	4,600
q, 10 in. l Btu/hrft^2	47,500	52,600	51,700	54,000	44,100	32,000	23,100	33,200	24,100	44,800	50,300	42,000	47,300	34,800	29,200	26,400	20,300	18,300	13,600
q, 4 in. l. Btu/hrft^2	36,300	41,200	42,500	43,800	35,700	33,400	27,600	30,200	29,800	49,700	51,900	46,500	49,200	28,600	29,000	28,500	22,500	34,700	33,600
Surface Temp.																			
T_s °F, 17 in. l.	123	127	129	126	120	-	-	-	-	-	-	-	-	-	-	-	-	-	-
T_s °F, 15 in. l.	230	267	262	271	263	-	-	-	-	-	-	-	-	-	-	-	-	-	-
T_s °F, 13 in. l.	310	345	338	342	313	105	93	109	98	127	135	130	138	110	102	100	90	96	97
T_s °F, 10 in. l.	277	295	291	308	264	207	168	215	175	207	293	256	283	224	199	186	159	152	129
T_s °F, 4 in. l.	209	234	239	245	208	199	166	188	177	264	272	251	262	182	181	179	155	202	199

Run No.	39	40	41	42	43	44	45	46	47	48	49[d]	50	51	52	53[c,e]	54[e]	55[e]	56[e]
G lb/hrft^2	4820	4200	4170	4160	4810	4790	4160	4110	4180	4890	4950	4180	4240	4130	4170	4180	4760	4760
Re	46,600	40,600	40,400	40,300	46,600	46,500	40,400	39,800	40,500	46,900	47,900	40,500	41,100	40,100	40,400	40,400	46,000	46,000
ϕ	0.680	0.895	0.769	0.665	0.842	0.677	0.895	0.670	1.027	0.901	0.897	0.766	0.905	0.899	0.760	0.777	0.783	0.690
Flameholder	S-2	S-2	S-2	S-2	S-2	S-2	S-2	S-2	S-2	S-2	S-2	S-2	F-4	F-5	F-5	F-5	F-5	F-5
L_b, in.	13-1/2	13-1/2	13-1/2	13-1/2	17-1/2	17-1/2	17-1/2	17-1/2	17-1/2	17-1/2	17-1/2	17-1/2	17-1/2	17-1/2	17-1/2	17-1/2	17-1/2	17-1/2
SPL, db	131	130	129	129	133	132	130	130	133	133	133	132	132	139	155	155	156-1/2	157-1/2
f, cps	-	-	-	-	-	-	-	-	-	-	-	-	-	80% 4175 20% 350	345	345	345	335
T_{SLR} °F, 4 in. l.	2630	3135	2910	2570	2970	2585	3110	2560	3295	3125	3100	2845	3270	3105	2525	2575	2605	2345
T_{SLR} °F, 10 in. l.	-	-	-	-	2960	2490	3150	2460	3275	3135	3115	2820	3320	3140	2645	2710	2750	2450
T_b °F, 4 in. l.	2190	2605	2420	2140	2465	2145	2580	2125	2735	2600	2575	2365	2715	2580	2105	2145	2175	1960
T_b °F, 10 in. l.	-	-	-	-	2470	2075	2625	2050	2725	2615	2595	2350	2765	2620	2225	2275	2320	2070
E_{SLR}%, 4 in. l.	75	74	76	75	74	77	75	77	75	75	74	75	80	76	75	75	76	76
E_{SLR}%, 10 in. l.	-	-	-	-	71	71	73	71	69	72	70	71	77	73	72	73	74	73
$E_{\Delta P}$%, 2 in. l.	80	83	84	80	75	73	79	72	79	80	78	76	86	91	-	-	-	-
h, 4 in. l. Btu/hrft^2°F	14.0	11.8	11.5	11.9	10.1	9.5	8.9	8.9	8.6	11.2	11.8	8.3	8.5	10.6	16.6	16.6	19.5	18.9
h, 10 in. l. Btu/hrft^2°F	-	-	-	-	14.2	12.5	12.5	12.5	11.9	14.6	15.1	12.5	13.2	13.7	26.8	25.9	30.0	35.0
$h/(h_\infty h'/h'_\infty)$, 4 in. l.	1.12	1.00	1.00	1.07	0.89	0.86	0.86	0.92	0.82	0.93	1.01	0.82	0.91	1.19	1.96	1.95	20.6	20.5
$h/(h_\infty h'/h'_\infty)$, 10 in. l.	-	-	-	-	0.99	0.90	0.95	1.02	0.89	0.95	1.01	0.98	1.14	1.22	2.54	2.44	2.55	3.06
T_1 °F	81	79	79	80	79	79	80	86	86	85	85	76	70	83	77	77	80	80
Q_{water} Btu/hr	30,700	40,300	31,900	27,400	51,000	38,900	47,200	37,700	51,800	56,400	57,500	46,100	52,400	58,900	73,900	74,100	88,000	78,300
Q_1 Btu/hr	29,400	39,700	30,700	25,500	48,600	38,400	45,900	36,200	49,800	53,400	54,600	41,800	50,600	55,400	71,500	72,500	84,100	75,000
Q_{fh} Btu/hr	4,300	5,000	4,600	3,700	5,200	4,300	5,200	4,000	4,700	5,200	5,200	4,300	8,500	8,600	9,700	10,000	9,800	8,900
Local Heat Fluxes[g]																		
q, 17 in. l. Btu/hrft^2	-	-	-	-	4,000	3,600	5,200	3,900	5,000	5,300	6,100	2,600	5,600	6,300	5,200	6,500	6,700	5,500
q, 15 in. l. Btu/hrft^2	-	-	-	-	14,900	11,000	16,200	10,900	19,600	15,700	14,000	12,300	17,500	16,700	33,800	32,000	36,600	26,700
q, 13 in. l. Btu/hrft^2	3,900	4,900	3,300	3,000	24,200	17,900	27,400	17,500	31,100	27,100	28,200	21,500	28,300	25,600	54,300	53,500	58,700	50,600
q, 10 in. l. Btu/hrft^2	13,600	25,900	16,400	13,500	36,200	26,500	34,500	26,200	35,500	39,400	40,400	30,700	39,100	37,800	54,600	54,400	62,700	62,900
q, 4 in. l. Btu/hrft^2	31,000	33,300	29,600	26,500	27,500	22,000	26,400	20,600	27,700	31,800	32,900	22,400	27,300	30,400	34,600	35,500	41,400	35,700
Surface Temp.																		
T_s °F, 17 in. l.	-	-	-	-	101	98	110	102	111	103	118	91	113	118	111	121	124	105
T_s °F, 15 in. l.	-	-	-	-	149	129	160	127	174	153	144	138	160	156	145	136	157	210
T_s °F, 13 in. l.	93	98	89	87	191	160	207	157	224	207	210	175	208	197	338	334	360	319
T_s °F, 10 in. l.	127	188	144	131	232	185	223	182	223	257	243	205	242	240	314	313	349	351
T_s °F, 4 in. l.	189	199	183	171	175	153	171	147	176	205	197	155	175	187	203	207	224	207

Run No.	57	58[b]	59	60	61	62	63	64	65	66	67	68	69	70	71	72	73[f]	74[f]
G lb/hrft^2	4210	4710	4760	4760	4760	4720	4250	4340	4350	4220	4220	4250	4910	4910	4910	4570	4570	4570
Re	40,600	45,900	46,000	45,900	45,900	45,500	41,000	41,800	41,800	40,700	40,600	40,900	47,300	47,400	47,300	44,000	44,000	44,100
ϕ	0.768	0.570	0.583	0.685	0.677	0.673	0.926	0.919	0.826	0.757	0.815	0.900	0.749	0.811	0.896	0.896	0.910	0.905
Flameholder	F-5	F-5	F-5	F-5	F-6L	S-3L	S-3R	S-3R	S-3R	S-4R	S-4R	S-4R	S-4R	S-4R	S-4R	S-1	S-1	S-1
L_b, in.	17-1/2	17-1/2	17-1/2	17-1/2	17-1/2	17-1/2	17-1/2	17-1/2	17-1/2	17-3/4	17-3/4	17-3/4	17-3/4	17-3/4	17-3/4	17-1/2	17-1/2	17-1/2
SPL, db	130	160	131	132	131	132	148	147	133	147-1/2	131	151-1/2	149	132	154-1/2	153	156	157
f, cps	-	350	-	-	-	-	4100	4100	-	4030	-	4200	4030	-	4200	4175	4190	4190
T_{SLR}°F, 4 in. l.	2870	1930	2345	2610	2625	2640	3085	3075	3020	2820	2945	2870	2710	2970	2915	3005	3045	3060
T_{SLR}°F, 10 in. l.	2830	2000	2100	2480	2560	2600	3155	3135	3050	2880	3000	2980	2750	2990	2985	3055	3150	3140
T_b°F,4 in. l.	2385	1620	1945	2165	2180	2190	2565	2560	2505	2345	2445	2390	2255	2465	2430	2505	2550	2580
T_b°F,10 in. l.	2360	1690	1745	2060	2135	2170	2635	2620	2545	2405	2500	2495	2300	2490	2495	2555	2650	2655
E_{SLR}%, 4 in. l.	79	77	78	76	79	80	75	75	79	81	78	74	78	79	73	76	77	79
E_{SLR}%, 10 in. l.	73	72	67	69	73	74	72	72	75	78	75	71	75	75	70	73	74	75
$E_{\Delta P}$%, 2 in. l.	77	-	80	76	81	78	-	-	79	-	81	-	-	83	-	-	-	-
h, 4 in. l. Btu/hrft^2°F	10.1	20.8	8.7	9.5	10.2	10.3	12.9	12.5	9.4	11.6	9.7	15.3	14.1	10.1	17.5	15.3	16.7	16.9
h, 10 in. l. Btu/hrft^2°F	12.0	36.4	7.8	9.6	13.4	15.3	17.3	17.6	15.3	16.7	13.4	19.6	18.4	14.3	21.1	19.9	20.7	22.0
$h/(h_\infty h'/h'_\infty)$, 4 in. l.	1.13	2.39	0.95	0.99	1.06	1.01	1.34	1.27	0.95	1.23	1.01	1.62	1.34	0.93	1.65	1.74	1.92	1.98
$h/(h_\infty h'/h'_\infty)$, 10 in. l.	1.08	3.36	0.69	0.80	1.12	1.23	1.45	1.46	1.27	1.44	1.13	1.67	1.42	1.07	1.61	1.67	1.77	1.92
T_i°F	75	85	70	72	72	70	71	68	68	69	70	69	68	67	67	68	67	67
Q_{water} Btu/hr	44,000	78,900	26,700	35,100	39,300	41,900	69,300	70,500	54,100	57,400	52,800	77,600	64,900	56,700	80,200	80,600	-	-
Q_i Btu/hr	42,000	73,600	25,100	33,500	38,200	40,200	67,700	68,000	50,900	55,600	51,200	74,800	61,900	54,500	78,400	78,200	78,800	78,000
Q_{fh} Btu/hr	6,300	9,000	6,000	6,400	5,200	4,100	5,900	5,900	5,400	8,600	7,500	9,000	8,900	7,700	9,300	8,000	8,500	8,400
Local Heat Fluxes[g]																		
q, 17 in. l. Btu/hrft^2	4,300	10,600	3,000	3,400	2,800	2,000	6,900	6,100	4,500	14,000	18,800	17,200	15,900	19,000	18,200	11,500	7,900	8,300
q, 15 in. l. Btu/hrft^2	12,800	45,500	7,600	8,700	6,800	6,500	31,600	32,700	15,400	20,300	20,900	28,600	25,100	21,300	33,000	40,700	33,600	33,300
q, 13 in. l. Btu/hrft^2	19,600	61,600	10,400	13,000	12,400	14,900	44,300	45,100	31,400	30,200	26,300	49,800	38,200	26,800	53,700	53,000	51,500	54,100
q, 10 in. l. Btu/hrft^2	29,800	52,300	14,500	21,200	29,100	33,100	46,200	46,500	39,800	40,200	35,200	48,600	41,500	36,800	51,100	50,300	52,000	53,600
q, 4 in. l. Btu/hrft^2	26,500	31,300	18,100	22,400	23,900	24,400	35,500	34,400	26,600	29,200	26,600	37,800	32,700	27,900	43,000	39,900	42,600	42,000
Surface Temp.																		
T_s°F, 17 in. l.	100	142	93	94	91	85	118	111	99	147	172	163	150	165	157	123	265	269
T_s°F, 15 in. l.	136	312	110	115	105	104	227	233	146	169	170	207	190	172	228	262	393	399
T_s°F, 13 in. l.	168	374	125	137	134	146	288	291	222	215	196	308	246	193	321	312	458	475
T_s°F, 10 in. l.	210	302	130	158	193	212	271	274	243	241	218	254	238	231	287	273	384	457
T_s°F, 4 in. l.	171	191	133	139	151	149	203	199	156	177	159	207	189	157	228	215	301	390

Footnotes and Flameholders are listed on the following two pages.

Footnotes

[a]In this run the sonic plate is upstream of the mixing chamber. In the other runs the sonic plate is located between the flanges joining the mixing and combustion chambers.

[b]In this run a spray-quench muzzle is not attached to the end of the burner. In the other runs the muzzle is attached.

[c]This run was taken on a particularly humid day, i.e., it was raining.

[d]For this run all of the data were taken during injection of the sodium bicarbonate. In the other runs, sodium bicarbonate is injected only during the SLR measurements.

[e]In this run the screen that is normally in the muzzle is not in place.

[f]In this run the tube's cooling water was decreased to approximately 1/2 gpm and boiled in the jacket.

[g]The local heat fluxes, q, are listed for the five levels above the exhaust end of the burner, i.e., the subscript 4 in. l. refers to 4 inches from the end of the burner exclusive of any spray quench.

List of Flameholders

All are bluff-body flameholders.

Designation	F.h. Blockage of Tube Cross-Section, per cent[a]	Thickness, inches	Screen-in-annulus (10 mesh, 47 mil diameter wire)
F-1	90.8	1/8	No
F-2	90.8	5/8	No
F-3	92.7	1/8	No
F-4	95.0	1/8	No
F-5	94.6	5/16	No
F-6L[b]	95.3	5/16	No
S-1	96.5	1/8	Yes
S-2	96.5	1-3/8	Yes
S-3L[b]	98.3	1/8	Yes
S-3R[c]	98.3	1/8	Yes
S-4R[d]	97.1	1/4	Yes

Footnotes:

[a]Blockage includes that of the screen in the annulus.

[b]This flameholder is used with a 1/32-inch thick asbestos liner cemented to the tube wall from the 12-1/2-inch level to the 22-1/2-inch level.

[c]This flameholder is used with a 1/32-inch thick asbestos liner cemented to the tube wall from the 17-1/4-inch level to the 22-1/2-inch level.

[d]This flameholder is used with a 1/8-inch thick asbestos ring 1/2-inch wide cemented to the tube wall from the 17-1/2-inch level to the 18-inch level.

APPENDIX B

SAMPLE CALCULATION

APPENDIX B

SAMPLE CALCULATION

Run Number 48

Data

Air rate = 131 SCFM

Propane rate = 4.97 SCFM

Inlet mixture temperature = 85°F

Tube-water rate = 11.4 gpm

Flameholder rate = 24 cc per sec

Temperature rise of tube water = 10.2°F

Inlet water temperature = 66.8°F

Temperature rise of tube water without combustion = 0.3°F

Temperature rise of flameholder water = 27.1°F

Sodium-line-reversal temperature at 4-inch level (i.e., 13-1/2-inches from flameholder) = 3125°F

Sodium-line-reversal temperature at 10-inch level (i.e., 7-1/2 inches from flameholder) = 3135°F

Pressure drop (25-inch level to 2-inch level) = 16.30 inches H_2O

Pressure drop without combustion = 15.52 inches H_2O

Sound pressure level = 133 decibels

No predominant frequencies

Burning length = 17-1/2-inches (excluding muzzle)

Muzzle on end (with a screen in muzzle)

Sonic plate 10 inches above flameholder

Flameholder: number S-2 (screen-in-annulus)

blockage = 96.5 per cent (including screen)

annulus length = 1-3/8 inches

Temperatures at the measuring station, 4-1/2 inches below flameholder with the thermocouple locations:

T°F	Radius, inches
203.2	2.480
167.5	2.690
133.1	2.909

Heat Flux and Heat Balances

The calculation of the local heat flux is shown only at the section 4-1/2 inches below the flameholder, because all five local fluxes are calculated in the same manner.

$$Q/A_s = \frac{k_{av}}{r_s} \frac{(T_i - T_j)}{\ell n\ r_j/r_i} \qquad (6)$$

Using the inner and outer thermocouples,

$$Q/A_s = \frac{153\ (203.2 - 133.1)}{2.480\ \ell n\ \frac{2.909}{2.480}} = 27{,}100\ \text{Btu/hrft}^2$$

Using the inner and middle ones,

$$Q/A_s = \frac{154\ (203.2 - 167.5)}{2.480\ \ell n\ \frac{2.690}{2.480}} = 27{,}200\ \text{Btu/hrft}^2$$

The second value merely serves as a check on the first. The heat flux

at the other four stations are found in a similar manner and are

L, inches (from flameholder)	Q/A_s, Btu/hrft^2	T_s °F
1/2	5,300	103
2-1/2	15,700	153
4-1/2	27,100	207
7-1/2	39,400	257
13-1/2	31,800	205

The temperatures for each station as a function of tube radius are shown in Figure 53, where the inside or outside surface temperature can easily be read. A plot of the local fluxes as a function of distance along the tube from the flameholder can be made. An integration of the area under the curve gives Q_i. Here, Q_i = 53,400 Btu/hr.

The heat absorbed by the tube's cooling water gives a check for the heat transferred through the wall. The net rise in the water temperature is 10.2 - 0.3 = 9.9°F, at a water rate of 11.4 gpm.

$$Q_w = 11.4 \times 9.9 \times 8.33 \times 1.0 \times 60 = 56,400 \text{ Btu/hr}$$

The difference between the two methods is 5.4 per cent.

One other heat loss is that transferred to the flameholder's cooling water.

$$Q_{f.h.} = 24 \times 27.1 \times .2642 \times 10^{-3} \times 8.33 \times 3600 \times 1 = 5160 \text{ Btu/hr}$$

Reynolds Number and Fuel-to-Air Ratio

The molal average viscosity for the inlet mixture is 0.0177 cp. Its density is 0.0778 lbs/ft^3 under standard conditions, 60°F and 1 atm.

$$Re = \frac{D \rho V}{\mu A} = \frac{4.92 \times 0.0778 \times 135.97 \times 60 \times 144}{12 \times 18.71 \times 0.0177 \times 2.42}$$

$$Re = 46,900$$

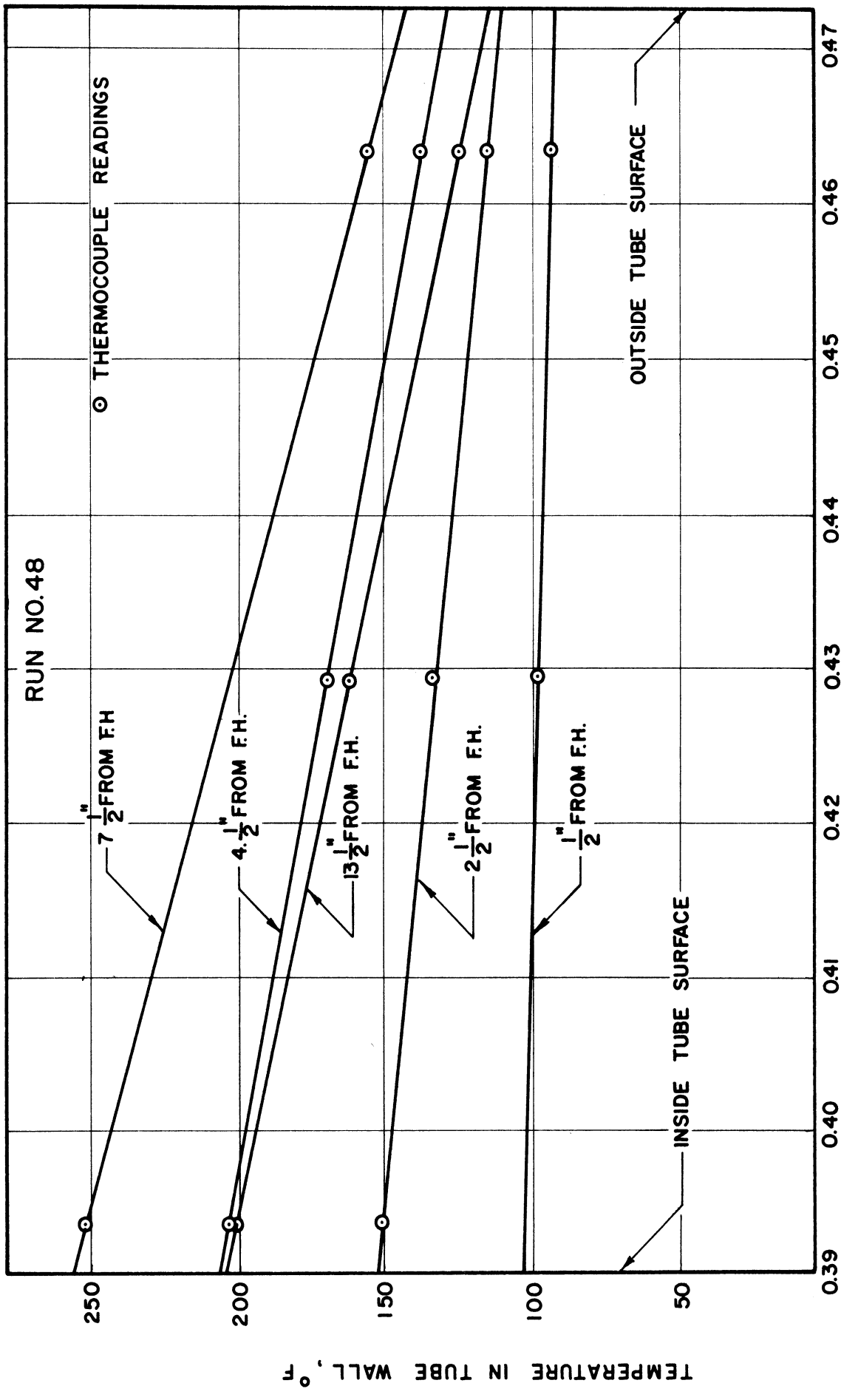

Figure 53. Temperature Gradient in the Tube Wall at the Five Measuring Stations.

The ratio of the moles of air to the moles of fuel, 98 per cent propane and 2 per cent propylene, is 23.75 for a stoichiometric mixture. The ratio of the fuel-to-air ratio to that of a stoichiometric mixture, ϕ, is then

$$\phi = 23.75 \times \frac{4.97}{131} = 0.901$$

Bulk Temperature and Combustion Efficiency

The bulk temperature is readily evaluated, knowing the sodium-line-reversal temperature and the inside surface temperature as read from Figure 53.

13-1/2-inches from flameholder,

$$T_b = 0.82\ (3125 - 205) + 205 = 2600°F$$

7-1/2-inches from flameholder,

$$T_b = 0.82\ (3135 - 257) + 257 = 2615°F$$

The composition must first be estimated to evaluate $\overline{C}_{p2}$ before the combustion efficiency can be calculated. So the combustion efficiency is assumed to be 75 per cent and the compositon is calculated assuming complete combustion to CO_2 and H_2O. The basis for calculation is 18.75 moles of nitrogen. Five moles of oxygen, 0.12 moles of H_2O, and ϕ moles of propane, i.e., 0.901, are present with this nitrogen in the unburned gases. For the burned gases,

	moles	mole fraction y		M		yM	C_p 60°-2600°F		yC_p
N_2	18.75	0.7370	x	28	=	20.63	0.0198		0.0146
O_2	1.62	0.0637	x	32	=	2.04	0.0198		0.00126
C_3H_8	0.22	0.0087	x	44	=	0.38	0.080		0.0007
CO_2	2.03	0.0798	x	44	=	3.51	0.0319		0.00255
H_2O	2.82	0.1108	x	18	=	1.99	0.0261		0.00289
	25.44	1.0000		$\overline{M}_2$	=	28.55		$\overline{C}_{p2}$ =	0.02200

The heat capacities in this table are the mean heat capacities from 60°F to 2600°F obtained from Perry[59] in the units of Btu/ft^3°F, with the volume measured at 60°F. The density of the burned gases at 60°F is 0.0752 lb/ft^3 and thus $\overline{C}_{p2}$ in mass units is 0.293 Btu/lb°F.

$$E = \frac{\overline{C}_{p2} (T_b - T_i) + Q_t}{Q_R} \qquad (14)$$

Q_t is the heat lost from the flame to the point of flame temperature measurement. Integration of the local fluxes from the flameholder to the 13-1/2-inch distance gives 41,100 Btu/hr. The loss to the flameholder is added on giving 46,300 Btu/hr.

$$Q_t = Q/W = 46,300/635.6 = 73 \text{ Btu/lb mixture}$$

The heat of combustion of the fuel, 98 per cent propane and 2 per cent propylene, is 19,924 Btu/lb fuel. Since at the stoichiometric point there are 15.7 lbs of air per lb of fuel, then

$$Q_R = 19,924 \times \frac{0.901}{15.7 + 0.901} = 1082 \text{ Btu/lb mixture}$$

$$E = \frac{0.293 (2600 - 85) + 73}{1082} \times 100 = 75 \text{ per cent}$$

Since this value agrees with the estimated one, the heat capacity does not have to be reevaluated.

Similarly, at 7-1/2-inches from the flameholder

$$Q_t = 36, \qquad \overline{C}_{p2} = 0.292$$

and

$$E = \frac{0.292(2615 - 85) + 36}{1082} \times 100 = 72 \text{ per cent}$$

Radiant Heat Fluxes

Radiant heat transfer is calculated from the method presented by McAdams,[48] using the SLR temperature measurement. The mean beam length for the core gases is 0.61 D or 0.25 feet.

At the 13-1/2-inch distance, the partial pressure of CO_2 is 0.08 atm and that of H_2O is 0.111 atm from the composition determined earlier for E = 75. For CO_2, $P_cL = 0.020$ and for H_2O, $P_wL = 0.028$. At 3585°R, T_{SLR}, $\epsilon_g = 0.016 + 0.0058 = 0.022$. Also by McAdams' methods, $\alpha_g = 0.086$.

$$q_R = 0.173\left(\frac{1+\epsilon_s}{z}\right)\left[\epsilon_g\left(\frac{T_g}{100}\right)^4 - \alpha_g\left(\frac{T_s}{100}\right)^4\right] \tag{23}$$

The tube emmissivity, ϵ_s, is estimated to be 0.6.

$$q_R = .173 \times 0.8 \times \left[.022\left(\frac{3585}{100}\right)^4 - .086\left(\frac{665}{100}\right)^4\right]$$

$$q_R = 5000 \text{ Btu/hrft}^2$$

Similarly for the 7-1/2-inch distance from the flameholder where E = 72 and T_{SLR} = 3595°R,

$$q_R = 4900 \text{ Btu/hrft}^2$$

Convective Coefficient

The convective heat transfer coefficient is now readily evaluated, at the 13-1/2-inch distance

$$h = \frac{Q/A_s - q_R}{T_b - T_s} = \frac{31,800 - 5000}{2,600 - 205} \qquad (24)$$

$$h = 11.2 \text{ Btu/hrft}^2\text{°F}$$

and at the 7-1/2-inch distance

$$h = 14.6 \text{ Btu/hrft}^2\text{°F}$$

Temperature Profile

The temperature profile along the burner length is now calculated, using the data taken without combustion, i.e., the cold flow data. For the S-2 flameholder, the h'/h'_∞ values are

L, inches (from flameholder)	h'/h'_∞	h_x Btu/hrft^2°F
13-1/2	1.7	11.2
7-1/2	2.2	14.5
4-1/2	2.8	18.4
2-1/2	3.6	23.7
1/2	4.8	31.6

The h_x values are obtained by multiplying h'/h'_∞ by the factor, h at

13-1/2-inches ÷ 1.7 = 6.59. In this manner the coefficients have been scaled up by a constant factor based on the coefficient measured during combustion at the 13-1/2-inch level.

Radiation fluxes must be estimated before the temperatures at the four stations can be calculated from the above convective coefficients. Therefore, gas temperatures are estimated and the radiant heat transfer calculated as demonstrated earlier.

L, inches	T_g °F (assumed)	Q_R/A_s Btu/hrft^2	Q/A_s Btu/hrft^2	Q_c/A_s Btu/hrft^2
13-1/2	2600	5000	31,800	26,800
7-1/2	2620	4900	39,400	34,500
4-1/2	1575	1900	27,400	25,500
2-1/2	800	400	15,700	15,300
1/2	265	0	5,300	5,300

The temperature differences are now found from

$$T_g = \frac{(Q_c/A_s)}{h_x} \tag{25}$$

L, Inches	ΔT_g	T_s °F	T_g °F
13-1/2	2395	205	2600
7-1/2	2380	257	2637
4-1/2	1385	207	1592
2-1/2	646	153	799
1/2	168	103	271

Since the calculated gas temperatures are essentially those assumed to evaluate the radiant heat transfer, the calculation need not be repeated.

Pressure-Drop Combustion Efficiency

The drag caused by the tube walls during combustion is calculated using friction factors for smooth tubes and the previously calculated temperature profile to evaluate the viscosity and density of the burned gases. The viscosity is evaluated using Sutherland's formula

$$\frac{\mu}{\mu_o} = \frac{273.1 + C}{T°K + C} \left(\frac{T°K}{273.1}\right)^{3/2} \qquad (26)$$

with $C = 114$ and $\mu_o = 0.0171$.

L, inches	Re	f	ρ lbs/ft^3	$\Delta P/L$ $\frac{\text{in.H}_2\text{O}}{\text{in.tube}}$
1/2	34,900	0.0058	0.0535	0.470×10^{-3}
2-1/2	23,900	0.0063	0.0310	0.885×10^{-3}
4-1/2	17,800	0.0068	0.0191	1.54×10^{-3}
7-1/2	14,300	0.0072	0.0126	2.48×10^{-3}
13-1/2	14,400	0.0072	0.0128	2.44×10^{-3}

where $\frac{\Delta P}{\Delta L} = \frac{4fG^2}{2g_c D\rho} = \frac{f}{\rho}(4.34 \times 10^{-3}) \frac{\text{inches } H_2O}{\text{inch tube}}$

The summation of the pressure drop per unit length is made with each local value taken to represent the few inches on either side of it as shown below.

L, inches	ΔL	$\frac{\Delta P}{\Delta L} \times \Delta L$
1/2	0 to 1-1/2 = 1-1/2	0.71×10^{-3}
2-1/2	1-1/2 to 3-1/2 = 2	1.77×10^{-3}
4-1/2	3-1/2 to 5-1/2 = 2	3.08×10^{-3}
7-1/2	5-1/2 to 10-1/2 = 5	12.40×10^{-3}
13-1/2	10-1/2 to 15-1/2 = 5	12.20×10^{-3}
		30.16×10^{-3} inches H_2O

Therefore, drag of tube walls is 0.03 inches of H_2O. The drag of the flameholder was measured under cold flow conditions and found to be 15.52 inches H_2O. The pressure drop due to the combustion then is $\Delta P_c = 16.30 - 15.52 - .03 = 0.75$ inches H_2O.

A combustion efficiency of 80 per cent is assumed to evaluate $\overline{M}_2$.

$$\frac{T_2}{T_1} = \frac{P_2}{P_1} \frac{\overline{M}_2}{\overline{M}_1} \frac{A_2}{A_1} \frac{g_c}{\rho_1 u_1^2} \left[\Delta P_c + \frac{\rho_1 u_1^2}{g_c}\right] \qquad (13)$$

$$T_2 = 545 \times \frac{14.7}{15.3} \times \frac{28.5}{29.4} \times \frac{19.01}{18.71} \times \frac{1}{0.749} \left[0.750 \times 5.2 + 0.749\right]$$

$$T_2 = 3200°R = 2740°F$$

To evaluate $\overline{C}_{p2}$, the combustion efficiency is estimated to be 80 per cent.

	Moles	mole fraction y	M		yM	C_p 60° to 2740°F		yC_p
N_2	18.8	0.736	x 28	=	20.60	0.0199		0.0147
O_2	1.4	0.055	x 32	=	1.76	0.0199		0.0011
C_3H_8	0.18	0.007	x 44	=	0.31	0.082		0.0006
CO_2	2.16	0.085	x 44	=	3.74	0.0322		0.0027
H_2O	3.00	0.117	x 18	=	2.10	0.0263		0.0031
				$\overline{M}_2$ =	28.51		$\overline{C}_{p2}$ =	0.0222

Again $\overline{C}_{p2}$ is in Btu/ft^3°F with the volume measured at 60°F and 1 atm. The density of the burned gases at 60°F is 0.0751 lb/ft^3 and $\overline{C}_{p2}$ becomes 0.296 Btu/lb°F.

The heat loss up to 2 inches from the end of the burner is 52,700 Btu/hr and Q_t = 83 Btu/hr lb.

$$E = \frac{\overline{C_{p2}} (T_2 - T_i) + Q_t}{Q_R} \times 100 \qquad (14)$$

$$E = \frac{0.296\ (2740 - 85) + 83}{1082} \times 100 = 80$$

Since $\bar{M}_2$ and $\bar{C}_{p2}$ were evaluated on an estimated combustion efficiency of 80 per cent, the calculation is complete.

Predicted Coefficients

The coefficient for convective heat transfer, h_∞, predicted for fully developed turbulent flow is calculated from the relation,

$$h_\infty = \frac{k_s}{D} \times 0.023\ Re_s^{0.8}\ Pr_s^{1/3}\ (T_b/T_s)^{.33} \qquad (18)$$

For the 13-1/2-inch distance, with T_2 = 205°F and E = 75 per cent, the properties of the gases at the surface were estimated using weight averages.

$$k_s = 0.0171 \qquad \mu_s = 0.0195 \text{ cp} \quad \text{and} \quad C_{ps} = 0.261 \quad Pr_s = 0.72$$

$$Pr_s^{1/3} = 0.896$$

Then

$$h_\infty = \frac{0.0171 \times 12}{4.92} \times 0.023 \times \left[\frac{4.92 \times 636 \times 12}{19 \times 0.0195 \times 2.42}\right]^{0.8} \times 0.896$$

$$\times \left(\frac{3060}{665}\right)^{.33}$$

$$h_\infty = 7.0 \text{ Btu/hrft}^2\text{°F}$$

Similarly, for the 7-1/2-inch distance, h_∞ = 7.01 Btu/hrft^2°F.

The cold flow ratio of coefficients is

at the 13-1/2-inch distance,

$$h'/h'_\infty = 1.7$$

at the 7-1/2-inch distance,

$$h'/h'_\infty = 2.2$$

Therefore,

at 13-1/2 inches,

$$h/(h_\infty\, h'/h'_\infty) = 0.929$$

at 7-1/2 inches,

$$h/(h_\infty\, h'/h'_\infty) = 0.946$$

The coefficient determined from the assumption of E = 80 per cent at the 13-1/2-inch distance, i.e., the 4-inch level, is easily evaluated.

$$T_2 = \frac{Q_R E - Q_t}{\bar{C}_{p2}} + T_i = \frac{1082 \times 0.80 - 73}{0.293} + 85 = 2700°F$$

Thus for E = 80 per cent,

$$h = \frac{Q/A - q_R}{\Delta T} = \frac{31,800 - 5600}{2700 - 205} = 10.5 \text{ Btu/hrft}^2\,°F$$

and

$$h/(h_\infty\, h'/h'_\infty) = \frac{10.5}{6.95 \times 1.7} = 0.889$$

APPENDIX C

DERIVATIONS

APPENDIX C

DERIVATIONS

Combustion Efficiency

The derivation of the equations used to evaluate the combustion efficiency from the measured pressure drops is presented. This derivation is adapted from that presented by Sundstrom.[78] The general mass, momentum, and energy relations can be reduced by reasonable assumptions to the following one-dimensional form.

Mass: $$\rho_1 u_1 A_1 = \rho_2 u_2 A_2 \tag{10}$$

Momentum: $$\left(P_1 + \frac{\rho_1 u_1^2}{g_c}\right) A_1 - F_D = \left(P_2 + \frac{\rho_2 u_2^2}{g_c}\right) A_2 \tag{11}$$

Energy: $$\overline{C}_{p_1}(T_1-T_o) + \frac{u_1^2}{2g_c} + Q_r(T_o) - Q_t = \overline{C}_{p_2}(T_2-T_o) + \frac{u_2^2}{2g_c} \tag{12}$$

The assumptions made in deriving these equations are

1) the flow is steady,
2) thermal diffusion is negligible,
3) μ' is negligible compared to μ,
4) C_{ps} = constant, and
5) there are no gradients in velocity temperature or pressure at either stations 1 or 2.

Assumptions 1, 2, and 3 are valid. The error introduced by assumption 4 is minimized by using the average value of C_{ps} between T_o and T_1 or T_2. In the experiments, stations 1 and 2 are located upstream of the flameholder and at 2 inches from the end of the tube, respectively.

Upstream of the flameholder, conditions are uniform, but gradients do exist at the tube exit. Since the region of most active combustion is upstream of the exit, the gradients are not severe.

From the ideal gas law

$$\frac{T_2}{T_1} = \frac{P_2}{P_1}\frac{\rho_1}{\rho_2}\frac{\bar{M}_2}{\bar{M}_1} \tag{27}$$

The mass and momentum equations are combined to give

$$\frac{\rho_1}{\rho_2} = \frac{u_2 A_2}{u_1 A_1} = \frac{g_c A_2}{\rho_1 u_1^2 A_1}\left[P_1 - P_2\frac{A_2}{A_1} - \frac{F_D}{A_1} + \frac{\rho_1 u_1^2}{g_c}\right] \tag{28}$$

Substitution of the expression for temperature ratio gives

$$\frac{T_2}{T_1} = \frac{P_2}{P_1}\frac{\bar{M}_2}{\bar{M}_1}\frac{g_c}{\rho_1 u_1^2}\frac{A_2}{A_1}\left[P_1 - P_2\frac{A_2}{A_1} - \frac{F_D}{A_1} + \frac{\rho_1 u_1^2}{g_c}\right] \tag{13}$$

The energy equation is solved for the heat released due to chemical reaction.

$$Q_r^{(T_o)} = \bar{C}_{p_2}(T_2 - T_o) - \bar{C}_{p_1}(T_1 - T_o) + \frac{u_2^2}{2g_c} - \frac{u_1^2}{2g_c} + Q_t \tag{29}$$

In the experiments, T_i had an average value of 76°F with the maximum deviation being 10°F for any run. Therefore, the reference temperature, T_o, is conveniently chosen as 76°F. The kinetic energy terms are much smaller than the exit sensible heat and heat transfer terms and are therefore eliminated. Equation (29) is then simplified

$$Q_r^{(T_1)} = \bar{C}_{p_2}(T_2 - T_1) + Q_t \tag{30}$$

The combustion efficiency is defined as the ratio of the heat released by chemical reaction to the heat which would be released if combustion were complete.

$$E = \frac{Q_r(T_1)}{Q_R(T_1)} = \frac{\overline{C}_{p_2}(T_2-T_1) + Q_t}{Q_R(T_1)} \tag{14}$$

Equation (13) is used to evaluate T_2 from the pressure-drop measurements.

Effect of Thermocouple Holes

The error caused by the presence of the thermocouples in the tube wall on the heat flux is estimated. The case to be analyzed is one that would cause the greatest error in the heat flux. The thermocouple assembly is assumed to be a perfect insulator and the analysis employs a conformal mapping technique. The error, caused by the presence of the thermocouple, in the temperature distribution and temperature indication of the thermocouple is covered by Beck and Hurwicz[6] in a generalized manner.

Since the thermocouple section is approximately one-inch wide in both the longitudinal and the circumferential directions and since the angle subtended by the section is only 20°, the two-dimensional view for the analysis may be either a longitudinal one or a circumferential one. The longitudinal plane, shown as section A-A' in Figure 54, is the easier to analyze and is used here. The analysis using the radial plane has also been done with the results agreeing within one per cent.

The thermocouple hole nearest the inside tube surface will have the greatest effect and is placed at the origin of the x-y plane. The

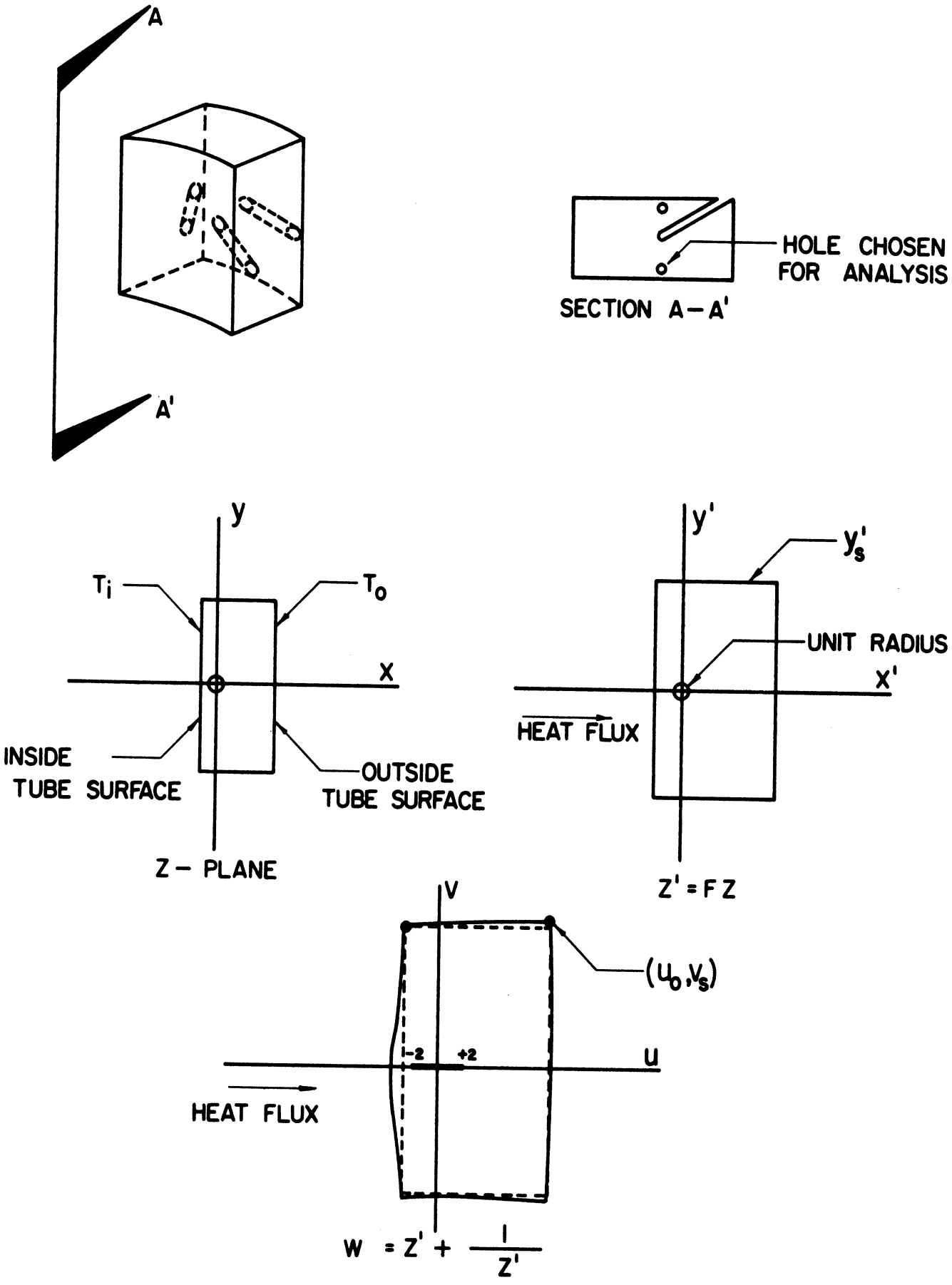

Figure 54. Complex Mapping Technique for Analysis of Error Caused by a Thermocouple Hole on the Heat Flux.

conditions of the problem are

1) $T = T_i$ at $x = -0.040$ inches

2) $T = T_o$ at $x = +0.468$ inches

3) $\frac{dT}{dy} = 0$ at $y = \pm 1/2$ inches

4) $dT/d\theta = 0$ at $\theta = \pm 10°$

5) 0.042-inch diameter thermocouple hole at the orgin.

The coordinates of the z plane are first multiplied by a factor F of 47.6 to convert the hole with a radius of 0.021 inches to one of unit radius. Then the hole is collapsed in the W plane by the transformation $W = z' + \frac{1}{z'}$. The heat flux through the approximate rectangle of the W plane compared to the heat flux through the rectangle of the z' plane, ignoring the hole, will show the effect of the hole.

The coordinates of the important points in the three planes are given in the following table:

x	y	x'	y'	u	v
-0.040	0	-1.90	0	-2.43	0
+0.468	0	+22.30	0	+22.35	0
0	0.5	0	23.80	0	23.76
-0.040	0.5	-1.90	23.80	-1.90	23.76
+0.468	0.5	+22.30	23.80	+22.32	23.78

$$u = Fx + \frac{Fx}{(Fx)^2 + (Fy)^2} \tag{31}$$

$$v = Fy - \frac{Fy}{(Fx)^2 + (Fy)^2} \tag{32}$$

The average coordinates of the approximate rectangle in the W plane are used to estimate the heat flux. The distortion of the rectangle is exaggerated in the drawing. The average coordinates are $u_i = -2.17$, $u_o = 22.34$, and $v_s = 23.76$. Since the heat flow is one-dimensional, the heat fluxes are given by the relation

$$q_{\text{no holes}} = 2\, k y'_s \frac{\Delta T}{\Delta x'} \tag{33}$$

$$q_{\text{holes}} = 2\, k v_s \frac{\Delta T}{\Delta u} \tag{34}$$

$$\frac{q_{\text{holes}}}{q_{\text{no holes}}} = \frac{v_s}{y'_s} \frac{\Delta x'}{\Delta u} \tag{35}$$

$$= \frac{23.76}{23.80} \frac{(-1.90 - 22.30)}{(-2.17 - 22.34)}$$

$$= 0.98$$

Therefore, the estimated error in the heat flux caused by the presence of the thermocouple is 2 per cent.

APPENDIX D

CONDUCTIVITY OF TUBE WALL AND LAMP CALIBRATION

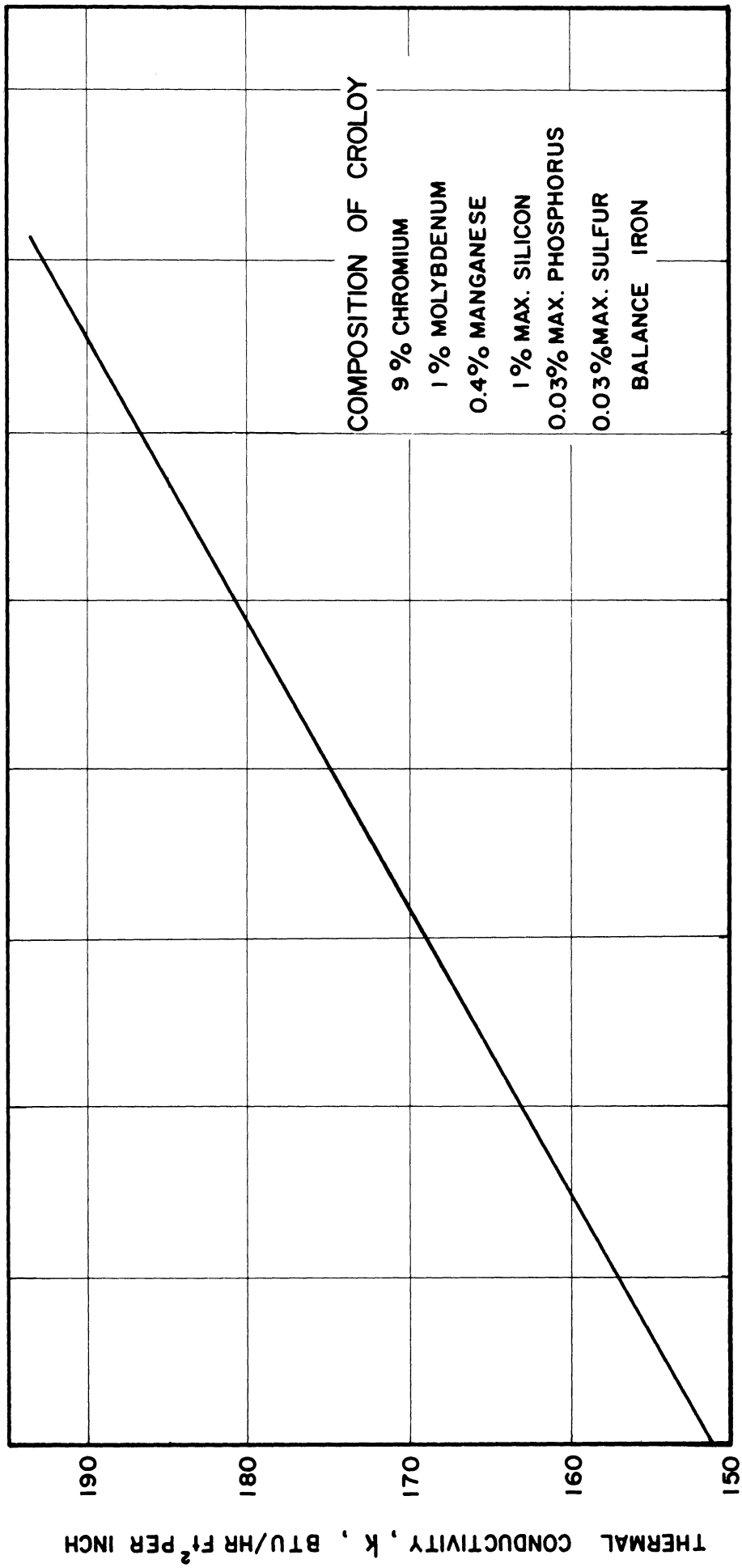

Figure 55. Thermal Conductivity of TubeWall, Croloy, as a Function of Temperature.

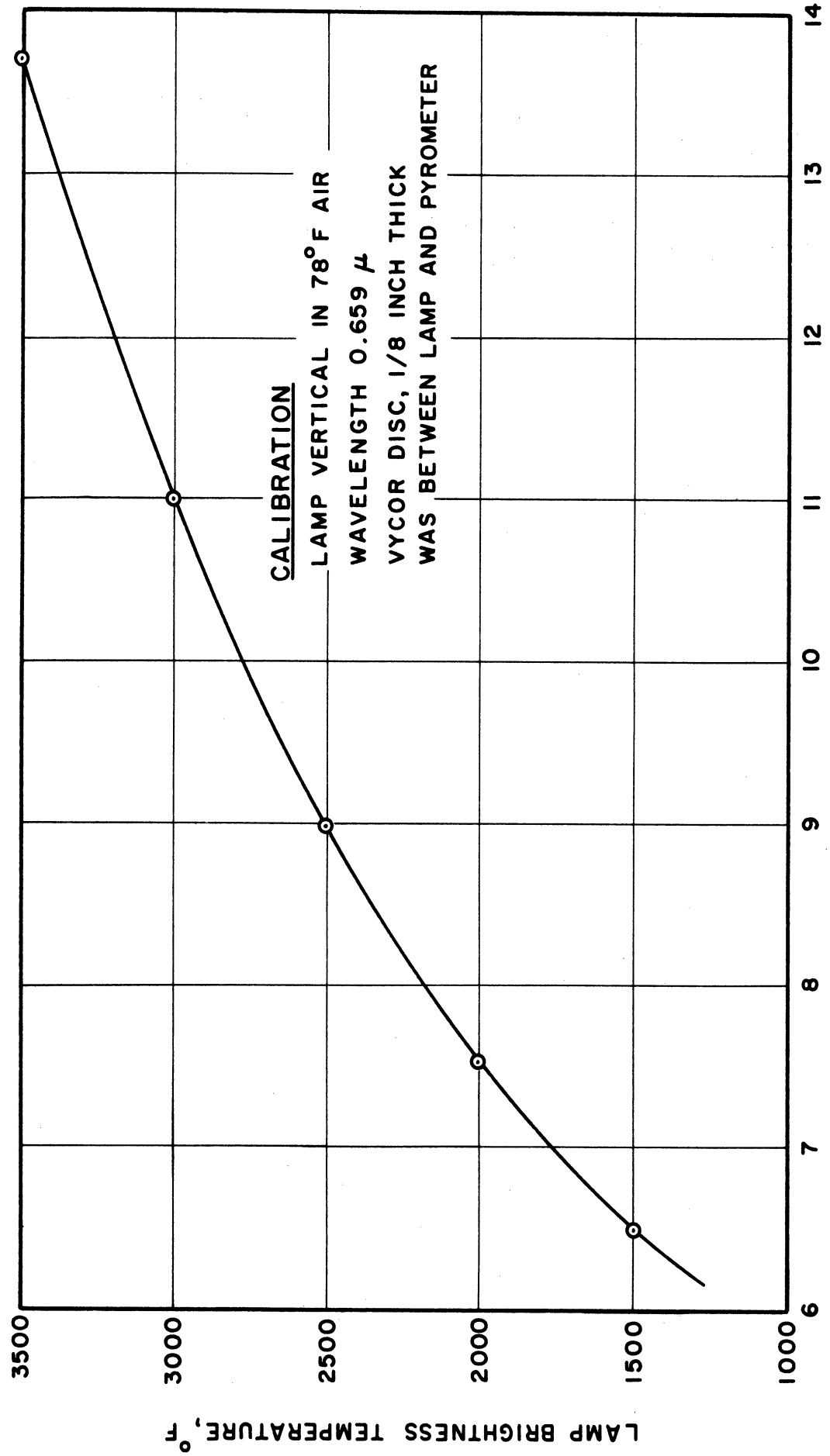

Figure 56. Calibration Curve of Tungsten Ribbon Lamp with Vycor Window in Line of Sight.

BIBLIOGRAPHY

1. Avery, W. H. and Hart, R. W. Ind. Eng. Chem., 45, (Aug., 1953), 1634-1637.

2. Bailey, J. J. J. Appl. Mech., 79, (Sept., 1957), 333-339.

3. Barker, C. L. Calif. Inst. Tech., Jet Prop. Lab., Progr. Rep. 20-356, (Aug. 1, 1958).

4. Bartz, D. R. Jet Propulsion, 27, (Jan., 1957), 49-51.

5. Bayley, F. J. J. Roy. Aeron. Soc., 61, (1957), 208.

6. Beck, J. V. and Hurwicz, H. Trans. ASME, 82, Series C, No. 1, (Feb., 1960), 27.

7. Berman, K. and Cheney, S. H., Jr. J. Am. Rocket Soc., 23, (1953), 89.

8. Blackshear, P. L., Rayle, W. D. and Tower, L. K. NACA, TN 3567, (Oct., 1953).

9. Brokaw, R. S. NACA, RM E57K19a, (March, 1958).

10. Cheng, S. I. and Kovitz, A. A. Sixth Symposium on Combustion, Reinhold, New York, (1957), 418.

11. Cheng, S. I. and Kovitz, A. A. Seventh Symposium on Combustion, Butterworths, London, (1958), 476.

12. Churchill, S. W. Convective Heat Transfer from a Gas Stream at High Temperature to a Cylinder Normal to the Flow. Ph.D. Thesis, University of Michigan, 1953.

13. Crocco, L., Grey, J. and Harrje, D. T. Jet Propulsion, 28, (Dec., 1958), 841.

14. Damkoehler, G. Z. Electrochem., 46, (1940), 601.

15. Dunlap, R. A. University of Michigan, Rept. No. UMM-43, (March, 1950).

16. Fand, R. M. and Kaye, J. USAF, Wright Air Development Center, Tech. Note 59-18, (March, 1959).

17. Friedman, R. and Grover, J. H. Ind. Eng. Chem., 49, (Sept., 1957), 1470.

18. Greenfield, S. J. Aero. Sci., 18, (1951), 512.

19. Hahnemann, H. and Ehret, L. NACA, TM 1271, (July, 1950).

20. Hammaker, F. G., Jr. and Hampel, T. E. Amer. Gas Assoc. Labs., Research Rept. No. 1255, (1956).

21. Harp, J. L., Jr., Velie, W. W. and Bryant, L. NACA, RM E53L24b, (March, 1954).

22. Harrje, D. T. Calif. Inst. Tech., Jet Prop. Lab., Progr. Rep. 20-362, (Aug. 27, 1958).

23. Havemann, H. A. J. Indian Inst. Sci., 37B, (1955), 58, 121.

24. Havemann, H. A. and Rao, N. N. Nature (London), 174, (1954), 41.

25. Hirschfelder, J. O. J. Chem. Phys., 26, (Feb., 1957), 274.

26. Holman, J. P. and Mott-Smith, T. P. Wright Air Development Center, Tech. Note 58-352, (Dec., 1958).

27. Jackson, E. G. and Kilham, J. K. Ind. Eng. Chem., 48, (Nov., 1956), 2077-2079.

28. Jackson, T. W., Harrison, W. B. and Boteler, W. C. Trans. ASME, 81, Series C, (Feb., 1959), 68.

29. John, R. R. and Summerfield, M. Jet Propulsion, 27, (Feb., 1957), 169.

30. Jost, W. Explosion and Combustion Processes in Gases. New York: McGraw-Hill, New York, 1946.

31. Karlovitz, B. Seventh Symposium on Combustion, Butterworths, London, (1958), 519.

32. Karlovitz, B., Denniston, D. W., Jr. and Wells, F. E. J. Chem. Phys., 19, (1951), 541.

33. Kaskan, W. E. and Noreen, A. E. Trans. ASME, 77, (Aug., 1955), 885-895.

34. Khitrin, L. N. and Goldenberg, S. A. Sixth Symposium on Combustion, Reinhold, New York, (1957), 545.

35. Kilham, J. K. Third Symposium on Combustion, Flame, and Explosion Phenomena, Williams and Wilkins, Baltimore, (1949), 733.

36. Kippenham, C. J. and Croft, H. O. Trans. ASME, 74, (1952), 1151.

37. Koffel, W. K., Harp, J. L., Jr. and Bryant, L. NACA, RM E54H27, (Nov., 1954).

38. Kreith, F. Trans. ASME, 81, Series C, (Feb., 1959), 74.

39. Kubanskii, P. N. Zh. Tekh. Fiz., 22, (1952), 585-592.

40. Kubanskii, P. N. Akust, Zh., 5, (1959), 51-57.

41. Ladenburg, R. W., Lewis, B., Pease, R. N., and Taylor, H. S., (Editors), High Speed Aerodynamics and Jet Propulsion, IX: Physical Measurements in Gas Dynamics and Combustion, Princeton University Press, 1956.

42. Landau, L. J. Exp. Theor. Phys., 14, (1944), 240.

43. Lemlich, R. Ind. Eng. Chem., 47, (June, 1955), 1175.

44. Lewis, B., Pease, R. N. and Taylor, H. S. (Editors), High Speed Aerodynamics and Jet Propulsion, II: Combustion Processes, Princeton University Press, 1956.

45. Lewis Laboratory Staff, NACA, RM E54B02, (April, 1954).

46. Longwell, J. P., Frost, E. E. and Weiss, M. A. Ind. Eng. Chem., 45, (1953), 1629.

47. Loshaek, S., Fein, R. S. and Olsen, H. L. J. Acoust. Soc. Am., 21, (1949), 605.

48. McAdams, W. H. Heat Transmission. 3rd ed., New York: McGraw-Hill, 1954.

49. Marble, F. E. and Adamson, T. C., Jr. Selected Combustion Problems. London: Butterworths, (1954), 111.

50. Markstein, G. H. J. Chem. Phys., 17, (1949), 428.

51. Martinelli, R. C., Boelter, L. M. K., Weinberg, E. B. and Yakahi, S. Trans. ASME, 65, (1943), 789.

52. Merk, H. J. Appl. Sci. Res., Sect. A, 8, No. 1, (1958), 1-27.

53. Mickelsen, W. R. NACA, TN 3983, (May, 1957).

54. Moore, F. K. and Maslen, S. H. NACA, TN 3152, (May, 1954).

55. Morrell, G. Jet Propulsion, 28, (Dec., 1958), 829.

56. Morse, P. M. Vibration and Sound. New York: McGraw-Hill, 1948.

57. Mueller, W. K., Jr. Ph.D. Thesis, University of Illinois, 1956.

58. Pass, I. and Tischler, A. O. NACA, RM E56C10, (June, 1956).

59. Perry, J. H. (Editor), Chemical Engineers Handbook. New York: McGraw-Hill, 1950.

60. Petrein, R. J., Longwell, J. P. and Weiss, M. A. Jet Propulsion, 26, (1956), 81.

61. Prudnikov, A. G. Seventh Symposium on Combustion. London: Butterworths, (1958), 221.

62. Putnam, A. A. and Dennis, W. R. Trans. ASME, 75, (Jan., 1953), 15-28.

63. Putnam, A. A. and Dennis, W. R. Trans. ASME, 77, (Aug., 1955), 875-883.

64. Putnam, A. A. and Dennis, W. R. J. Acous. Soc. Amer., 28, (1956), 246.

65. Putnam, A. A. and Dennis, W. R. J. Acous. Soc. Amer., 28, (1956), 260.

66. Rayleigh, Lord. The Theory of Sound, II. Dover Publications, 1945.

67. Rogers, D. E. and Marble, F. E. Jet Propulsion, 26, (June, 1956), 456-462.

68. Scadron, M. D. and Warshawsky, I. NACA, TN 2599, (1952).

69. Schmidt, E., Steinicke, H. and Neubert, V. Fourth Symposium on Combustion, Baltimore: Williams and Wilkins, (1953), 658.

70. Schotte, Wm. Ind. Eng. Chem., 50, (April, 1958), 683-690.

71. Scurlock, A. C. Project Meteor Rept. 19, Mass. Inst. Technol. Fuels Research Lab., (1948).

72. Shetinkov, E. S. Seventh Symposium on Combustion. London: Butterworths, (1958), 406.

73. Shieber, H. ARS Journal, 29, (June, 1959), 446.

74. Shorin, S. N. and Pravoverov, K. N. Izvest. Akad. Nauk. USSR, Otdel. Tekh. Nauk., 1953, 1122.

75. Smith, R. P. and Sprenger, D. F. Fourth Symposium on Combustion. Baltimore: Williams and Wilkins, (1953) 893.

76. Spalding, D. B. Some Fundamentals of Combustion. London: Butterworths Scientific Publications, 1955.

77. Summerfield, M. Heat Transfer Symposium, University of Michigan, 1952.

78. Sundstrom, D. W. Heat Transfer from Gas Flames in Cooled Tubes. Ph.D. Thesis, University of Michigan, 1958.

79. Tailby, S. R. and Ashton, M. D. Trans. Instn. Chem. Engrs., 36, (1958), 1-12.

80. Tailby, S. R. and Berkovitch, I. Trans. Instn. Chem. Engrs., 36, (1958), 13-28.

81. Tailby, S. R. and Saleh, M. A. Trans. Instn. Chem. Engrs., 31, (1953), 36.

82. Timofeev, V. N. and Uspenskii, V. A. Izvest. Akad. Nauk. USSR, Otdel. Tekh. Nauk., 1956, No. 9, 111.

83. Tischler, A. O. and Male, T. Proceedings of the Gas Dynamics Symposium on Aerothermochemistry, Northwestern University, (1956), 71-81.

84. Truman, J. C. and Newton, R. T. Ind. Eng. Chem., 47, (1955), 1183.

85. Usow, K. A., Meyer, C. L. and Schulze, F. W. NACA, RM E53I01, (Dec., 1953).

86. West, F. B. and Taylor, A. T. Chem. Eng. Prog., 48, (1952), 39.

87. Westenberg, A. A. J. Chem. Phys., 22, (1954), 814.

88. Williams, G. C., Hottel, H. C. and Scurlock, A. C. Third Symposium on Combustion, Flame, and Explosion Phenomena, Baltimore: Williams and Wilkins, (1949), 21.

89. Winter, E. F. Fuel, 34, (1955), 409.

90. Wright, F. H. and Becker, J. L. Jet Propulsion, 26, (1956), 973.

91. Zellnik, H. E. Heat Transfer from Hot Gases Inside Circular Tubes. Ph.D. Thesis, University of Michigan, 1956.

92. Ziebland, H. J. Brit. Interplan. Soc., 14, (1955), 249.

93. Zukoski, E. E. and Marble, F. E. Proceedings of the Gas Dynamics Symposium on Aerothermochemistry, Northwestern University, (1956), 205-210.